A Study on Cheap Robust Sensing for Obstacle Avoidance Guidance Based on Bio-Sonar Strategy of Bats

by

Yasufumi Yamada

Doshisha University
Faculty of Life and Medical Sciences

November 2016

Doshisha University

Faculty of Life and Medical Sciences

ABSTRACT

A Study on Cheap Robust Sensing
for Obstacle Avoidance Guidance Based on Bio-Sonar Strategy of Bats

by Yasufumi Yamada

SUPERVISOR: Professor Yoshiaki Watanabe

Bats (Microchiroptera) possess a highly developed biosonar system that can be regarded as the minimum sensor requirement (one transmitter and two receivers) for three-dimensional spatial sensing. Despite this, bats can realize robust navigation in a complex environment. The present study 1) experimentally investigated changes in the pulse direction, pulse emission timing and flight path of *Rhinolophus ferrumequinum nippon* during an obstacle avoidance flight as the bats became familiar with the space around them and 2) expressed behavioral principles observed in the bats during flight, especially in an unfamiliar space, using an algorithm and then embedded the principles into an autonomous vehicle equipped with simple ultrasound sensors. A cross-correlational investigation provide useful solutions for technical problems of recent technology trends that rely on careful sensing using multiple sensors. 1) During successive long-term flights, bats repeated the same flight path after several tens of seconds of flight and decreased the number of pulse emissions by a) prolonging the interpulse interval while b) replacing the triple pulse (sonar sound group of three pulse emissions with short intervals) with a double or single pulse, suggesting that bats complete much spatial learning in a short time and then adapt their flight motor control and time-temporal control of sonar sound to achieve economical flight. 2) Further investigation of the pulse direction control during repeated flights through an obstacle course revealed that while flying in unfamiliar space bats often produced two emissions as a pair (double pulses) and alternately shifted the pulse direction between immediate obstacles and the intended flight direction. Meanwhile, as the bats became familiar with the space around them, they reduced the number of pulse emissions and controlled the pulse direction primarily in the intended flight direction. 3) To confirm the practical effectiveness of the bat's behavior, a multi-obstacle avoidance model (MOA model) was constructed as a platform for a bat-inspired navigation algorithm. 4) Using the MOA model, the observed behavioral principles of bats in unfamiliar spaces was embedded into an autonomous vehicle equipped with simply designed ultrasonic sensors. A practical vehicle demonstration suggested that simple procedures inspired by animals, such as the spatial and temporal integration of sensing information from double-pulse scanning, can greatly benefit the performance of acoustical navigation. The findings of this world-leading biomimetic research offer new possibilities for artificial-intelligence navigation systems.

TABLE OF CONTENTS

LIST OF FIGURES

ACKNOWLEDGEMENTS

Chapter 1. *Introduction*

1.1 *Bio-sonar System of Bats*

Bats and dolphins possess a highly developed sonar (acronym for SOund NAvigation and Ranging) system, called an echolocation system, which emits ultrasound pulses and analyzes the echoes returning from surrounding objects. The echolocation system acquired by evolutionary adaptation allows biosonar animals to navigate by processing echoes using their auditory system without using good visual information in complete darkness.

The use of ultrasound by bats for localization was first reported by Griffin in the 1950s (Griffin, 1958). Bats emit brief sounds at high frequencies (Neuweiler, 1984) from 15 kHz to over 200 kHz through their mouth and/or nostrils when echolocating. Echolocating bats can be classified according to whether the ultrasound they emit is constant-frequency (CF) ultrasound and/or frequency-modulated (FM) ultrasound (Simmons, 1979; Neuweiler, 1984). Bats that use only FM sounds to echolocate are known as FM bats. Meanwhile, most bats that use CF components for echolocation combine the CF component with FM components in their pulses and are known as CF–FM bats. The capability of the biosonar system of bats has been gradually revealed. For instance, an FM echolocating bat species, *Eptesicus fuscus*, can detect changes of less than 1 μs in the arrival time of echoes (Simmons, 1979; Simmons *et al.*, 1990). In contrast, a CF-FM bat species, *Pteronotus parnellii parnellii,* is able to detect differences as small as 50 Hz in the echo frequency of the second harmonic (Riquimaroux *et al.*, 1991; 1992). Such a sophisticated biosonar system allows bats to freely fly while avoiding obstacles (Gustafson and Schnitzler, 1979; Jen and Kamada, 1982) and to hunt small flying prey, typically insects (Griffin *et al.*, 1960; Novick and Vaisnys, 1964; Schnitzler and Kalko, 2001; Ghose and Moss, 2006).

1.2 Motivation

An artificial sensing system that includes sonar is expected to be a useful application of new advanced technology in the Internet of things. The Internet of things is the internetworking of physical devices, buildings and other items embedded with electronics, software, sensors and actuators and the network connectivity that allows these objects to collect and exchange data (Ashton, 2009; Atzori *et al.*, 2010). A representative technology of the Internet of things is the autonomous vehicle, where a mobile robot is able to sense its environment and navigate without human input. The spatial sensing is performed by multiple sensors, such as radar, Global Positioning System, odometry and stereovision sensors, accompanied with the processing of a wealth of data using a high-performance central processing unit (CPU) so that careful sensing eliminates any chance of collision. The development of an artificial navigation system is thus directed toward expensive design.

Echolocating bats emit ultrasound pulses from the nose or mouth and detect the returning echoes with the left and right ears; this can be regarded as the minimum sensor requirement for three-dimensional (3D) spatial sensing. From an engineering perspective, echolocation processes one-dimensional sound information. Echolocation seems to require fewer data and have a lower processing cost than visual sensing, which requires the reconstruction of two-dimensional images. Here, the term "cheap design" is a concept proposed in studies of mobile robots that leads to low operational energy cost, simple mechanical design and a low-resolution sensor system (Pfeifer and Lambrinos, 2000; Iida, 2005). Although the echolocation of bats is considered to be based on cheap design sensing in some respects, bats achieve robust navigation in a complex environment; i.e., bats avoid randomly located obstacles and fly with other conspecifics (Griffin, 1958; Jen and Kamada, 1982; Surlykke *et al.*, 2009a; Barchi *et al.*, 2013). Such behavioral evidence suggests that bats employ not only a physiological specialization of the auditory system but also behavioral strategies adapted to cheap design sensing. Our motivation is to determine the behavioral principle of the sensing strategy of bats and to construct bio-inspired algorithms as useful applications for a cheap and robust navigation system based on artificial sonar. To accomplish the two aspects of our purpose, a cross-correlational investigation was

conducted as biomimetic research through the behavioral measurement of bats and practical demonstration of a bat-inspired autonomous vehicle.

The present study was the first attempt to comprehensively investigate the acoustic navigation system of bats by conducting biological analysis, mathematical modeling and a practical demonstration. Top-down and bottom-up investigations accelerate the search for a general representation of the biosonar system; a bottom-up investigation is a study of bats from the output behavior to the behavioral principle while a top-down investigation is a study of a vehicle realized from the input design concept responding to the output movement.

1.3   Purpose

To extract a decision-making process of navigation from animals, it is necessary to measure the directional attention relative to surroundings. Behavior associated with the spatial perception of visually guided animals has been extensively studied by measuring eye movement (for humans) and the heading angle (for flies, fish and birds), which is considered equivalent to the eye-gaze direction (Land and Collett, 1974; Land and Lee, 1994; Eckmeier *et al.*, 2008). These behavioral studies suggest that there are theoretical strategies involving relationships between the eye gaze and steering motions among visually guided animals that vary according to the navigation task. In contrast, the dynamics of the relationship between the acoustic gaze (i.e., the direction of ultrasound pulses emitted by bats relative to the flight direction) and flight control are also assumed to relate to a practical behavioral solution that sustains the highly developed navigation system of, for example, aerial-feeding echolocating bats (Ghose and Moss, 2003; Ghose *et al.*, 2006; Ghose and Moss, 2006; Fujioka *et al.*, 2014). For example, while chasing multiple target prey in a field during natural foraging, Japanese house bats (*Pipistrellus abramus*) emit pulses towards not only their immediate target but also their next intended target, which helps plan the future flight path for the effective capture of consecutive prey (Fujioka *et al.*, 2011; Fujioka *et al.*, 2014). The acoustic gaze of bats is considered to be equivalent to the eye gaze of visually guided animals that obtain spatial information sequentially by moving their eyes (or head) during locomotion (Land and Collett, 1974; Land and Lee, 1994;

Eckmeier *et al.*, 2008). Visual perception, however, is based on passive sensing, in which spatial information is received continuously, whereas bats receive spatial–temporal information intermittingly by actively sensing each pulse emission. The echolocation of biosonar animals is thus a unique model that can be used to understand spatial sensing from a perspective different from visual sensing, and measurement of the acoustic gaze of bats during flight allows us to directly compare visual and acoustical sensing from both biological and engineering perspectives. Bat behavioral was thus measured in the present study by mainly focusing on the dynamics of the acoustic gaze and flight motor control.

The aim of the behavioral investigation in the present study was to find an adaptive navigation strategy that optimized the animal's own behavior to the surrounding environment when the animal becomes familiar with the environment. Adaptive navigation behavior has been reported for human drivers who first control their position in a lane using their foveal vision and then increasingly learn to use their peripheral vision to obtain information from more distant road regions as they become familiar with the route (Land and Horwood, 1995). To change the own path planning and/or sensing strategy in a stable environment was a unique and intelligent strategy relying on animal behavior. If behavioral differences between navigating unfamiliar and familiar spaces can be analyzed in detail, we can obtain the essentials of navigating both types of spaces simultaneously. We therefore investigated the obstacle avoidance navigation strategy of bats in the present study by comparing behaviors of flight through unfamiliar and familiar spaces.

1.4   Organization

The remainder of the dissertation is organized as follows. Chapter 2 briefly describes the echolocation of bats, an artificial navigation system and previous related works. Chapter 3 describes the time-temporal alteration of flight paths and sonar sounds of echolocating bats during long-term flight through an obstacle chamber to confirm the presence of adaptation behavior. Chapter 4 presents the adaptation strategy of bats, mainly focusing on the directional control of sonar sound during repeated flights through an obstacle course. How echolocating bats adapt their acoustic gaze and flight path as they become familiar with the space around them is discussed. Chapter 5 constructs a

mathematical model for obstacle avoidance navigation specialized to ultrasound sensing using one transmitter and two receivers. Avoidance movement in this model is evaluated in a mathematical simulation with the intention that the model can be used as a platform for a bat-inspired navigation algorithm. Chapter 6 presents an experiment involving an actual vehicle controlled by an obstacle avoidance algorithm using ultrasonic sensors, which is inspired from the behavioral principles of bats during obstacle avoidance flight through an unfamiliar space. The movement of the vehicle reveals how the observed behavioral strategies of bats improve the robustness of obstacle avoidance navigation. Finally, conclusions and possible directions of future research are presented in chapter 7.

Chapter 2. *Background*

2.1 *Echolocation by CF-FM and FM Bats*

Echolocation can be categorized into two main types according to the spectral and temporal characteristics of the emitted sounds. Rhinolophidae, Hipposideridae, and some species of Mormoopidae are narrowband CF echolocators, emitting long calls dominated by a single CF and separated by brief periods of silence (i.e., a high duty cycle) (Fenton *et al.*, 2012). Narrowband CF bats employ Doppler-shift compensation, adjusting the frequency of their calls to maintain the echo frequency within the acoustic fovea and thus avoiding masking effects by using frequency to separate pulses and their echoes (Schnitzler and Denzinger, 2011). Broadband FM bats, meanwhile, emit broadband pulses of short duration, with long intervals of silence between them, using time rather than frequency to separate pulses and echoes and avoiding masking effects (i.e., a low duty cycle). Narrowband CF and broadband FM echolocation differ in several respects, and bats from each group are thought to adapt their acoustic and flight behaviors according to their foraging habitats (Simmons and Stein, 1980; Neuweiler, 1984; Fenton, 2010; 2013).

2.2 *Echolocation Flight by Bats*

Using a directional beam of ultrasound to echolocate in the air, where sounds are quickly attenuated, bats rely on beamforming to optimize their acoustical field of view. The beam directionality of echolocation pulses has been evaluated for several types of bats, such as the narrowband CF species *Rhinolophus ferrumequinum* (Grinnell and Schnitzler, 1977), *Hipposideros terasensis* (Hiryu *et al.*, 2006) and *Pteronotus parnellii* (Hartley and Suthers, 1990) and the broadband FM species *Eptesicus fuscus* (Hartley and Suthers, 1989), *Carollia perspicillata* (Hartley and Suthers, 1987) and *Myotis* (Shimozawa *et al.*, 1974). Recently, microphone arrays have been used to measure the echolocation beam directionality during flight in both field and laboratory settings (Surlykke *et al.*, 2009b; Jakobsen and Surlykke, 2010; Jakobsen *et al.*, 2013; Jakobsen *et al.*, 2015). The cited studies reported that bats actively adjust their beam width according to the situation.

Mouth-emitting FM bats have been observed to adjust their mouth gape to optimize their acoustical fields of view, using a narrow beam width when entering a confined space and a wider beam width as they approach spaces that are more open (Surlykke *et al.*, 2009b; Kounitsky *et al.*, 2015). Active beam adjustment has also been observed for the narrowband CF bat *R. ferrumequinum nippon*, a nostril-emitting species, during prey-capture flight in a laboratory setting (Matsuta *et al.*, 2013). During the final stages of prey capture, *R. ferrumequinum nippon* actively expands its beam width without changing its call frequency to retain a moving target within its acoustical field of view. Such dynamic beam control is considered a common behavioral strategy among both broadband FM and narrowband CF bats.

Most broadband FM bats emit echolocation pulses through their mouths. The beam directionality of mouth-emitting species can be modeled as a circular piston in an infinite baffle, with the diameter determined by the size of the mouth opening (Strother and Mogus, 1970; Mogensen and Møhl, 1979; Jakobsen and Surlykke, 2010; Jakobsen *et al.*, 2013). According to the acoustical principle of the circular piston model, directivity is determined by the interaction of the mouth aperture and wavelength (i.e., higher call frequencies create a narrower beam if the aperture size remains constant). Jakobsen *et al.* (Jakobsen *et al.*, 2013) found that six aerial hawking vespertilionid species with different body sizes produced calls at different frequencies, with smaller bats emitting higher-frequency calls. The different frequencies created sonar beams with extraordinarily similar patterns of directivity, following the rule that decreasing the emitter size creates a narrower beam if the frequency remains constant. This finding indicates that the bats adjust their calls to create similar acoustic fields of view under similar flight conditions, regardless of body size.

Acoustic scanning is another important behavioral mechanism used by echolocators to determine their acoustical field of view and explore their environment during echolocating flight. The acoustic gaze, defined as the angular difference between the direction of flight and direction of pulse emission, has been experimentally investigated in the case of flying bats in both field (Seibert *et al.*, 2013; Fujioka *et al.*, 2014; Seibert *et al.*, 2015) and laboratory settings (Ghose and Moss, 2003; Ghose *et al.*, 2006; Surlykke *et al.*, 2009a; Kinoshita *et al.*, 2014). Using acoustic scanning, the flying *Eptesicus fuscus* can aim its directional beam to within 3 degrees of a stationary target (Ghose and Moss, 2003).

Rhinolophus ferrumequinum nippon approaching a moving moth in flight in a laboratory chamber can track its target to within less than 5 degrees (Matsuta *et al.*, 2013). The acoustic gaze is a useful index of a bat's attention when selecting targets, and it is analogous to gaze control in visually guided animals. Interestingly, *Eptesicus fuscus* has been observed to conduct sequential gaze shifts between multiple objects when simultaneously performing tasks involving obstacle avoidance and prey capture (Surlykke *et al.*, 2009a). Such sequential gaze shifting has also been reported for the free-swimming harbor porpoise *Phocoena phocoena* when discriminating between two targets (Wisniewska *et al.*, 2012) and for the flying *R. ferrumequinum nippon* when choosing between two moths (Kinoshita *et al.*, 2014). The cited studies demonstrated that echolocating bats will display species-specific behavioral strategies to control their acoustic gaze on the basis of their particular beam directionality to adjust the sensory volume of echo information when navigating complex environments.

The above findings may account for the achievement of both flight and echolocation among bats, and the evolution and ecology of bats have been affected by flight and echolocation (Speakman and Racey, 1991; Arita and Fenton, 1997). We therefore assume that bats manage both flight and echolocation effectively using a well-refined strategy. A large gap exists between echolocation and flight strategy. It is important to understand the adaptive echolocation behavior of bats.

2.3 *Obstacle avoidance navigation by an artificial navigation system*

Recently, inexpensive ultrasonic sensors have become useful for spatial sensing in the navigation of autonomous vehicles (Burgard *et al.*, 1996; Lu, 2013; Aihara *et al.*, 2015). In conjunction with other sensor information, such as that of a radio-frequency identification device tag or stereo vision that refers to a pre-memorized spatial map (Royer *et al.*, 2007), a vehicle can estimate its current position using ultrasonic sensors in an indoor environment (Cox, 1991; Kortenkamp and Weymouth, 1994; Choi *et al.*, 2011; Volos *et al.*, 2013). Meanwhile, when a vehicle needs to map its position in real time to navigate without prior information or any other sensor information in an unfamiliar space (Thrun *et al.*,

2001), recent technology trends lead to careful sensing in which the whole of the surrounding space is covered by multiple sensors, accompanied by the processing of a wealth of data using a high-performance CPU. That is to say, such a concept of spatial sensing is totally the opposite of a bat's biosonar system; i.e., bats achieve high-performance navigation relying on cheap design sensing that provides surrounding information through a restricted acoustical field of view.

Chapter 3. *Echolocation behavior of CF-FM bats during long-term flight in an obstacle-filled environment*

3.1 Introduction

The highly developed sonar navigation of bats has been investigated by making behavioral measurements using a microphone array system in both field (Seibert *et al.*, 2013; Fujioka *et al.*, 2014; Seibert *et al.*, 2015) and laboratory settings (Ghose and Moss, 2003; Ghose *et al.*, 2006; Surlykke *et al.*, 2009a; Kinoshita *et al.*, 2014). During feeding flight, *Eptesicus fuscus* has been observed to make sequential gaze shifts between multiple objects when simultaneously performing tasks involving obstacle avoidance and prey capture (Surlykke *et al.*, 2009a) (Surlykke *et al.*, 2009a). Such sequential gaze shifting has also been reported for flying *R. ferrumequinum nippon* when choosing between two moths (Kinoshita *et al.*, 2014).

Meanwhile, there have been fewer reports on obstacle avoidance navigation than purchasing navigation because the directional attention during obstacle avoidance flight is more frequently switched relative to the multiple surrounding objects and it is thus difficult to determine a rule that is consistent for all obstacle layouts. Moreover, it is possible that the navigation rule changes continuously in a stable environment as the obstacle layout is memorized and the working memory is fed back to the path planning and sensing strategy. An analysis of the behavioral differences in navigation through unfamiliar space and familiar space in the same environment would reveal the essentials of the navigation strategies for the two spaces simultaneously. Moreover, finding the successive rule transited from the unfamiliar navigation to the familiar navigation may allow an adaptation model to be established. As a first step, this chapter investigates whether *R. ferrumequinum nippon* changes its navigation behavior during long-term flight in an environment containing obstacles.

3.2 Materials and Methods

3.2.1 Subject

Eleven adult Japanese horseshoe bats (*R. ferrumequinum nippon*, body length: 6.0–8.0 cm, body mass: 20–30 g) were used (figure 3-1). *Rhinolophus ferrumequinum nippon* were captured from natural caves in Hyogo and Osaka prefectures in Japan. The animals were housed in a temperature- and humidity-controlled colony room [4 m (L) × 3 m (W) × 2 m (H)] at Doshisha University in Kyoto, Japan. The bats were allowed to fly freely and given access to mealworms and water. The day/night cycle of the room was set to 12 h of dark followed by 12 h of light. Captures were conducted under license and in compliance with current Japanese law. All experiments complied with the Principles of Animal Care, publication no. 86-23, revised 1985, of the National Institutes of Health, and with current Japanese law. All experiments were approved by the Animal Experiment Committee of Doshisha University.

The echolocation pulses emitted by *R. ferrumequinum nippon* are compound signals, each of which consists of a CF component, with the second harmonic (CF_2) around 68–70 kHz being the strongest, plus an accompanying initial short upward FM sweep (iFM_2: 2–8 kHz, ending at 68–70 kHz) and a terminal short downward FM sweep (tFM_2: beginning at 68–70 kHz and extending 8–12 kHz lower; figure 3-2A). *Rhinolophus ferrumequinum nippon* produces sonar sound groups more often in unknown environments (Yamada *et al.*, 2016). A sonar sound group (multiple pulses) of three or two pulses is referred to as a triple pulse and double pulse, respectively, and were used in the investigation of the temporal control for the pulse emission timing of bats (figure 3-2A).

Figure 3-2B shows a top view of the measurement system used. The experiments were conducted in a flight chamber that was constructed from steel plates [9 m (L) × 4.5 m (W) × 2.5 m (H)] under lighting with red filters (>650 nm) to avoid visual effects on the bats. An obstacle-filled environment was constructed using plastic chains (diameter, 4 cm) that were suspended from the ceiling of the chamber. Ten bats were used for this experimental layout(layout 1). Each bat was observed for only one successive flight over 100 s so that echolocation behaviors at the start and end of long-term flight could be compared. Furthermore, we recorded the echolocation behavior of another bat for different

obstacle layouts to confirm that the same navigation behavior was observed for different obstacle layouts.

Figure 3-1 Japanese horseshoe bats (*R. ferrumequinum nippon*).
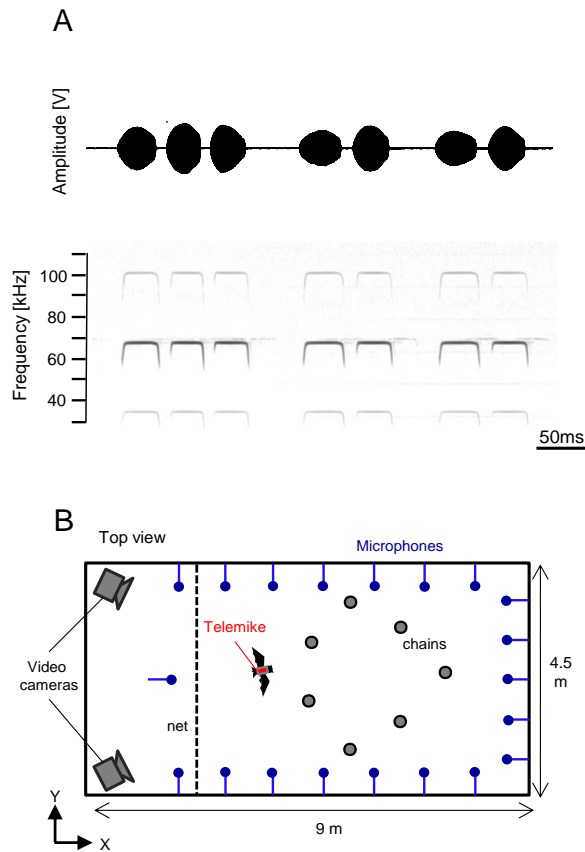
Figure 3-2 Measurement system for echolocation pulses and flight path of a bat during flight. (A) Amplitude pattern (top) and sonograms (bottom) of typical pulse emission sequences of *R. ferrumequinum nippon* during flight in the flight chamber. Sounds were recorded with an on-board microphone mounted on the back of the bat. (B) Arrangement of the obstacles and microphone array in the flight chamber.

3.2.2 Video recordings

Flights were recorded using two digital high-speed video cameras (IDT Japan, Inc., MotionPro X3, Tokyo, Japan; 125 frames per second) located in the left and right rear corners of the flight chamber to map the 3D position of bats during flight. Cameras were placed behind the start position so that they would not interfere with the bat's flight path. 3D flight paths were reconstructed from video footage using motion analysis software (Ditect Corporation, DIPPMotionPro ver.2.2.1.0, Tokyo, Japan). Before flights were filmed, a 3D reference frame was placed at known coordinates at the center of the flight chamber and briefly recorded by the two video cameras. The analysis software used the cameras' stereo view of the reference frame to calibrate the 3D flight path reconstruction system. Employing a direct linear transformation technique using the coordinates of the reference frame, the successive positions of the flying bats, as well as the locations of other objects, were reconstructed from the pair of two-dimensional video images. The flight path of each bat was determined using 3D coordinate data, and a polynomial equation was fitted to the data to create a smooth flight path. The instant 3D flight direction of the bat was obtained, in conjunction with the acoustic characteristics of the echolocation sounds, from the 3D coordinates at a frame rate of 125 frames per second.

3.2.3 Sound recordings by an on-board telemetry microphone

A custom-made telemetry microphone (Telemike) was mounted on each subject to record the timing and amplitude of sounds emitted during flight ((Hiryu *et al.*, 2008; Matsuta *et al.*, 2013; Hase *et al.*, 2016) (figure 3-3). The Telemike consisted of a 1/8-inch omnidirectional condenser microphone (Knowles, Model FG-3629, Itasca, Illinois, USA), a miniature custom-designed FM transmitter unit, a 1.5-V hearing aid battery (Sony, Type SR521SW, Tokyo, Japan) and a transmitting antenna. The total mass of the Telemike was approximately 0.6 g. The Telemike was attached to the back of the bat with a piece of double-sided adhesive tape. The microphone pointed forward and was positioned approximately 1 cm above the noseleaf of *R. ferrumequinum nippon*. The microphone was centered between the bat's pinnae. An FM antenna (RadioShack Corporation, Model 15-1859, TX, USA) suspended from the ceiling of the flight chamber received radio signals

transmitted by the Telemike. The received signals were digitized with a high-speed data acquisition card (Model NI PXIe-6358, 16-bit, f_s = 500 kHz; National Instruments, Tokyo, Japan) with a control signal that triggered and synchronized the frames of the video cameras so that the data were synchronously stored as files on the hard disk of a personal computer.

Telemike

Figure 3-3 A custom-made telemetry microphone (Telemike) mounted on the *R. ferrumequinum nippon*. The microphone pointed forward and was positioned approximately 1 cm above the noseleaf on *R. ferrumequinum nippon*.

3.2.4 Sound recordings from the microphone array

The recording procedure for the microphone array was the same as that used previously by Matsuta *et al*. (Matsuta *et al.*, 2013). To measure the horizontal beam width and direction of the pulse emitted by bats during flight, a 20-channel microphone array was set up on the walls surrounding the chamber on a horizontal (X–Y) plane, 1.2 m above the floor (figure 3-2B). Microphones were placed 0.8 m apart along the X-axis and 0.5 m apart along the Y-axis. The electrical design of the microphone array circuit board was the same as that used in the study cited above. We used 1/8-inch omnidirectional (± 3 dB, from 0° to 90°) condenser microphones (Knowles, Model FG-3629, Itasca, Illinois, USA) for the array. Urethane acoustic absorption material (20 cm × 20 cm) was attached to the rear of each microphone to reduce unexpected echoes from the walls and ceiling of the chamber. The data recording system for microphone array signals was independent of the telemetry microphone recording system. All signals recorded by the microphone array system were

digitized using a high-speed data acquisition card (Model NI PXIe-6358, 16-bit, f_s = 500 kHz; National Instruments, Tokyo, Japan). The digitized signals were stored as files on the hard disk of a personal computer using a custom program in LABVIEW (NI, Model NI LABVIEW 8.0, Tokyo, Japan) beginning with the control signal that triggered and synchronized the video recording. Microphone array data were thus synchronized with flight coordinates and the sound recordings made by the Telemike.

3.2.5 Sound analysis

Telemike recordings

Custom MATLAB routines were used to extract individual pulses from a spectrogram of Telemike recordings. The second harmonic component of pulses was analyzed for *R. ferrumequinum nippon* to determine the time at which the bats emitted pulses. The inter-pulse interval (IPI) was defined as the interval between the onsets of successive calls. The energy maximum in the spectrogram of each component was measured to quantify changes in the sound pressure levels of pulses emitted during flight. These values are represented as solid lines with lengths proportional to the pulse pressure level that indicate the pulse direction along the flight path.

Microphone array recording

The times at which emitted pulses arrived at each microphone of the array were estimated from the bat's 3D position and the time of pulse emission. This allowed us to use custom MATLAB routines to extract recorded pulses from the individual channels of the microphone array. The maximum energy of the second harmonic component of the pulse was measured from the spectrograms extracted from individual channels in the microphone array. In the case of *R. ferrumequinum nippon*, the energy maximum appears at the CF_2 components of the pulses. However, the CF_2 components were long in duration and overlapped with echoes from the surrounding walls in the microphone array recordings, making it inappropriate to quantify their sound pressure level. Therefore, a frequency 2 kHz below CF_2, which appeared within the terminal FM component of the second harmonic

(tFM$_2$), was designated as the peak frequency for *R. ferrumequinum nippon* and used to quantify changes in the sound pressure levels of pulses emitted by this species. The intra-individual variations in peak frequency were 1–2 kHz. Such small variations in frequency are unlikely to affect the measurement of beam width.

The sound pressure levels of the pulses were then corrected for the propagation loss of sound in the air between the bat and each microphone and the sensitivity differences among the microphones in the array. Sound absorption was calculated from measured absorption coefficients, which were determined for the average frequencies at the peak energy in the tFM$_2$ component of *R. ferrumequinum nippon* (2.4 dB/m at 65 kHz). The sensitivity of the microphone array elements was measured by presenting tone bursts at 65 kHz to each microphone of the array (a 3-ms burst at 65 kHz; sound pressure level of 107 dB at 1 m from the loudspeaker) using an ultrasonic loudspeaker (PT-R7 III, Pioneer Corporation, Kanagawa, Japan), allowing recorded sounds to be calibrated according to sensitivity differences among the microphones.

For emitted sound, the corrected sound pressure levels of each microphone within the array were converted into vectors (red arrows, figure 3-4) and the pattern of pulse directivity was fitted with a Gaussian shape using the corrected sound pressure vectors across all microphones for each pulse (red dashed line). The peak direction of the Gaussian fitted directivity pattern was defined as the pulse direction (blue arrow, figure 3-4). The beam width was defined as the portion of the pulse directivity pattern between −6 dB (half-amplitude) off-axis angles from the pulse direction (green double-headed arrow, figure 3-4). The measurement errors in the pulse direction and beam width generated by our microphone array system were previously investigated using ultrasound tone bursts from a loudspeaker (PT-R7 III, Pioneer) set in the chamber. The pulse direction and beam width were measured as the loudspeaker was moved between 0.5 and 6 m from the front wall. The measurement errors of the pulse direction and beam width were less than approximately 3° and 5° at a distance of 1 to 6 m from the chamber's front wall.

Top view

Pulse direction

Beam width

Bat
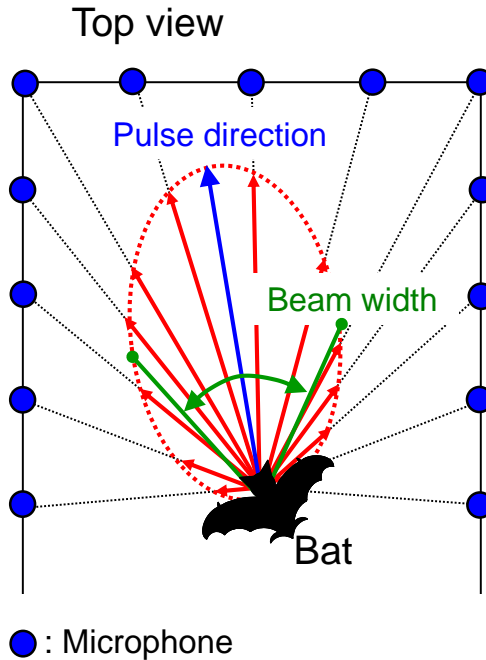
●: Microphone

Figure 3-4 Calculation procedure of the horizontal pulse direction and beam width using the microphone array. The pattern of pulse directivity (dashed red line) was fitted with a Gaussian shape using the sound pressure vectors across all microphones (red arrows). Then, the horizontal pulse direction was determined at peak direction of the pulse directivity pattern (blue arrow). The green double-sided arrow indicates the beam width of the pulse.

The call parameters investigated in this study were the IPI and pulse direction emitted by bat. The IPI was measured from Telemike recordings, whereas the pulse direction was analyzed using recordings from the microphone array (as described above). In this study, we measured the pulse and flight direction to quantify how bats change their path planning and navigation behavior to become familiar with the space around them. We used a Student's t-test or an *F*-test to test for significant differences in call parameters between data sets.

3.3   Results

3.3.1 Stable path planning for long-term flight

When an experimenter released an individual bat at one end of the flight chamber, all 11 bats continued to fly in the obstacle-filled environment for a period of 100 s. Representative horizontal flight paths of three bats during long-term obstacle avoidance flights are shown in figure 3-5. The initial part of the flight path for each individual is shown in figure 3-5A and a later part is shown in figure 3-5B. The distribution of the horizontal flight path probability during long-term flight is shown in figure 3-5C. The figures show that bats flew randomly with various path patterns at the beginning of flight whereas from several seconds to several tens of seconds, bats repeated their flight along a stable path. In particular, the geometrical pattern of the stable flight path of all 10 bats tended to encircle all seven obstacle chains or the three rightmost obstacle chains in layout 1 (figure 3-5A and B). Interestingly, when the bats began flying again after landing by experimenter releasing the bats to turn in the opposite direction, the bats rapidly adopted the same stable path before landing. In the case of tight obstacles in the environment, the bat followed a stable path that traced out a figure-of-eight (figure 3-5C). The result of two-dimensional cross correlation analysis of the convergence time required for a stable path for each of the three bats is shown in figure 3-6. Bat A rapidly adopted a stable path within 3 s of flight whereas bats B and C took 20 s.

The findings suggest that bats employ stable path planning for long-term flight in any environment to become familiar with the space around them. In this chapter, the flight time of 20 s was assumed to separate pre- and post-accustomed phases; i.e., all bats followed a stable path within 20 s at this chamber scale.
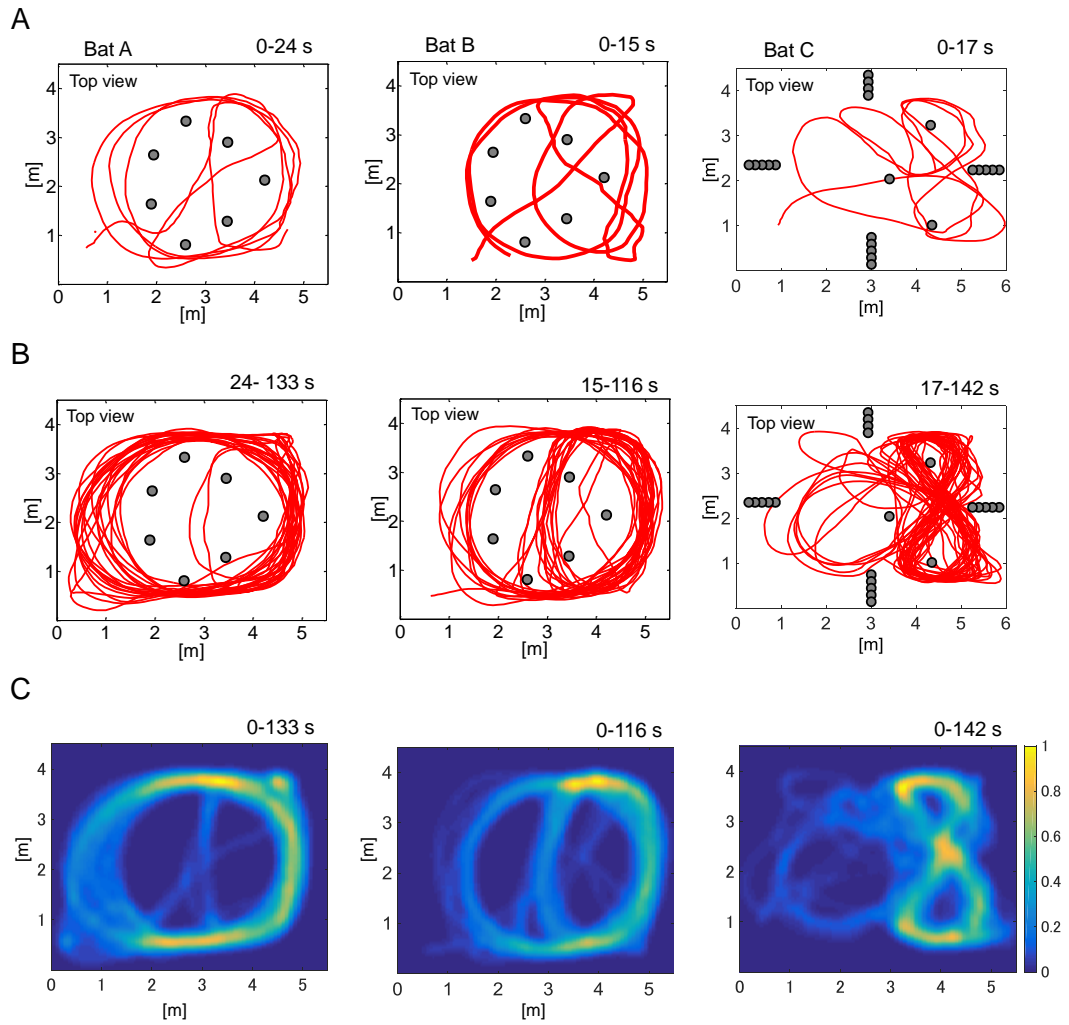
Figure 3-5 Flight control behavior of *R. ferrumequinum nippon* during long term successive flight. Top views of initial (A) and after part (B) of flight paths in each bats . (C) Distribution of horizontal flight path probability during long term successive flight.
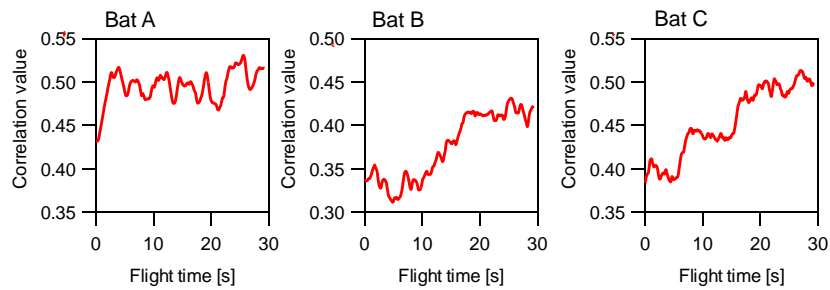
Figure 3-6 Cross correlation analysis for convergence time to be stable path in each three bats. Cross correlation was conducted by total flight path and apart of the flight path (time window is constant at 10 s).

3.3.2 Temporal shift of the pulse emission

Figure 3-7 shows changes in the pulse repetition rate for the three bats within the first 30 s of flight. The pulse repetition rate is the number of emission pulses per second. The figure shows that the pulse repetition rates of all three bats decreased to approximately 50% of the initial rates over the 30 s. The bats thus reduced the pulse emissions synchronized to obtain a stable flight path. This section investigates how bats shift the timing of pulse emissions to reduce the number of emission pulses focusing on the IPI and the number of multiple-pulse emissions.
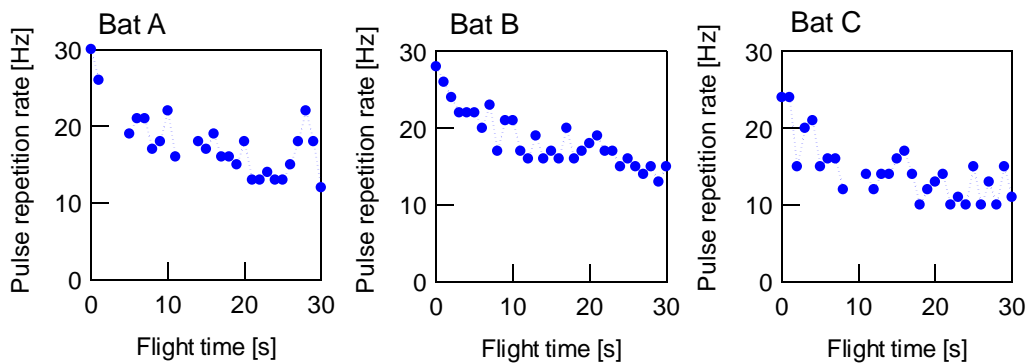
Figure 3-7 Changes in pulse repetition rate as a function of a time during long term flight of each three bats. All bats reduce the pulse emissions approximately 50% as time proceeds until 30s.

Figure 3-8 shows changes in the IPI for bats A and B during obstacle avoidance flight in the case of layout 1. The IPI analysis compared pre-accustomed (C, E) and post-accustomed (D, F) phases, which are the phases before and after 20 s of flight, respectively, as previously mentioned. The figure indicates that both bats more often repeated pulse emissions with long and short intervals than with intermediate intervals. The long interval exceeding 40 ms in the post-accustomed phase seems to be longer than that in the pre-accustomed phase whereas there was little change in the short interval between the two phases.
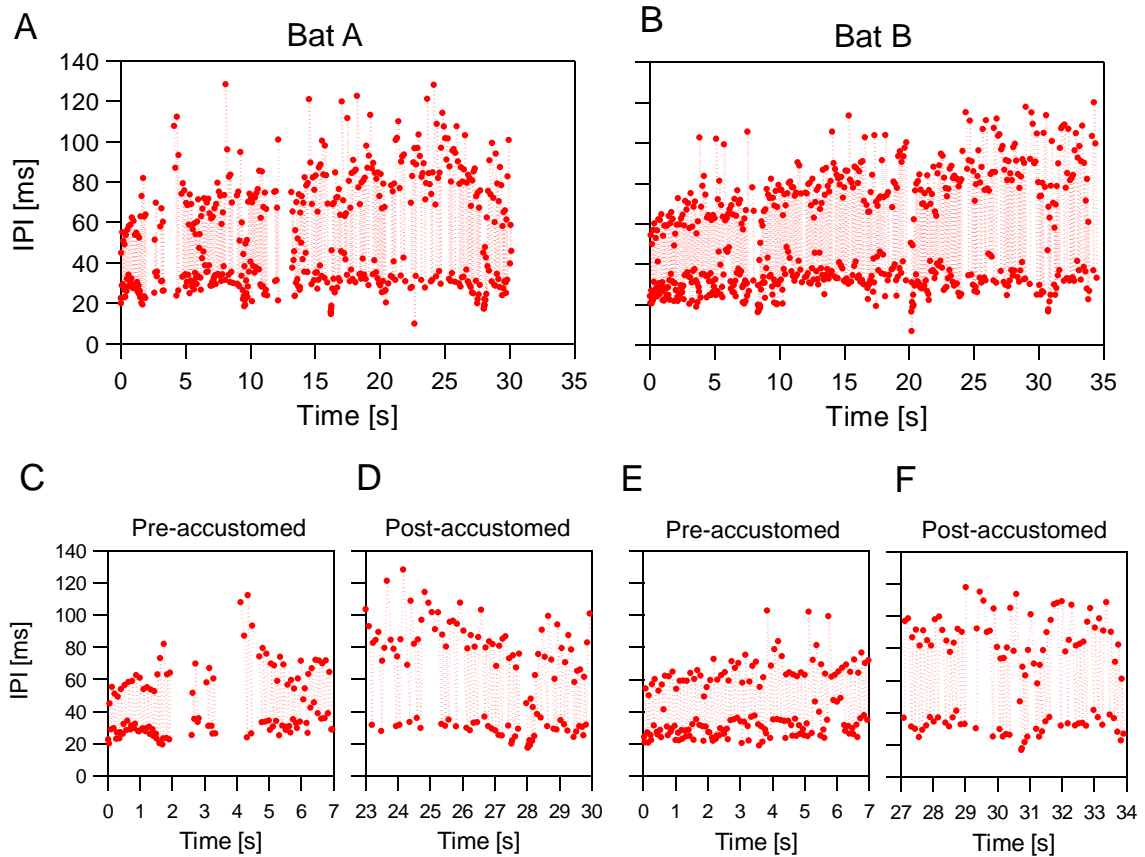
Figure 3-8 (A, B) Examples of changes in IPI during long term obstacle avoidance flight. The IPI analysis was conducted by comparing between the pre- (C, D) and post- (D, F) accustomed phase note that pre- and post-accustomed phase is defined as before and after the 20s past at the beginning of the flight, respectively. long interval pulse over the 40ms in post-accustomed phase seems to be prolonging compared to that in pre-accustomed phase whereas short interval pulse was few changing.

Figure 3-9A shows histograms of the IPI for all 10 bats taken from pre- and post-accustomed phases. The IPI (mean ± standard deviation) was 43 ± 21 ms (n = 1468) for the pre-accustomed phase and 65 ± 31 ms (n = 1054) for the post-accustomed phase. Both histograms of IPIs have two distinct peaks owing to the prevalence of multiple-pulse emission where the minimum value between the two distinct peaks is defined as the boundary separating the longer and shorter IPIs in each phase; the shorter IPI was 27 ± 5.8 ms (<45 ms, n = 887) and the longer IPI was 66 ± 13.2 ms (>45 ms, n = 581) in the pre-accustomed phase whereas the shorter IPI was 31 ± 5.7 ms (<55 ms, n = 427) and the longer IPI was 88 ± 14.9 ms (>55 ms, n = 627) in the post-accustomed phase. In both pre-

and post-accustomed phases, the peak around the shorter IPI was significantly narrowly distributed whereas the second peak at the longer IPI had a broader distribution (pre-accustomed phase: F-test, $F_{580,886} = 5.19$, $P < 0.001$, post-accustomed phase: F-test, $F_{426,626} = 6.83$, $P < 0.001$). Moreover, both shorter and longer IPIs in the post-accustomed phase were significantly longer than those in the pre-accustomed phase (Student's t-test, $P < 0.001$). Evaluation of the effect size r obtained from the Student's t-test reveals that the longer IPI ($r = 0.60$) was significantly more prolonged than the shorter IPI ($r = 0.28$). These findings suggest that bats did not prolong the IPI for pulses overall but prolonged the longer IPI instead of the shorter IPI (Figure 3-9B).
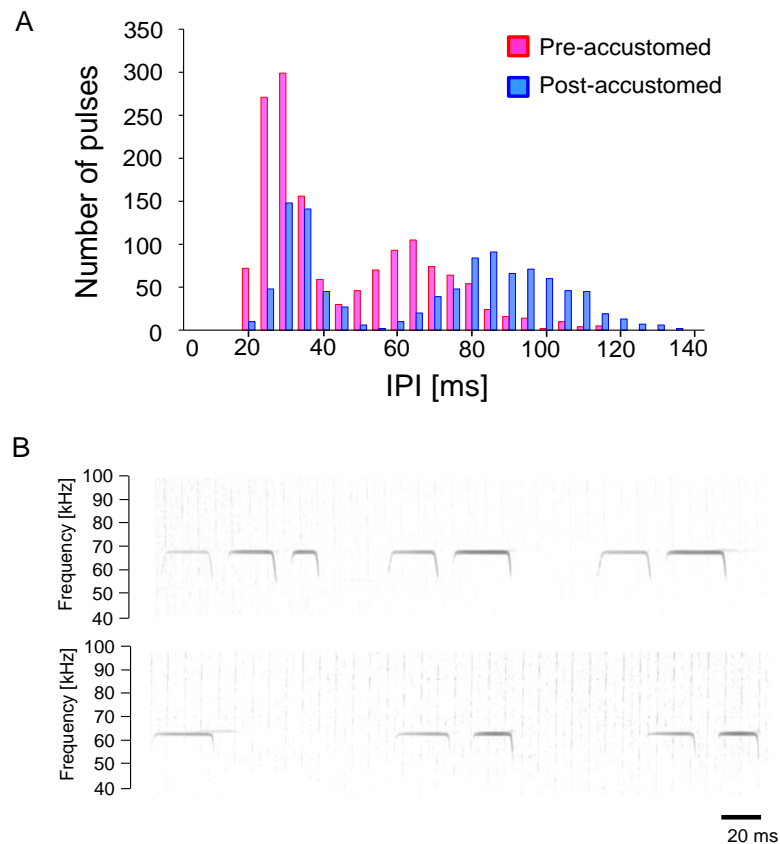
Figure 3-9 Temporal shifting of pulse emission timing during long term obstacle avoidance flight in the chamber. (A) IPI histograms of pre- and post-accustomed phase combined with all ten bats. (B) Sonograms of typical pulse emission sequences in *R. ferrumequinum nippon* during pre- (top) and post-accustomed phase (bottom).

Rhinolophus ferrumequinum nippon produce two or more pulses within a group having a stable shorter IPI. We refer to successive pulses repeated with a shorter interval as pulses in a clustered group, or a multiple pulse, and we investigated the frequency of appearance of each type of multiple pulse in pre- and post-accustomed phases. Figure 3-10 shows the numbers of triple+ (i.e., a group of three or more pulses), double and single pulses for all 10 bats in pre- and post-accustomed phases. Triple+ pulses were frequently observed in the pre-accustomed phase, occurring 256 times, whereas they were rarely observed in the post-accustomed phase, occurring only 18 times. With the reduction in the frequency of triple+ pulses, the frequency of single pulses increased fivefold from the pre-accustomed phase (45 pulses) to the post-accustomed phase (241 pulses). The frequency of double pulses slightly increased from the pre- accustomed phase (304 pulses) to the post-accustomed phase (380 pulses).

The above findings suggest that bats reduce their pulse emission rate as time proceeds by 1) increasing the silent time by prolonging the longer IPI and at the same time 2) replacing triple pulses with single or double pulses (Figure 3-10). It is noted that the bats did not replace all multiple pulses with single pulses in the post-accustomed phase; both double and single pulses were used more in the post-accustomed phase.
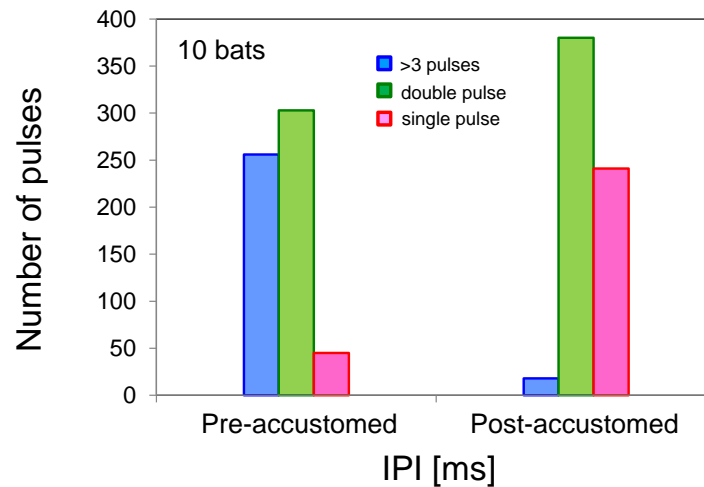
Figure 3-10 Number of over the triple (blue), double (green) and single (red) pulse emissions combined with all ten bats results in pre- and post-accustomed phase. Over the triple pulse was decreased whereas double and single pulse was increased from pre- to post-accustomed phase.

3.3.3 Pulse direction control for flight in unfamiliar and familiar spaces

The horizontal flight paths and pulse directions for bats A and B during pre- and post- accustomed phases are shown in figure 3-11A and B. The flight path, encircling all seven obstacle chains, was almost the same in each case. The pre-accustomed phase was defined to correspond to the first circle of a path and the post-accustomed phase was defined to correspond to several subsequent circles of the path. In all flights, bats emitted almost all pulses toward the inside of their turn without emitting pulses toward the closest walls on the outside of their turn. Changes in the absolute angle of the pulse direction in these flights are shown in figure 3-11C and D. The color of each plot indicates the classification of the triple+, double and single pulses. The figure shows that triple+ pulses were emitted more often than double or single pulses in the pre-accustomed phase whereas single pulses were emitted more often in the post-accustomed phase. The change from triple+ pulses to single pulses was observed in each case. Triple+ pulses were more often directed toward 0° and $\pm 180°$ in the pre-accustomed phase and replaced with both double and single pulses in the post-accustomed phase. The findings suggest that bats did not change the emission pulse type in a step-by-step manner; i.e., they did not change from a triple pulse to double pulse and then from a double pulse to a single pulse.

Figure 3-12A and B shows examples of the flight path and pulse direction of bat A in pre- and post-accustomed phases. In each example, a triple pulse was replaced with a single pulse and the emitted pulses were directed around chains 1 and 2. Changes in the absolute angle of the pulse direction and obstacle directions of chains 1 and 2 during the flights are shown in figure 3-12C and D. The figure also shows the beam width of a pulse for *R. ferrumequinum nippon*, which has been reported to be approximately $\pm 22°$ [22]. A comparison of the two phases reveals that the bats directed pulses toward the obstacles, shifting from chain 1 to chain 2, in the pre-accustomed phase whereas they directed pulses between chains 1 and 2 in the post-accustomed phase. It is considered that bats facilitated obstacle localization by emitting multiple pulses toward a certain target point in the

unfamiliar space and then adjusted the pulse direction to cover multiple obstacles within the beam width (red shaded area: figure 3-12D) for scanning with few pulse emissions after learning the obstacle-filled environment.
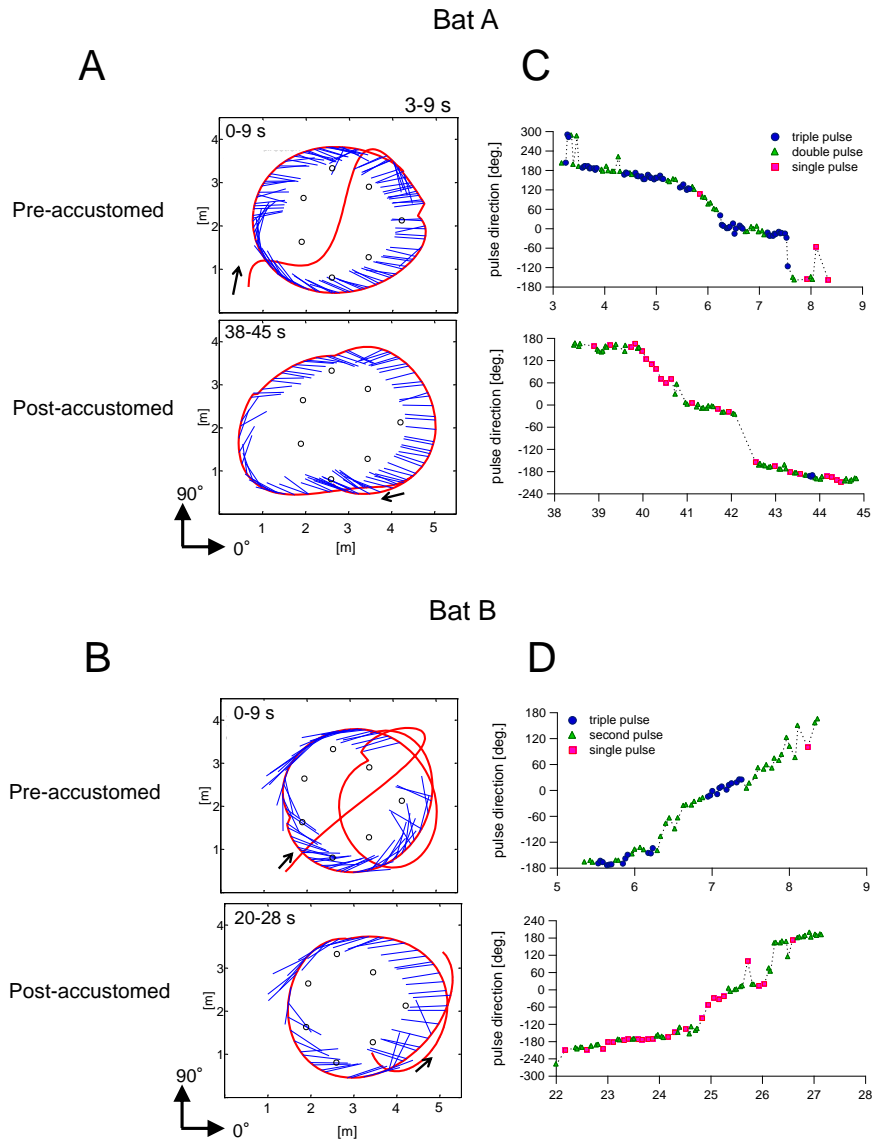
Figure 3-11 Echolocation of *R. ferrumequinum nippon* during long term obstacle avoidance flight. (A, B) Top views of flight path (red line) and pulse direction (blue line) during pre- (top) and post- (bottom) accustomed phase. (C, D) Changes in pulse direction (blue line) and flight direction (red line) as a function of flight time during each flight. It should be note that longitudinal axis was defined as 0° and anticlockwise rotation was defined as positive value. Color of each plot in these figures was indicated the classification of the triple, double and single pulses.
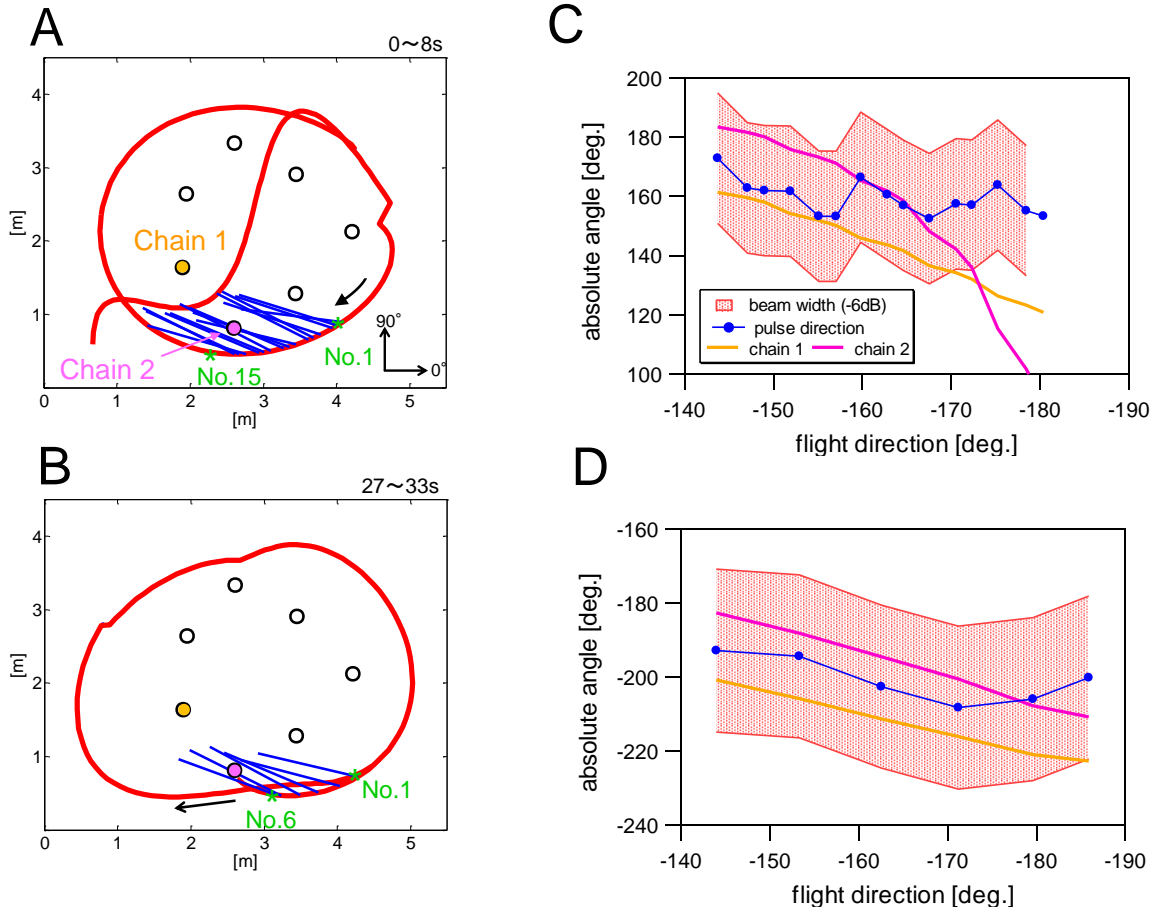
Figure 3-12 Typical part of changing the pulse direction control law replaced the triple pulse with single pulse. Top views of flight path (red line) and pulse direction (blue line) in the pre- (A) and post- accustomed phase (B). (C, D) Changes in pulse direction (blue line) and flight direction (red line) as a function of flight direction during the flights shown in (A) and (B). Yellow and magenta lines indicate the angles of chain 1 and chain 2 direction relative to the *x*-axis, respectively. The red shaded area indicates the beam width of the echolocation pulses of *R. ferrumequinum nippon* (-6 dB off-axis angle from the pulse direction, approximately ±20° in (Matsuta *et al.*, 2013)).

3.4 Discussion

Results presented in this chapter show that bats reduce their number of pulse emissions synchronized with their flight path to be stable during long-term flight through an obstacle-filled environment, suggesting that bats are capable of spatial learning and that they adapt their flight path and pulse emissions to their environment using spatial memory.

Eptesicus fuscus have also been reported to learn and then follow stable flight paths as they become familiar with a cluttered space by repeating flights across days (Barchi *et al.*, 2013). During successive flights, bats repeat the same flight path after several seconds to several tens of seconds of flight, suggesting that bats complete much spatial learning in a short time. In the present study, the stable flight path was circular or followed a figure-of-eight (figure 3-5), which matches stable flight paths observed for *Eptesicus fuscus* (Barchi *et al.*, 2013) and *R. ferrumequinum nippon* (Aihara *et al.*, 2015) during free flight through environments without obstacles. A circular or figure-of-eight flight path may therefore suit the flight motor control of bats.

Further investigation of the temporal shifting of pulse emissions revealed that bats adaptively reduce pulse emissions by 1) prolonging the longer IPI and 2) replacing the triple+ pulse with a double or single pulse.

The pulse emissions of bats are synchronized with the wingbeat cycle (SUTHERS *et al.*, 1972). Because the activity of flight muscles helps produce high airflow for the emission of intense pulses, the synchronization of the wingbeat with the respiratory cycle may reduce the cost of echolocation during flight (Speakman and Racey, 1991). Bats are well known to reduce the IPI when they approach a target object so as to frequently update spatial information during flight in various situations (Hiryu *et al.*, 2008). Our results suggest that bats not only frequently adjusted the longer IPI according to the surrounding environment but also prolonged the longer IPI to reduce pulse emissions.

The shorter IPI was slightly prolonged and the distribution in the histogram of the shorter IPI was significantly narrower than that in the histogram of the longer IPI so that bats did not change the duration of the IPI within a multiple pulse, suggesting that it was necessary to keep the emission interval as short as possible within the sonar sound group to use a multiple pulse effectively. In previous studies, *Eptesicus fuscus* produced a sonar

multiple pulse more often in complex environments or when performing complicated tasks (Moss *et al.*, 2006; Kothari *et al.*, 2014; Warnecke *et al.*, 2016). The emission of sonar sound groups has been reported for a number of bat species, which suggests that exercising temporal control over emissions helps bats negotiate complex or unfamiliar environments (Moss and Surlykke, 2010). In particular, it was suggested that the emission of double pulses allows bats to receive immediate and more detailed information of the surroundings for planning flight paths (Moss *et al.*, 2006) or for improving the resolution of the uncertain position of a target (Kothari *et al.*, 2014). In the present study, double pulses were increasingly used by bats in the post-accustomed phase despite triple+ pulses being decreasingly used, suggesting that the double pulse is a special pulse that is used not only to explore an unfamiliar space in the process of being accustomed to that space but also to negotiate a cluttered environment irrespective of whether the bat is familiar with the space.

From typical part of changing the pulse direction control law replaced the triple+ pulse with a single pulse after learning the obstacle-filled environment (figure 3-12), bats adjusted the pulse direction to cover multiple obstacles within the beam width so as to scan the obstacles with few pulse emissions. These findings suggest that the pulse direction could be adapted by spatial scanning with the beam width effectively. Further investigation of the pulse direction during flight through familiar and unfamiliar space is described in the next chapter. These spatio-temporal analyses of the long-term flight of bats suggest that the adaptation behavior of bats is optimized to be economical in conjunction with time-temporal and directional control of sonar sound.

3.5   *Summary*

Ultrasonic sonar emissions and 3D flight paths of *R. ferrumequinum nippon* during long-term obstacle avoidance flight were measured to confirm the presence of adaptation behavior. Analysis of the flight path revealed that bats repeated the same circular or figure-of-eight flight path after several seconds to several tens of seconds of flight. Simultaneously, bats reduce their pulse emissions by half over a period of 30 s by 1) prolonging the longer IPI and 2) replacing the triple+ pulse with a double or single pulse. In addition, the shorter IPI was slightly prolonged and the distribution in the histogram of the shorter IPI was

significantly narrower than that in the histogram of the longer IPI such that bats did not change the duration of the IPI within the multiple pulse, suggesting that it is necessary to keep the emission interval as short as possible within the sonar sound group to use the multiple pulse effectively. The use of the double pulse increased from the pre- to post-accustomed phase, suggesting that the double pulse is a special pulse that is used not only to explore an unfamiliar space in the process of becoming accustomed to the space but also to negotiate a cluttered environment irrespective of whether the space is familiar. The findings of this chapter suggest that bats are capable of spatial learning and that they adapt their flight path and pulse emissions to fly economically through their surrounding environment by using spatial memory.

Chapter 4. *Echolocation behavior of CF-FM bats during repeated flight through a high-clutter obstacle course*

4.1　Introduction

　　　Chapter 3 demonstrated that bats adapt their behavior, in terms of planning a stable path and reducing the number of pulse emissions, through spatial learning. This chapter investigates the echolocation behavior of bats during repeated flights through an obstacle course. An S-shaped obstacle course is produced using many more obstacle chains to restrict the avoidance path, thus requiring sensitive flight control with left and right turns. A dynamic change in the attention direction (i.e., pulse direction) is also expected for the surroundings. In addition, there is a possibility that a high-clutter environment will evoke a different acoustical navigation behavior in bats. Behavioral changes in repeated trials of flying through a highly cluttered environment will reveal the behavioral principle of the adaptation behavior of bats. Behavioral strategies employed by bats may also provide useful solutions to technical problems of recent technology trends that rely on careful sensing using multiple sensors.

4.2　Materials and Methods

4.2.1 Subjects and experimental condition

　　　Seven adult Japanese horseshoe bats (*R. ferrumequinum nippon*, body length: 6.0–8.0 cm, body mass: 20–30 g) were used in the experiments.

　　　The experiments were conducted in a flight chamber constructed from steel plates [9 m (L) × 4.5 m (W) × 2.5 m (H)] under lighting with red filters (>650 nm) to avoid visual effects on the bats. An obstacle-filled environment was constructed using plastic chains (having a diameter of 4 cm) that were suspended from the ceiling of the chamber. Figure 4-1 shows one of constructed obstacle layouts, in which chains were arranged at 15-cm

intervals along the X-axis and at 22 cm intervals along the Y-axis, so that the bat was forced to fly in an S-shaped pattern without passing between chains. Three naïve bats were used for this layout. Each bat was observed for 12 continuous repeated flights so that echolocation behaviors in unfamiliar and familiar spaces could be compared. Furthermore, we recorded echolocation behavior using another four naïve bats flying through different obstacle layouts. Each bat was observed only once (<20 s), focusing on exploratory behavior in an unfamiliar place.
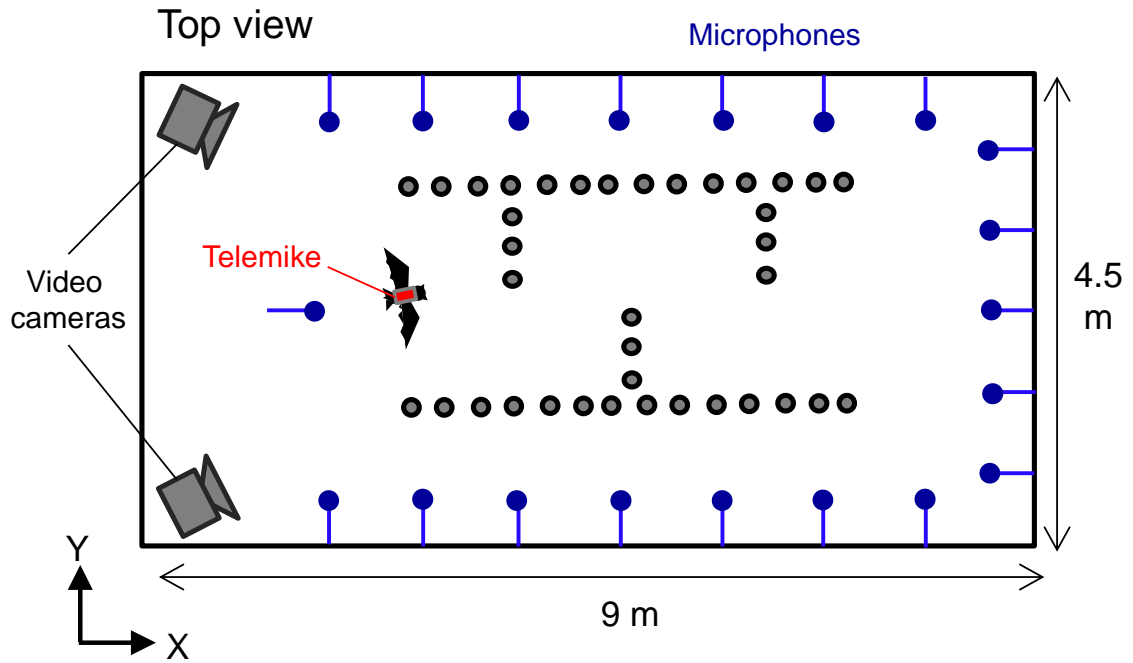
Figure 4-1 Arrangement of the obstacle course in the flight chamber. Experiment was conducted 12 times repeated flight in this obstacle course which was constructed by chains suspended from the ceiling.

4.2.2 Video and Sound recordings

The flight behavior of the bats was recorded using two digital high-speed video cameras (MotionPro X3; IDT Japan, Inc., Tokyo, Japan [125 frames per second]) located in the left and right corners of the flight chamber. The video recording procedure was the same as that used previous study (Hiryu *et al.*, 2008). Applying a direct linear transformation, the successive 3D positions of the flying bats and the locations of other

objects were reconstructed using motion analysis software (DIPPMotionPro [ver. 2.2.1.0]; Ditect Corp., Tokyo, Japan). The flight velocity vector of the bat was calculated as the time derivative of the coordinates of the flight path.

Echolocation sounds emitted by flying bats were recorded using a custom-made telemetry microphone (Telemike (Hiryu *et al.*, 2008)) that was mounted on the bat. The Telemike was attached to the back of the bat with a piece of double-sided adhesive tape, with the microphone pointed forward and positioned ~1 cm above the noseleaf of the *R. ferrumequinum nippon*, between the left and right pinnae of the bat. The received signals were digitized with a high-speed data acquisition card (Model NI PXIe-6358, 16-bit, f_s = 500 kHz; National Instruments, Tokyo, Japan) and a control signal that triggered and synchronized the frames of the video cameras so that the data were synchronously stored as files on the hard disk of a personal computer.

To measure the horizontal pulse direction and beam width of the pulse emitted by the bat during flight, a 20-channel microphone array was set up on the walls surrounding the chamber in the *xy*-plane 1.2 m above the floor. All signals recorded by the microphone array system were digitized with two high-speed data acquisition cards (Model NI PXIe-6358, 16-bit, f_s = 500 kHz; National Instruments). The digitized signals of all channels were stored as files on the hard disk of a personal computer using a custom program in LABVIEW (ver 8.0; National Instruments) with the control signal that triggered and synchronized the frames of the video cameras so that the microphone array data were synchronized with the flight coordinates and with the sound recordings made using the Telemike.

4.2.3 Sound analysis

Each pulse was extracted from a spectrogram produced from Telemike recordings using custom MATLAB (MathWorks, Natick, MA, USA) routines on a personal computer to determine the time at which the bat emitted the pulse. The energy maximum in the spectrogram of each pulse was measured to quantify changes in sound pressure levels of emitted pulses (see the lengths of blue solid lines in figure 4-5A and B). In this study, the IPI was defined as the interval between the onset of successive calls.

For microphone array recordings, the energy maximum of each terminal FM component of the second harmonic of the pulse was extracted from the spectrogram of each pulse for the individual channel recording of the microphone array. For each emitted sound, the sound pressure levels of each microphone within the array were converted into vectors (figure 3-4, red arrows) and the pattern of pulse directivity was fitted with a Gaussian shape using the sound pressure vectors across all microphones for each pulse. The horizontal pulse direction was then determined at the peak direction of the pulse directivity pattern fitted by the Gaussian shape (Ghose and Moss, 2006). The beam width was defined by −6 dB (half-amplitude) off-axis angles from the direction of the emitted pulse in the pulse directivity pattern.

We defined the directions of the X-axis and Y-axis as 0° and 90°, respectively, in the horizontal plane. The acoustic gaze was defined as the angular difference between the pulse direction and flight direction (Ghose and Moss, 2006). The sign (+/−) of the acoustic gaze is positive when the direction of the emitted pulse is counterclockwise from the flight direction and negative when the direction is clockwise. In this study, we also measured the absolute change in the acoustic gaze between successive pulses, Δgaze, to quantify how much bats shifted their acoustic gaze between emissions when scanning the space around them. A Student's t-test, two-way factorial analysis of variance (ANOVA), test of no correlation, Mann–Whitney U test and F-test were used, as appropriate, to test for significant differences in call parameters between datasets.

4.3 Results

4.3.1 Flight path and flight speed adaptation for the S-shaped obstacle course

All three bats passed through the obstacle course without collision during each of the 12 trials (giving a total number of 36 flight trials). Figure 4-2A shows the flight path data for all three bats across the 12 trials. The figure shows that the flight path changed across repeated trials. Figure 4-2B shows changes in the bulge width of the three bats as a function of the flight trial. Here, the bulge width is the separation on the Y-axis between the

maximum bulge points of left and right turns (Figure 4-2C). The figure shows that the maximum bulge width for each bat was 0.56–0.72 m in the first and second trials and that it decreased to 0.23–0.40 m in the 12th trial. These results suggest that all three bats changed their flight paths to reduce curvature as the bats repeated their flight.
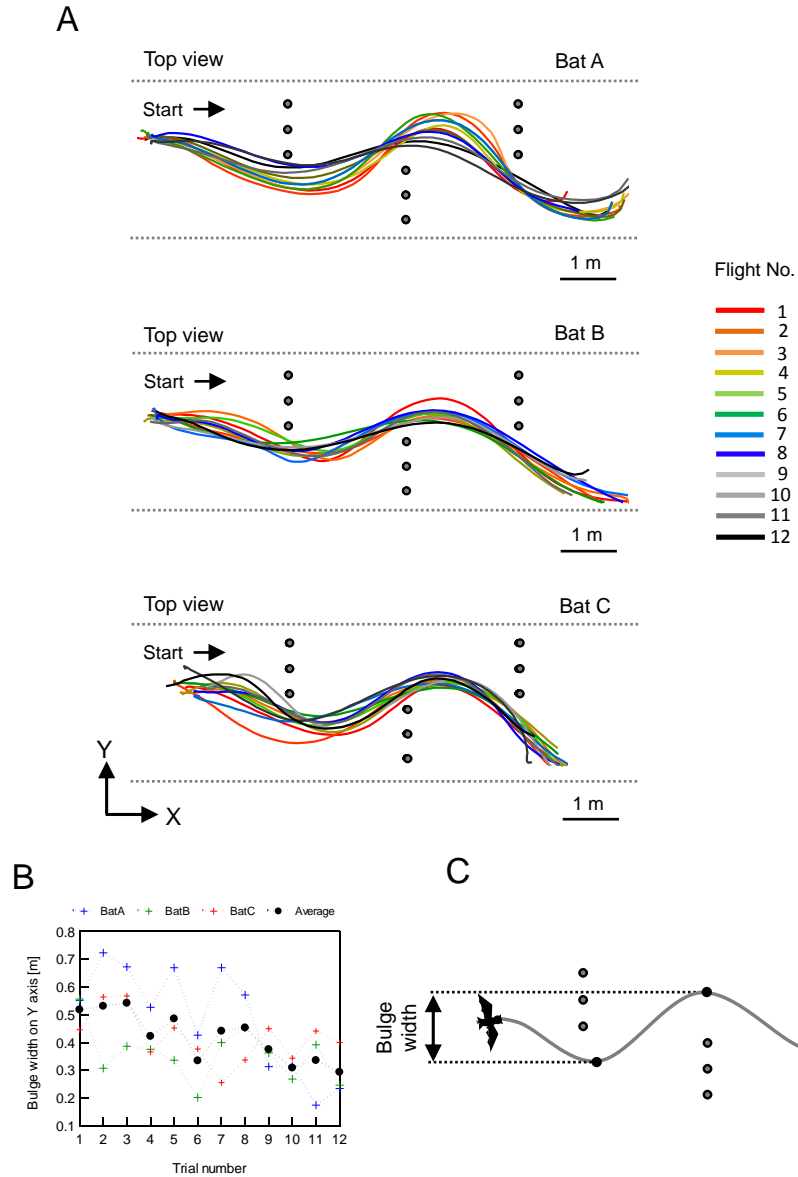
Figure 4-2 Flight control behavior of *R. ferrumequinum nippon* during repeated flight in the obstacle course. (A) Top views of flight trajectories in three bats (12 trials per the bat). (B) Changes in bulge width of the three bats as a function of flight trial. (C) Definition of the bulge width which is distance differences on Y-axis between the maximum bulge point of right and left turn.

Figure 4-3 shows changes in the flight speeds of bats A and B during obstacle-avoidance flight in the first and twelfth trials. A comparison of the first and twelfth trials of bat A or B reveals that the maximum flight speed increased slightly as the flight path curvature decreased. For all three bats, the average flight speed ranged from 2.7–3.0 m/s in the first trial to 3.2–3.8 m/s in the 12th trial. These findings suggest that bats also adapted their flight speed as they became familiar with the space around them.
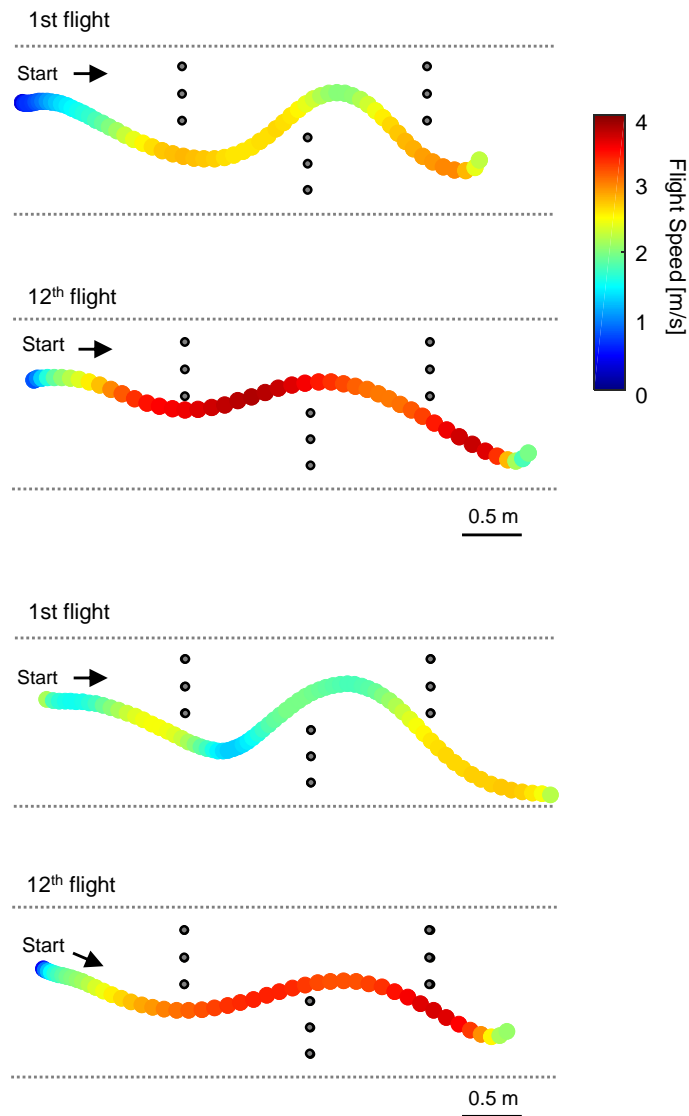
Figure 4-3 Comparisons of flight path and flight speed between the 1st and 12th trial flights of the bat. Color of each plot on flight path indicates the flight speed in place.

4.3.2 Temporal shifting of pulse emissions

Figure 4-4A shows IPI histograms for the first three trials (first, second and third trials) and last three trials (10th, 11th and 12th trials) combined for all three bats. The shorter IPI and longer IPI are defined as in chapter 3. The shorter IPI was 25 ± 6.0 ms (<42 ms, n = 488) and the longer IPI was 59 ± 9.1 ms (>42 ms, n = 178) in the first three trials whereas the shorter IPI was 26 ± 5.2 ms (<39 ms, n = 171) and the longer IPI was 59 ± 10.6 ms (>39 ms, n = 158) in the last three trials. Statistical analysis reveals that the shorter IPI in the last three trials was significantly longer than that in the first three trials (Student's t-test, $P < 0.001$) but it could be regarded as few because the effect size ($r = 0.15$) was smaller than the result for long-term flight in chapter 3 ($r = 0.28$). Moreover, there was no difference in the longer IPI between the first three and final three trials (Student's t-test, $P = 0.35$) despite the longer IPI vastly increasing from the pre- to post-accustomed phase in long-term flight. These results suggest that 1) bats do not always prolong the longer IPI when becoming familiar with the space around them and 2) control of the longer IPI is also affected by the complexity of the obstacle-filled environment.

Figure 4-4B shows changes in the number of pulse emissions of the three bats as a function of the flight trial. We found that the bats reduced the number of pulse emissions by 45% (66/148 pulses) from the first to the last of the 12 flight trials. The average rate of single pulses through all successive trials for the three bats was only 1% (14/1,302 pulses), whereas the rates of double and triple+ pulses were 38% (490/1,302 pulses) and 61% (798/1,302 pulses), respectively (figure 4-4B). This indicates that the bats depended primarily on sensing with multiple-pulse emissions (double or triple+ pulses, 99%) when exploring the obstacle-laden environment. Furthermore, the emission of triple+ pulses decreased significantly with increasing trial number (two-way factorial ANOVA, $F_{11,797} = 2.35$, $P < 0.05$) whereas the emission of double pulses did not change with repeated trials (two-way factorial ANOVA, $F_{11,490} = 1.48$, $P = 0.21$), suggesting that sensing with double pulses is necessary for echolocation in both unfamiliar and familiar spaces.

A
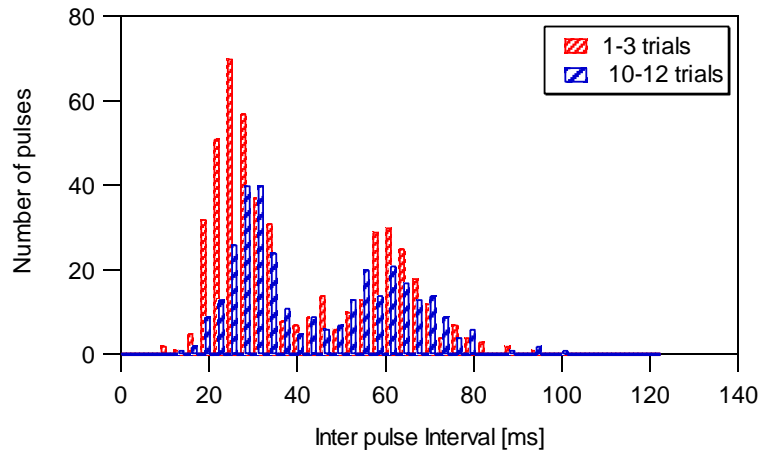
B
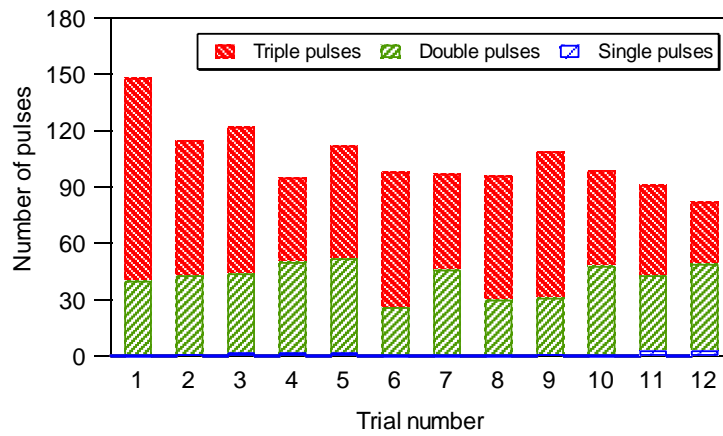
Figure 4-4 Temporal shifting of pulse emission timing by repeated flight of bats. (A) IPI histograms of initial three (1st, 2nd and 3rd trials) and terminal three trials (10th, 11th and 12th trials) combined with all three bats. (B) Changes in the number of pulse emissions as a function of trial number. Data were taken from three bats. Every pulse was classified into three types: single (blue), double (green), or triple pulses (red).

4.3.3 Pulse direction control for flight in unfamiliar and familiar space

Figure 4-5 shows the behavioral comparison of pulse direction control during echolocation between flight through unfamiliar and familiar spaces. The bats shifted the pulse direction dynamically relative to their flight direction in the first flight (figure 4-5A) whereas they shifted the pulse direction smoothly and directly towards the intended flight direction in the 12th flight trial (figure 4-5B). Figure 4-5C and D shows changes in pulse and flight directions as a function of flight time, respectively. In figure 4-5C, some emissions were aimed directly around each edge of the three obstacle chain arrays (marked as chains 1–3 in figure 4-5A) during the first flight, accompanying a dynamic shift in the pulse direction between successive pulses of as much as 90° (e.g., see the pulses around 1.0 s in figure 4-5C). These edges were supposed to be important markers to allow the bats to plan an avoidance path. In contrast, after a bat learned the map of the obstacle-laden environment, it shifted the pulse direction smoothly and adjusted the pulse direction to precede the intended flight direction, covering the edges of the chain obstacle array within the beam width (blue shaded area) (figure 4-5D). Moreover, the bats in the 12th flight increased the emitted pulses by +4.6 dB on average (from 4.3 to 4.9 dB for the three bats) compared with the pulses emitted during the first flight, suggesting that the bats emitted pulses that were more intense when they became familiar with the space around them. These findings demonstrate that the pulse direction and flight path controls of bats differ between flights in unfamiliar spaces and flights in familiar spaces, suggesting that the bats could learn their obstacle-filled environment by echolocation and adapt their acoustic gaze control for their own flight path planning.
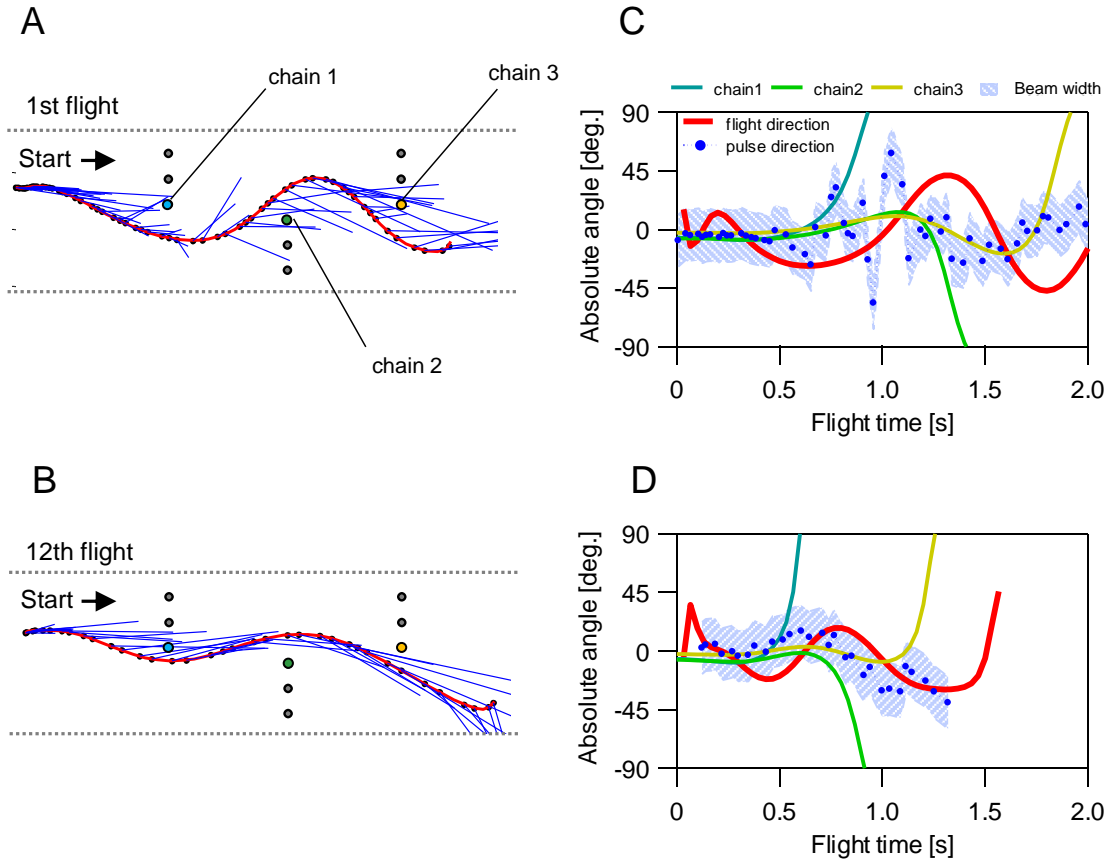
Figure 4-5 Echolocation of *R. ferrumequinum nippon* during the obstacle avoidance flight in the chamber. (A, B) Top views of flight path (red line) and pulse direction (blue line) during the 1st and 12th flights in the obstacle course. (C, D) Changes in pulse direction (blue line) and flight direction (red line) as a function of flight time during the flights shown in (A) and (C). Azure-blue, green, and yellow lines indicate the angles of chain 1, chain 2, and chain 3 direction relative to the x-axis, respectively. The light-blue shaded area indicates the beam width of the echolocation pulses of R. ferrumequinum nippon (-6 dB off-axis angle from the pulse direction, approximately ±20° in [34]).

4.3.4 Relationship between the acoustic gaze and turn rate

In further investigation, we analyzed the relationship between the turn rate of the bat's flight (i.e., angular velocity of the flight turn, $\varphi_d(t)$) and the acoustic gaze (i.e., the angle between pulse and flight directions, φ_{gaze}). Figure 4-6A shows the changes in the turn rate and acoustic gaze for the first and twelfth flights shown in figure 4-5. The figure reveals that the change in turn rate was basically synchronized with the change in the

39

acoustic gaze but with a time delay, which suggests that the change in the acoustic gaze preceded the change in the turn rate. Such a control law of the gaze and turn rate has also been reported for the chasing behavior of bats (Ghose and Moss, 2006). In the previous study, the relationship between the acoustic gaze and turn rate can be described by the simple equation

$$\varphi_d(t) = k\varphi_{gaze}(t + \tau) \qquad\qquad (4\text{-}1)$$

where τ is the delay time and k is the proportionality coefficient. Cross-correlation analysis of the turn rate and the acoustic gaze in each flight reveals that the time delay τ ranged from 0.1 to 0.3 s for all bats and that two of the three bats tended to reduce the time delay τ in repeated flights. Figure 4-6B shows a scatter plot of the turn rate versus acoustic gaze in the first flight and twelfth flight combining flight data of all three bats. The time delay τ is corrected in the figure. The figure indicates that the acoustic gaze had significant linear correlation with the turn rate with $k = 4.2$ (test of no correlation, R = 0.59, $P < 0.01$) in the first flight and with $k = 5.7$ (test of no correlation, R = 0.52, $P < 0.01$) in the 12th flight. Moreover, the proportionality coefficient k in the first flight was significantly higher than that in the 12th flight. These results suggest that the synchronized control of the acoustic gaze and turn rate is a basic strategy that bats adopt to avoid obstacles and that bats adapt their flight path planning to unfamiliar and familiar spatial environments by tuning the synchronization of the acoustic gaze and turn rate.

Figure 4-6A and B shows the distribution of the acoustic gaze φ_{gaze} during the first and twelfth flights for the combined data of all three bats. The acoustic gaze distribution was 7.9 ± 24.2° (mean ± standard deviation) in the first flight and 0.6 ± 12.7° in the 12th flight. The acoustic gaze distribution in the first flight was therefore significantly wider than that in the 12th flight (F-test, $F_{71, 99} = 3.63$, $P < 0.001$). Furthermore, the absolute change in acoustic gaze φ_{gaze} (Δgaze) between successive pulses was calculated. Figure 4-6C and D shows the distribution of Δgaze during the first and twelfth flights. Δgaze in the first flight was significantly different from that in the 12th flight (Mann–Whitney U test, $P < 0.001$), suggesting that bats widely and frequently shifted their acoustic gaze during flight in an unfamiliar space.

1st flight

12th flight

A

B
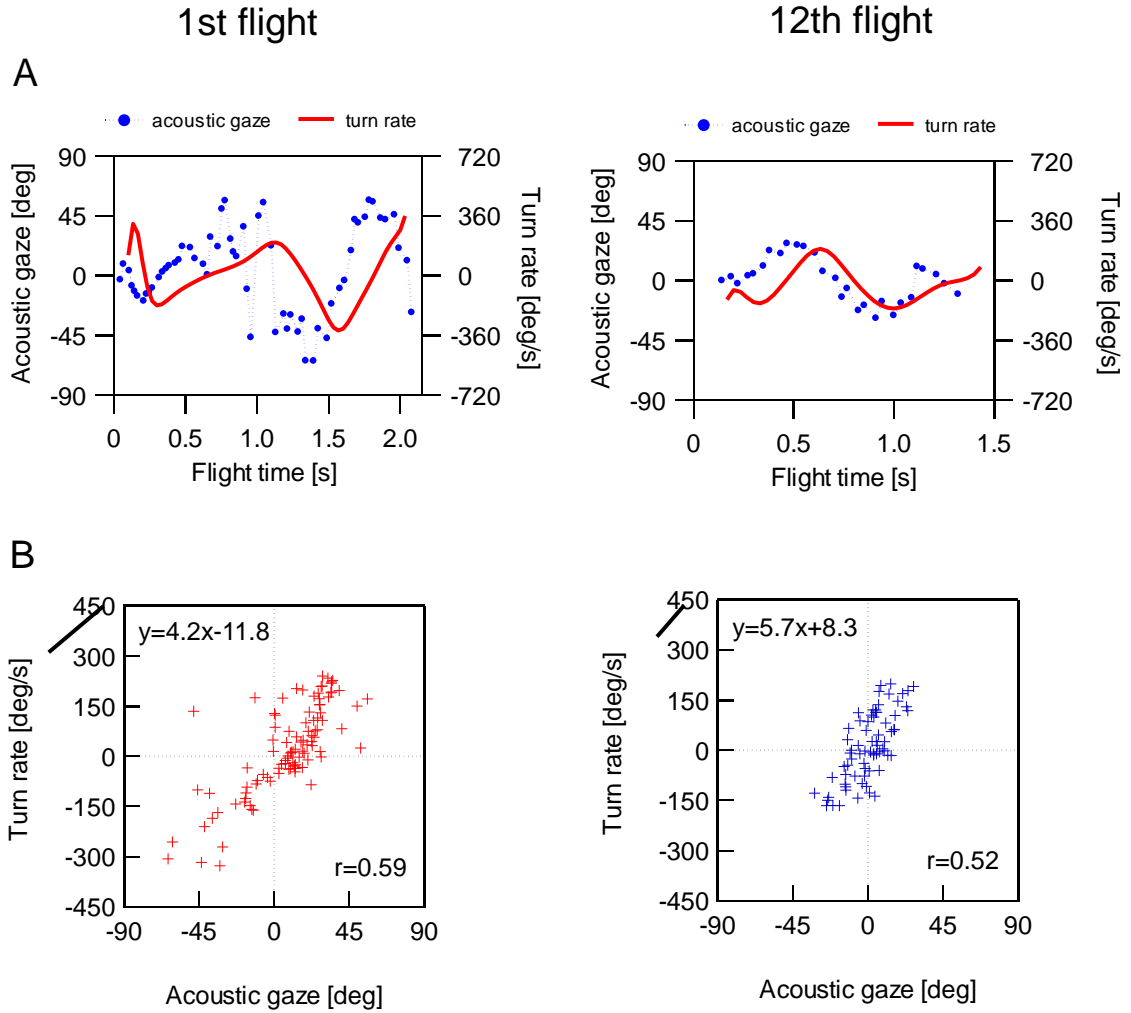
Figure 4-6 Acoustic gaze control synchronized with turn rate during flight in 1st and 12th trial. (A) Changes in turn rate and acoustic gaze as a function of time. (B) Scatter plot of turn rate and gaze angle at τ combined with all three bats for 1st (left) and 12th (right) trial. The regression line is shown in black.
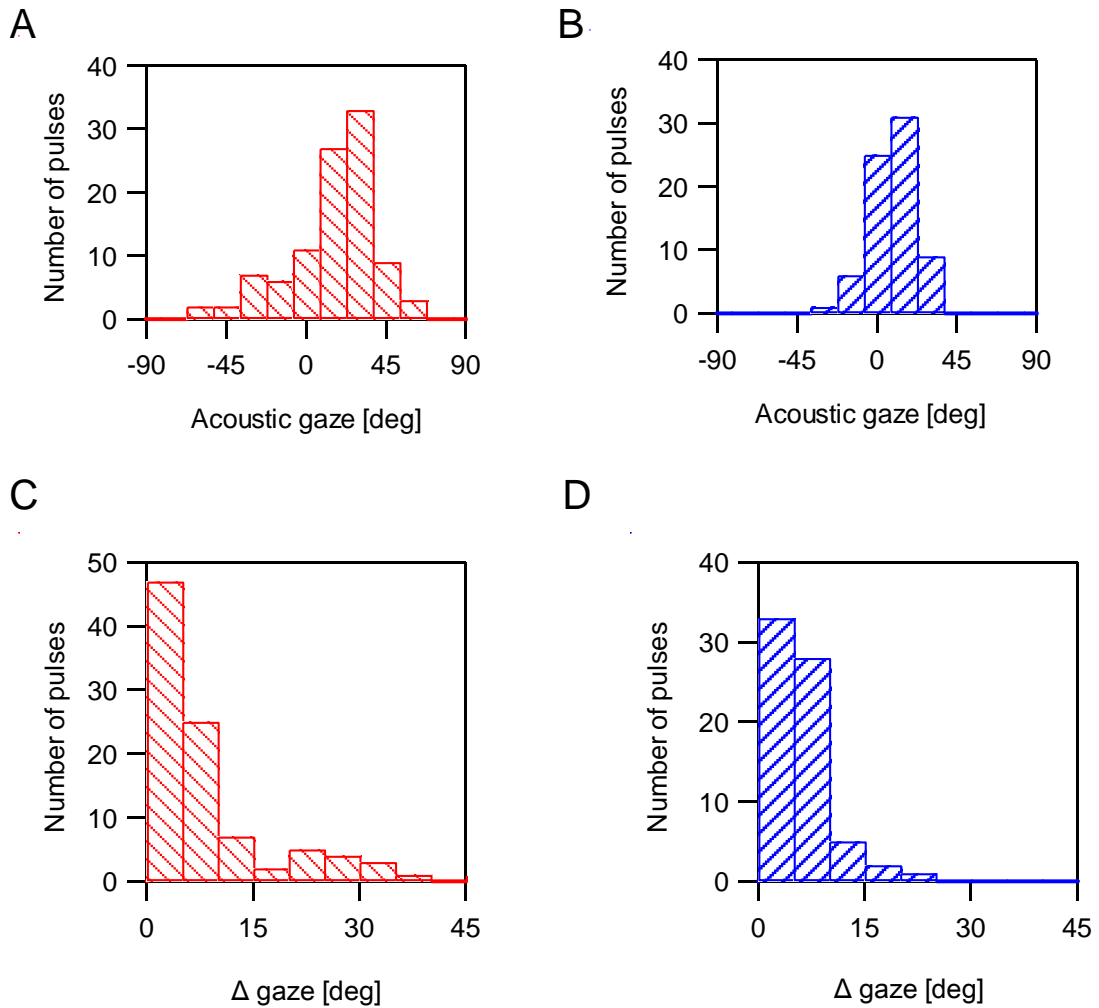
Figure 4-7 Comparison of acoustic gaze control of *R. ferrumequinum nippon* between the 1st and 12th trial. (A, B) Distributions of acoustic gaze combined with all three bats during flight in 1st and 12th trial. (C, D) Distributions of the amount of absolute change in acoustic gaze between successive pulses (Δgaze) during flight in 1st and 12th trial.

4.3.5 Frequently shifting the acoustic gaze during flight through an unknown space

Figure 4-7 shows other representative flights of four naïve bats with different obstacle arrangements. These animals were different from those used in the previous behavioral experiments, allowing the use of echolocation during the exploration of an unfamiliar setting to be investigated. All cases were picked up from only the beginning of

the first flight so as to obtain the echolocation behavior in an unfamiliar space. Double and triple pulses were the most sensing pulses used, and for some of the double pulses, one pulse in the pair was aimed directly towards a nearby obstacle among obstacles distributed around the bat while the other pulse in the pair was directed toward the bats' future flight path. Double-pulse scanning, in which the direction of the pulse emission alternatively shifted between the intended flight path and the nearby obstacle, appears to be a principal behavior of the bats during flight in an unfamiliar space.
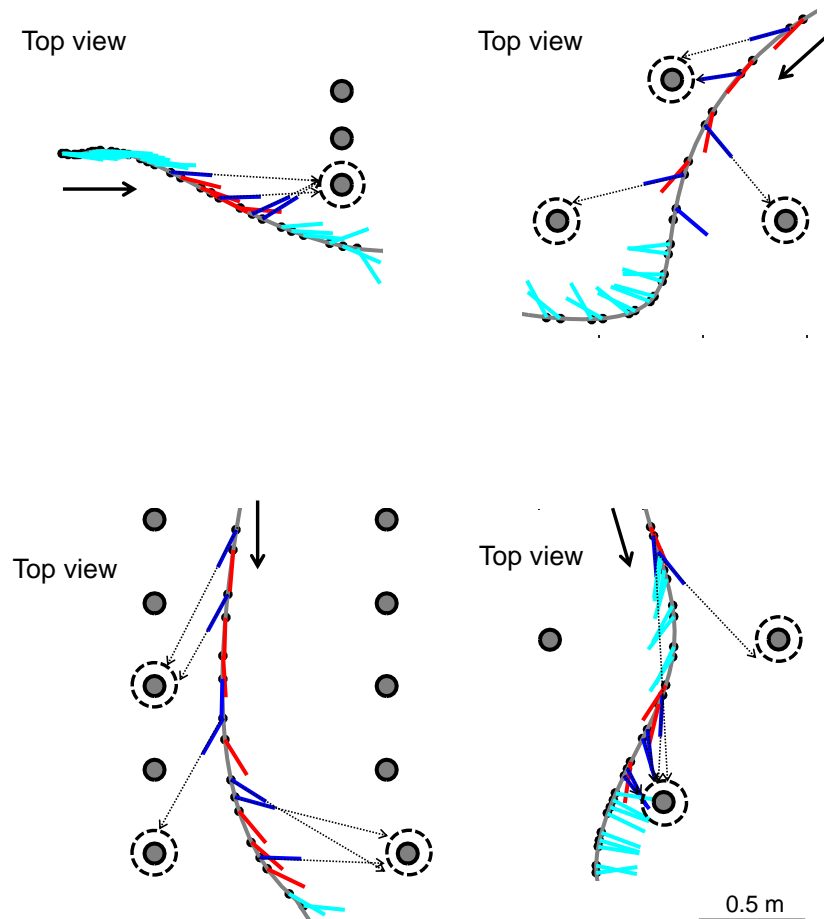
Figure 4-8 Examples of pulse direction control by the bats during flight in the various obstacle environments. The four obstacle layouts all differed from each other. Gray circles indicate obstacle chains suspended vertically from the ceiling to the floor. Red and blue lines indicate that the pulses were alternately emitted towards their own flight direction (red) and the obstacle direction (blue). Since the emission pulse was a broad beam, we could consider that bats aimed at the target obstacle if the pulse direction was directed towards the dashed-line circles.

4.4 Discussion

This chapter confirmed that bats adapt their flight path and pulse emission timing by spatial learning even in a highly cluttered environment. While flying through an S-shaped obstacle course, bats changed their flight path to reduce the curvature of the flight turn while increasing their flight speed after learning the obstacle-filled environment. These findings suggest that the adaptation strategy of bats is to reduce the energy cost of flight control by planning a shorter flight path that can be followed at a comfortable speed. The temporal shift of the pulse emissions reveals that bats did not prolong the longer IPI after learning the obstacle-filled environment despite prolonging the longer IPI during long-term flight through a low-density arrangement of obstacles. These behavioral changes indicate that the timing control of the long-interval pulse was strongly affected by the cluttered environment. Analysis of the appearance frequency of multiple pulses reveals that the average rate of single pulses in all successive trials for the three bats was only 1%, showing that double and triple pulses were needed to negotiate a more cluttered environment with or without spatial memory. The emission of triple pulses reduced significantly with the increasing trial number, suggesting that bats preferentially used the strategy of reducing the number of multiple pulses over the strategy of prolonging the pulse interval to reduce the number of pulse emissions in a cluttered environment.

Eptesicus fuscus relies on surrounding acoustic landmarks to guide its spatial orientation by echolocation when flying in a complex environment (Hiryu *et al.*, 2008). Moreover, *E. fuscus* has been reported to learn and then adopt stable flight paths as it becomes familiar with a cluttered space (Barchi *et al.*, 2013). In the present study, the measurement of the acoustic gaze allowed us to read spatial and temporal changes in the bat's attention so that we could investigate the decision-making process with respect to spatial perception. As a result, we experimentally demonstrated that *R. ferrumequinum nippon* makes adaptive behavioral changes when it becomes familiar with the space; i.e., the pulse direction was observed to shift smoothly relative to the flight direction whereas, during flight in unfamiliar space, the pulse direction (acoustic gaze) alternately shifted between surrounding immediate obstacles and the intended flight direction in a time-sharing manner.

Behavior regarding spatial perception has been studied extensively in visually guided animals by measuring eye movement (in the case of humans) or the heading angle (in the case of flies and birds) (Land and Collett, 1974; Land and Lee, 1994; Eckmeier *et al.*, 2008). For example, human drivers have been shown to control the steering wheel of a vehicle by aiming their eye gaze towards the inside pitch of a circuit course, so that the steering angle is synchronized with the eye gaze angle according to a certain time delay when driving a circuit course (Land and Lee, 1994). The results obtained in this chapter reveal that obstacle-avoiding bats basically control the angular velocity of their flight turn (turn rate) synchronized with the acoustic gaze according to a certain time delay (figure 4-6). These findings suggest that gaze control synchronized with a moving turn is a basic strategy widely used in navigation by both visually and acoustically guided animals. A previous study also reported that such a relationship between the acoustic gaze and turn rate could be described as equation (4-1). An investigation of the control law governing the acoustic gaze and flight turn according to equation (4-1) reveals that the proportionality coefficient *k* is different for flight in familiar and unfamiliar spaces. These findings suggest that bats may adapt their flight path planning to unfamiliar and familiar spatial environments by changing the synchronization of their acoustic gaze and turn rate.

As early as 1978, the engineer Edmund Donges used a driving simulator to demonstrate that there are basically two types of signal available to drivers: feedback and feedforward signals (Donges, 1978). The feedback signal is obtained from near-road information (i.e., information at lateral and angular deviations from the road center line) and allows drivers to control their lane position gradually (Land and Horwood, 1995). The feedforward signal comprises anticipatory signals that come from information in more distant regions of the road (i.e., far-road information) and allows drivers to match their driving path to the curvature of the road (Donges, 1978). Furthermore, Mourant and Rockwell (1970) reported that drivers first controlled their lane position using foveal vision and then increasingly learned to use their peripheral vision to obtain information from more distant road regions as they became familiar with the route (Mourant and Rockwell, 1970). This suggests that the steering control changes sequentially from feedback-dominant to feedforward-dominant control as drivers learn a route. Interestingly, bats during flight in an unfamiliar space were found to switch between feedback and feedforward control of their

acoustic gaze by the emission of double pulses. This hybrid scanning in which bats shift the pulse direction alternately between certain immediate obstacles and the future direction of their own movement is a good solution to the problem of the trade-off between feedback and feedforward control. When the bats became familiar with the space around them, they were observed to emphasize feedforward-dominant sensing (i.e., emitting intense pulses aimed at the goal of the obstacle course (figure 4-5)), which is thought to confirm the obstacle arrangement as far as possible in exchange for a decrease in pulse emission.

The findings suggest that bats adapt their acoustic gaze control synchronized with path planning and pulse emission timing in an obstacle-filled environment as they become familiar with the environment.

4.5 Summary

This chapter presented the adaptation strategy of bats, mainly focusing on the directional control of sonar emissions during repeated flights through a highly cluttered S-shaped obstacle course. The bats adapted their flight path to reduce the curvature of their flight path while increasing speed in repeated trials. The number of pulse emissions decreased but the longer IPI did not increase, indicating that the timing control of the long-interval pulse was strongly affected by the cluttered environment. In addition, the emission of triple+ pulses decreased significantly with increasing trial number, suggesting that bats preferentially used the strategy of reducing the number of multiple pulses over the strategy of prolonging the pulse interval to reduce pulse emissions in a cluttered environment. In further investigation of acoustic gaze control, bats showed an adaptive behavioral change as they became familiar with the space around them; i.e., the pulse direction was observed to shift smoothly relative to the flight direction whereas in the flight through unfamiliar space, the pulse direction (acoustic gaze) alternately shifted between surrounding immediate obstacles and the bats' own intended flight direction in a time-sharing manner. These findings suggest that bats adapt their acoustic gaze control synchronized with path planning and pulse emission timing as they become familiar with an obstacle-filled environment.

Chapter 5. *Mathematical modelling of obstacle avoidance navigation*

5.1 Introduction

The behavioral investigation of bats in chapters 3 and 4 indicated that bats memorize an obstacle-filled environment and adapt their flight path planning and sensing strategy as they become familiar with the space around them. To demonstrate the avoidance navigation using an autonomous vehicle embedded with the behavioral principles of bats, this chapter constructs a mathematical model named the multi-obstacle avoidance (MOA) model for obstacle avoidance navigation. The constructed model is based on ultrasound sensing using one transmitter and two receivers. Avoidance movement in this model is tested in a numerical simulation conducted using the S-shaped obstacle course that we used in chapter 4. In the simulation, the moving speed, IPI and beam width were fitted to values for actual echolocating bats so that the obstacle avoidance model is appropriate for the bat navigation scale.

In the actual flight of bats, the change in angular velocity of a flight turn (turn rate) is basically synchronized to the change in the acoustic gaze (pulse direction relative to flight direction) with a time delay so that the pulse direction is controlled toward the future fight direction. The relationship between the acoustic gaze and turn rate has a linear correlation with the time delay, with the correlation coefficient being different for bats flying through unfamiliar and familiar spaces (see section 4.3.4). The second half of this chapter constructs a synchronized control model for the acoustic gaze and turn rate on the basis of the original MOA model. We then investigate the coefficient of correlation of the acoustic gaze and turn rate effect on the flight path pattern using the new model.

These numerical simulation analyses demonstrate that the MOA model is a useful platform that can be used to reflect the navigation algorithm inspired by bats

5.2 *Mathematical modelling of obstacle avoidance navigation*

5.2.1 Multi Obstacle Avoidance model

This chapter presents our method of determining the direction of movement after sensing that is based on ultrasound sensing using one transmitter and two receivers. The simulated movement was determined using multiple-obstacle information obtained from one pulse emission (using the MOA model). The basic idea is schematically presented in figure 5-1. A brief explanation is that the timing of the ith pulse emission is denoted t_i and the direction of movement $\varphi_d(t_i)$ at the ith pulse emission is calculated using information of all detected obstacles, with the information being the obstacle distance $r(t_i, n)$ (i.e., the distance from the simulated bat to the obstacle n) and the obstacle direction $\theta(t_i, n)$ (i.e., the angle from the axis of the bat to the direction of obstacle n). The obstacle detection range is assumed as the inside of the maximum detection angle as viewing angle VA within the maximum detection distance d_{max}. (The obstacle detection method for actual ultrasound sensing is detailed in chapter 7.) The new direction of movement is determined according to the weighted sum of the vector of the current direction of movement and imaginary repulsive force vectors generated by the recognized obstacles. We set the repulsive force generated by obstacle n by integrating the imaginary pressure $g(r(t_i, n))$ with respect to the viewing angle θ from $\theta(t_i, n) - w(r(t_i, n))$ to $\theta(t_i, n) + w(r(t_i, n))$. The new direction of movement $\varphi_d(t_{i+1})$ is thus described by

$$\varphi_d(t_{i+1}) = \arg(e^{i\varphi_d(t_i)} - \sum_{n=1}^{N(t_i)} \int_{\theta(t_i,n)-W(r(t_i,n))}^{\theta(t_i,n)+W(r(t_i,n))} g(r(t_i,n)) e^{i\theta} d\theta) \qquad (5\text{-}1)$$

where $N(t_i)$ is the number of recognized objects at $t = t_i$. The positions of the recognized objects are calculated with the echolocation system. The distance factor $g(r(t_i, n))$ and the obstacle window factor $W(r(t_i, n))$ are given by
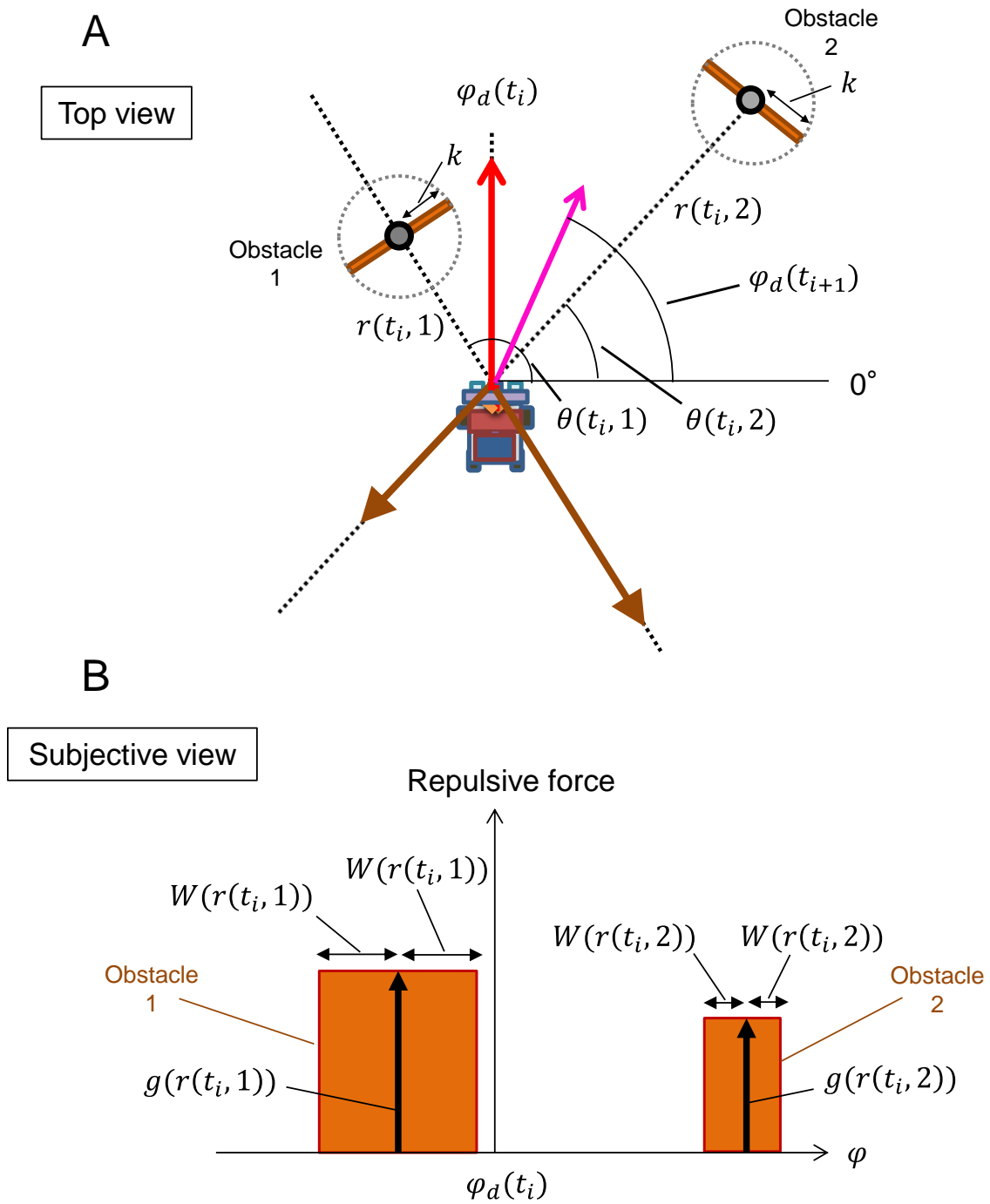
Figure 5-1 Schematics of top (A) and subjective (B) views of the bats and obstacles. The direction $\varphi_d(t_{i+1})$ of the vehicle motion is determined by the repulsive forces generated by the objects and the present direction of movement $\varphi_d(t_i)$.

$$g(r(t_i,n)) = \sqrt{\frac{\alpha}{r(t_i,n)}} \tag{5-2}$$

$$W(r(t_i,n)) = \arctan(\frac{k}{r(t_i,n)}) \tag{5-3}$$

where α and k are parameters with length dimensions. Here, k is the size of the imaginary objects (figure 5-1). Our model allows the imaginary objects to overlap. By substituting equations (5-2) and (5-3) into equation (5-1), we get the simple equation

$$\varphi_d(t_{i+1}) = \arg(e^{i\varphi_d(t_i)} - \sum_{n=1}^{N(t_i)} \sqrt{\frac{\alpha}{r(t_i,n)}} \sin(\arctan\frac{k}{r(t_i,n)})e^{i\theta(t_i,n)}) \tag{5-4}$$

An example path of motion obtained using the MOA model is shown in figure 5-2A. The detection distance and viewing angle were set at 1.4 m and $\pm30°$ respectively. In this case, the simulated bats detected two poles for each of the first three pulse emissions. The subjective view of these three pulse emissions (figure 5-2B) shows that an imaginary repulsive force becomes stronger and more widely distributed as a bat approaches an obstacle. By assuming the imaginary width of an individual obstacle according to the distance r_n, the MOA model calculates the imaginary repulsion force, which corresponds to the concept of a monoscopic depth cue of visual sensing; i.e., the relative change in the perceived object size decrease with distance. It is thus considered that the direction of movement is determined by adding reconstructed imaginary two-dimensional images of surrounding objects that are derived from one-dimensional sound information. If detected objects are classified according to the acoustic characteristics of returning echoes, the strength of repulsion felt by the simulated bat can be adjusted depending on information derived from each obstacle. A mathematical simulation was conducted using this model.
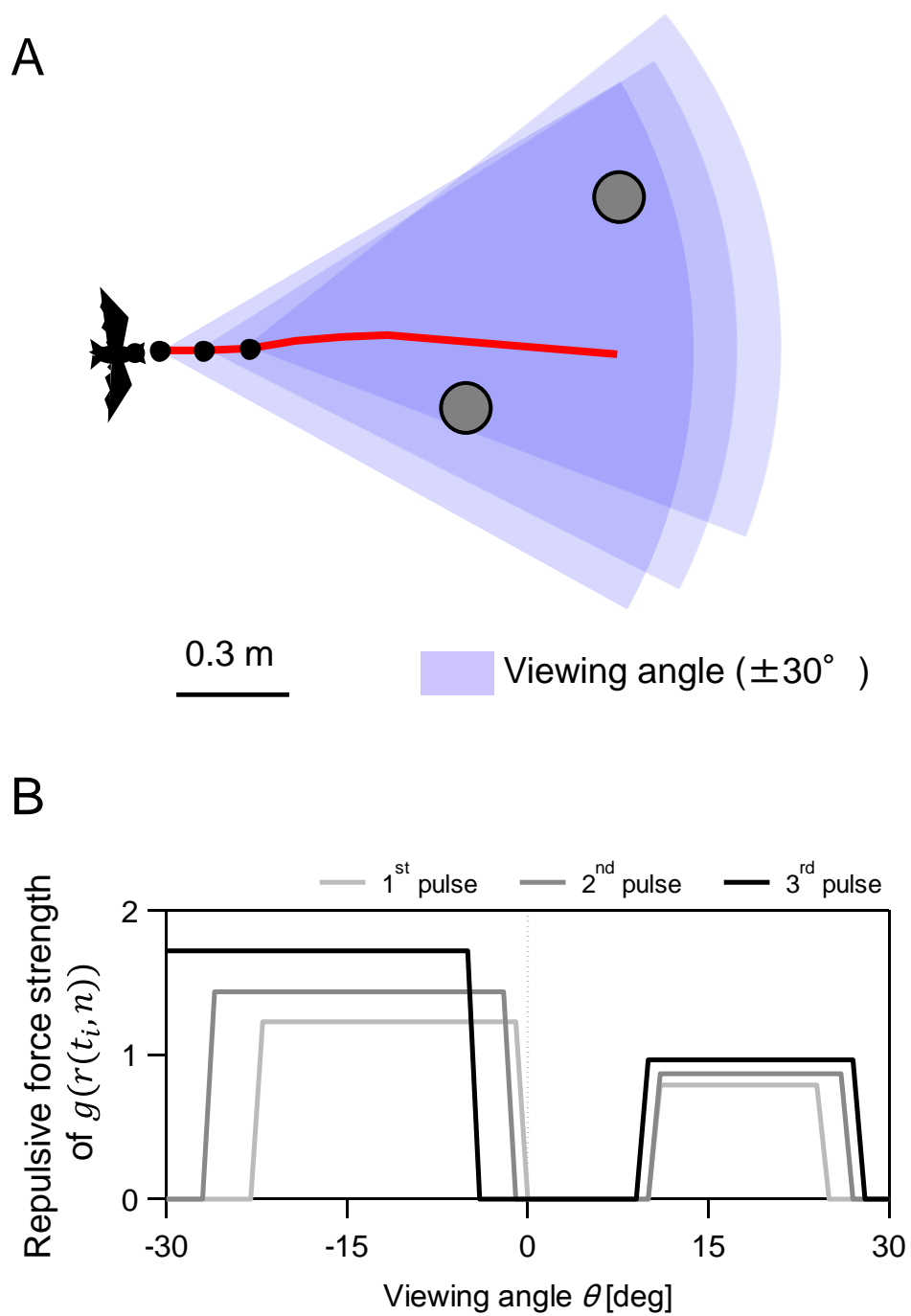
Figure 5-2 Example of obstacle avoidance movement by mathematical simulation of MOA model. (A) Horizontal moving path (red line) and sensing rage (blue shaded area) simulated by MOA model during obstacle avoidance movement (α =0.75m, k = 0.15m). (B) Subjective view from the bats to obstacles during initial three pulse emissions.

5.2.2 Simulation settings

The obstacle-filled environment and starting positions were set as for the bat measurement in Chapter 4 by inputting the coordinates of obstacle chains and bat flights into a personal computer. The speed of motion was set at a constant 3 m/s to match the average flight speed of the bats. After each sensing, the simulated bat changes the moving direction to avoid the obstacles calculated by MOA model. The pulse direction was fixed to the present direction of movement. The maximum detection distance was determined to be 1.4 m according to the sensing capacity of the actual vehicle (see chapter 6). The length parameter for an obstacle width k was set at 0.15 m so as to prevent the course out through the distance slit between each obstacle (0.3 m) formed a road pitch. A collision was defined as a simulated bat coming within 0.15 m of an obstacle.

This section investigates how the avoidance path simulated by the MOA model is affected by the IPI and viewing angle. Moreover, we demonstrate that the simulated bat can fly through the obstacle course without collision using actual values of the IPI and viewing angle of bats. The acoustic viewing angle of actual bats is unknown. However, a previous study reported that the beam width for *R. ferrumequinum nippon* was ±22° during free flight in a chamber (Yamada *et al.*, 2016). The acoustic viewing angle was therefore assumed as the beam width of bats. The IPI was set as 38 ms, which was the average IPI of bats measured.

5.2.3 Simulation result

Figure 5-3 shows examples of the path of motion and pulse direction simulated by the MOA model for three values of α. All simulated paths were categorized into three patterns: the bat flying through the obstacle course without collision, the bat colliding with an obstacle and the bat remaining outside the obstacle course. The three patterns are referred to as a success, miss and no count, respectively, and they were used to evaluate the probability of successful avoidance. A successful flight was specifically defined as the bat travelling a path length of 10 m and reaching the goal area without collision.
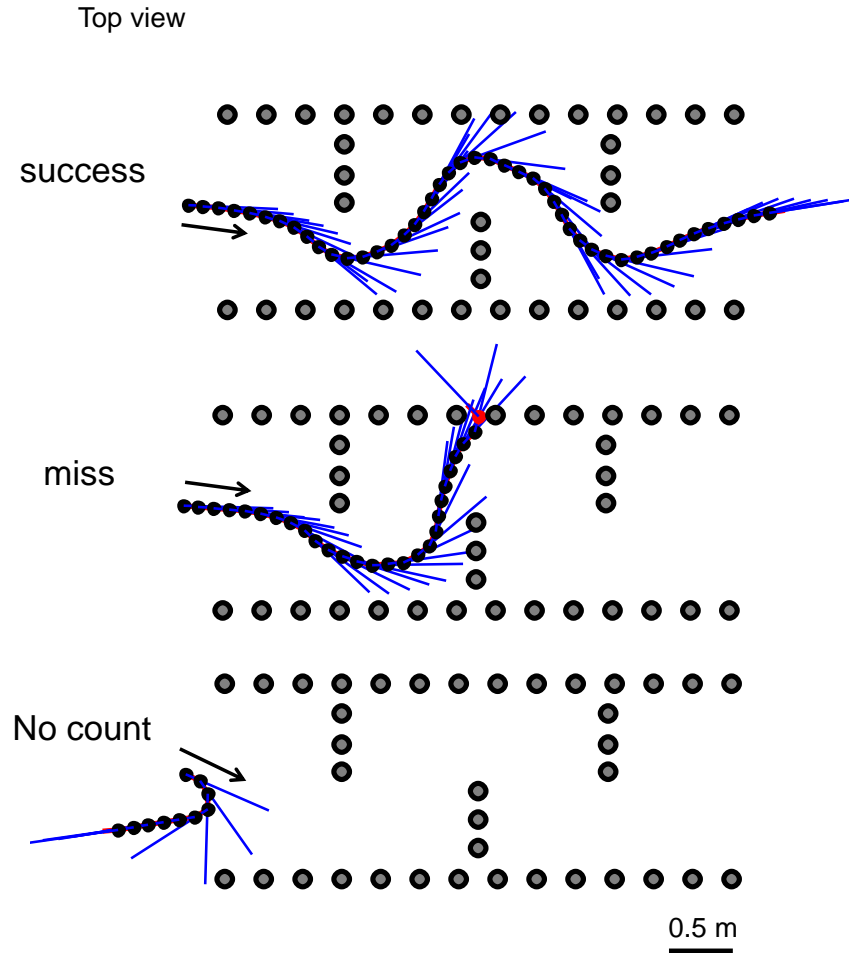
Figure 5-3 Examples of the path of motion and pulse direction simulated by the MOA model for three values of α (IPI of 0.4 s, viewing angle of 90°). All simulated paths were categorized into three patterns: successful navigation of the obstacle course, collision with an obstacle and remaining outside the obstacle course.

Figure 5-4A shows the probability map of the successful avoidance of obstacles as a function of the viewing angle and IPI. The probability of success for each viewing angle and IPI was calculated for 100 values of α ranging from 0.01 to 1 m in steps of 0.01 m. All 100 simulated paths were then categorized as successes, misses and no counts, and the success probability was finally calculated as the number of successes divided by the summation of the numbers of successes and misses. We therefore evaluated the avoidance difficulty for each viewing angle and IPI using the latitude of parameter α as an evaluation index. The figure shows that the probability of success decreased as the viewing angle

became narrower or the IPI became longer. Interestingly, the success probability map reveals that the bats' flight parameters (average IPI of 0.38 s, beam width of 22°) were almost suited for the threshold parameter that makes the success probability decline to less than 10% precipitously. Figure 5-4B shows an example of the path of motion and pulse direction obtained using the actual flight parameters of bats. It is seen that the simulated bats could fly through the obstacle course without collision. These results demonstrate that the MOA model reproduces the avoidance performance of bats when using the actual sensing and flight speed parameters of bats.

A

B

Top view

0.5 m
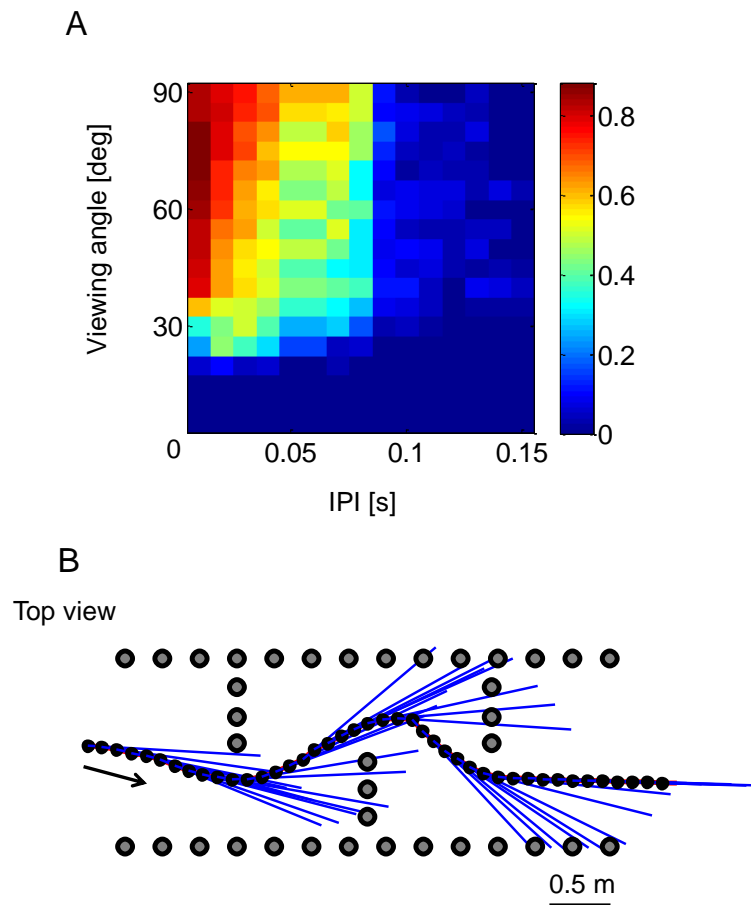
Figure 5-4 Evaluation of the MOA model during obstacle avoidance movement through the S-shaped obstacle course. (A) Probability map of successful avoidance as a function of the viewing angle and IPI. The color of each pixel indicates the success probability for a combination of the IPI and viewing angle. The calculation step for the IPI is 0.01 s and that of the viewing angle is 5°. (B) Horizontal path of motion and pulse direction simulated for the actual bat condition (IPI of 0.4 s, viewing angle of 30°, $\alpha = 0.75$ m).

5.3 Mathematical simulation of the synchronized control of the acoustic gaze and angular velocity of a flight turn

5.3.1 Pulse and flight direction control of the extended MOA model

In the actual flight of bats, the flight direction followed the pulse direction with a time delay. To reconstruct a similar behavior of pulse and flight direction control, the MOA model was modified such that the avoidance calculation responds to the control of pulse direction according to

$$\varphi_p(t_{i+1}) = \arg(e^{i\varphi_p(t_i)} - \sum_{n=1}^{N(t_i)} \sqrt{\frac{\alpha}{r(t_i,n)}} \sin(\arctan\frac{k}{r(t_i,n)})e^{i\theta(t_i,n)}) \qquad (5\text{-}5)$$

The direction of movement was calculated using another control law to follow the pulse direction. A previous study reported a control law for the pulse and flight direction of bats such that relationship between the acoustic gaze φ_{gaze} (pulse direction relative to the direction of movement) and turn rate $\dot{\varphi}_d$ (angular velocity of the turn) have linear correlation with a time delay (Ghose and Moss, 2006):

$$\dot{\varphi}_d(t) = k\varphi_{gaze}(t+\tau) \qquad (4\text{-}1)$$

where τ is the delay time and k is the proportionality coefficient. The proportionality coefficient of k for actual bats was significantly different between flight in unfamiliar space and flight in familiar space (Figure 4-6) whereas the delay time τ also changes but it has no trend between each space flight. To evaluate the effect of the correlation coefficient on the flight path pattern without a delay time τ effect, we use a simple equation based on the tangent function:

$$\dot{\varphi}_d(t_i) = \gamma\tan(\varphi_{gaze}(t_i)) \qquad (5\text{-}6)$$

where $-90° < \varphi_{gaze}(t_i) < 90°$ and γ is a parameter. Using this equation, simulated bats was turned in the same direction as the acoustic gaze direction and the angular velocity of the

turn movement $\dot{\varphi}_d$ (turn rate) was controlled by angular differences between the pulse and direction of movement; i.e., acoustic gaze φ_{gaze}. The parameter γ was the main factor determining the strength of the effect of the acoustic gaze φ_{gaze} on the turn rate $\dot{\varphi}_d$, and it is a factor similar to the proportionality coefficient k (figure 5-5). Six values of γ were used in this study to investigate the effect of the control law for the acoustic gaze and turn rate on the flight path. The linear gradient near the origin was 4.4 at $\gamma = 250$ and 5.9 at $\gamma = 340$, and these values were almost the same as the proportionality coefficient k of data for flight through an unfamiliar space ($k = 4.2$) and data for flight through a familiar space ($k = 5.7$).
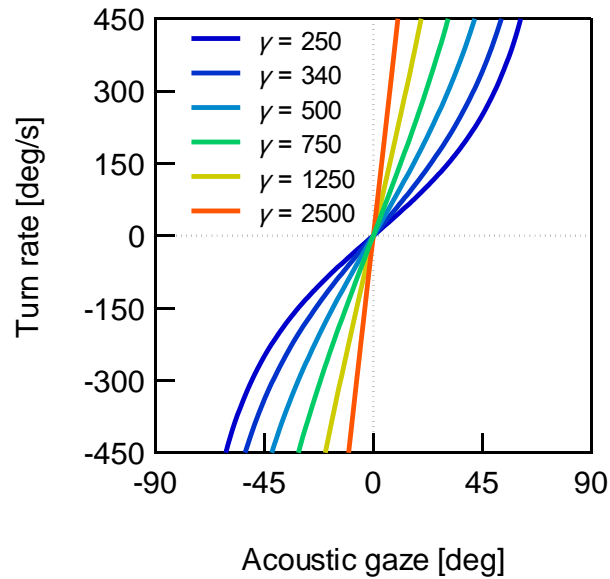
Figure 5-5 Control law between the acoustic gaze and turn rate for simulating the actual bats acoustic gaze control behavior. Six parameters of γ were used in this study to investigate the control law effect on the flight path.

In the case of equation (5-6), the turn rate $\dot{\varphi}_d$ was updated after every pulse emission because the acoustic gaze φ_{gaze} was calculated after every pulse emission. To calculate the turn rate $\dot{\varphi}_d$ in a time step shorter than the IPI, the calculation of the turn rate $\dot{\varphi}_d$ was modified as

$$\dot{\varphi}_d(t + \Delta t) = \gamma \tan(\varphi_p(t_i) - \varphi_d(t)) \tag{5-7}$$

where $t_i < t + \Delta t \leq t_{i+1}$ and Δt denotes the time step for the calculation of the turn that was sufficiently shorter than the IPI. The direction of movement φ_d was thus calculated as

$$\varphi_d(t + \Delta t) = \varphi_d(t) + \Delta t \dot{\varphi}_d(t + \Delta t) \tag{5-8}$$

Obstacle-avoidance navigation through the S-shaped obstacle course was conducted using equations (5-5), (5-7) and (5-8).

5.3.2 Simulation results

Figure 5-6A shows an example of the simulated path and pulse direction during free movement in a closed chamber without obstacles (where α and γ are 1.5 and 250, respectively). It is noted that the beam width was set at $\pm 90°$ because the echoes reflected from the walls were stronger than echoes reflected from the obstacle chains in actual sensing. Figure 5-6B shows the changes in the moving and pulse directions as a function of time in this simulation. It is seen that the simulated pulse was not directed toward the closest wall but to the inside of the turn. The flight direction follows the pulse direction with a time delay. The simulated bats thus followed a circular path according to the reflection of signals from the closed chamber walls. These trends were also observed for the actual flight of bats during free flight in a chamber of the same scale (figure 5-6C and D). We therefore confirm that the constructed model approximately described the synchronized control of the pulse and fight directions with a time delay that was observed for actual sensing by bats.

Using the constructed model, a simulation was conducted in an S-shaped obstacle-filled environment for the average flight speed and IPI of bats. The obstacle detection distance was 1.4 m. The beam width was set at $\pm 90°$ so that the situation of obstacle avoidance was assumed to be flight through a familiar space. Six values of γ were used to investigate how the flight path is affected by the correlation coefficient.
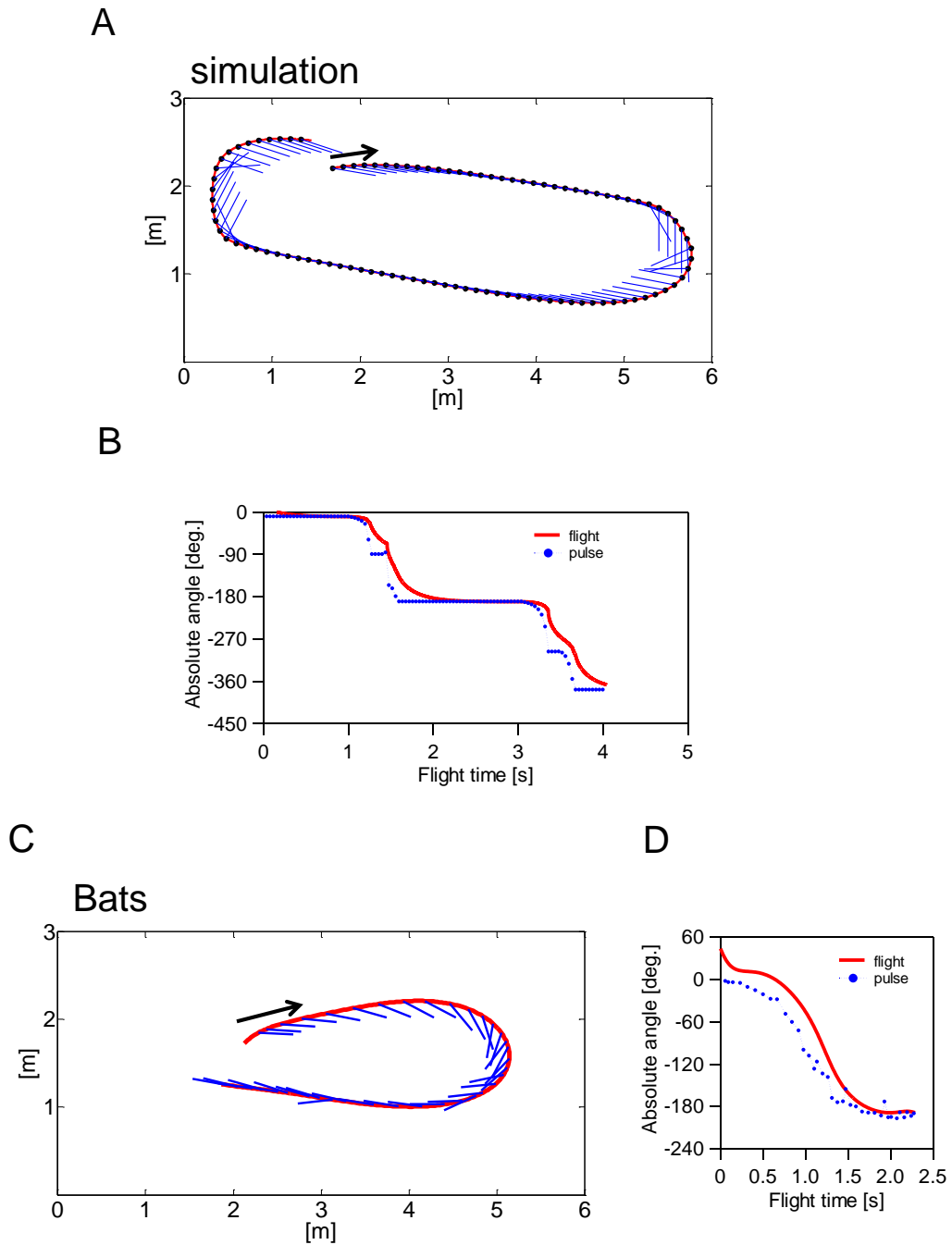
Figure 5-6 Behavioral comparison between the mathematical simulation of extended MOA model and *Pipistrellus abramus* during the free flight in the chamber. (A, C) Horizontal pulse direction (blue line) and moving path (red line) by extended MOA model and actual flying bats, respectively. (B, D).Changes in pulse (blue) and moving (red) direction as a function of a time in each movement.

Figure 5-7 shows simulation results for the horizontal flight path and pulse direction during obstacle avoidance for all six values of γ. When the avoidance parameters were set at $\alpha = 0.45$ m and $k = 0.15$ m, all simulated paths successfully passed through the obstacle course. A comparison of simulation results reveals that the avoidance path shifted to reduce the bulge width of the flight turn with an increase in the parameter γ. In addition, the mathematical simulation with high γ showed that the bat turned before coming close to the obstacles. The bulge width and the beginning of the flight turn were thus affected by the function parameter γ in that the acoustic gaze was synchronized with the turn rate. Furthermore, the trend that a high value of γ reduces the budge width was similar to the experimental results of the relationship between the bulge width and proportionality coefficient k for bats, indicating that bats indirectly control their flight path by adjusting the proportionality coefficient k, which synchronizes the acoustic gaze with the turn during flight through a familiar space.

γ=250

γ=750

γ=340

γ=1250

γ=500

γ=2500

all
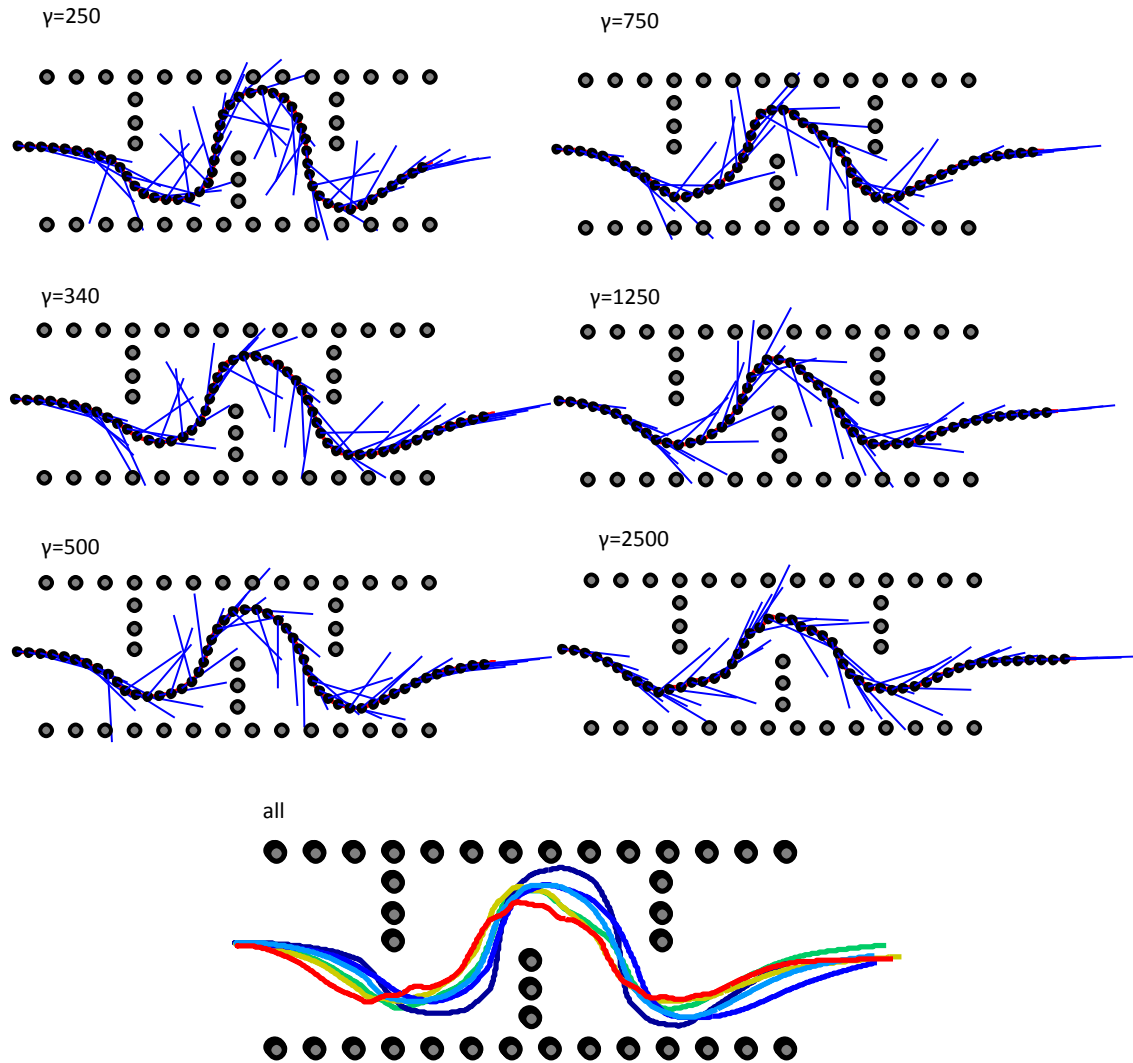
Figure 5-7 Comparison of the path of motion (red line) and pulse direction (blue line) simulated by the extended MOA model for six values of γ (IPI of 0.4 s, viewing angle of 90°). The bottom figure shows the overlapped flight paths in the six simulations.

5.4 Discussion

The behavioral measurement of the acoustic gaze revealed that bats sometimes emit a pulse toward a certain obstacle point, suggesting that bats process multiple echoes reflected from surrounding objects, and that bats then select the target echo from multiple echoes to determine the next pulse direction. Inspired by this suggestion, the MOA model was constructed as an avoidance model for calculations involving information of multiple obstacles. Mathematical simulation revealed that the MOA model can navigate an obstacle course using the actual navigation parameters of bats; i.e., the flight speed, IPI and beam width (figure 5-4B).

Bats essentially do not change the beam width of the pulse except during prey-capture flight and when approaching a wide open space whereas they flexibly control the pulse emission timing relative to the distance to a target object during flight (Hiryu *et al.*, 2008). Bats also reduce the number of pulse emissions by temporally shifting the pulse emission timing as they become familiar with the space around them, suggesting that bats use the minimum of pulse emissions that can maintain robust navigation to reduce the energy cost of sensing. Interestingly, according to the success probability map built using the MOA model and changing the IPI and viewing angle (figure 5-4A), the bat flight parameters (i.e., the IPI and beam width) were almost the threshold values that dramatically reduce the success probability to less than 10%. In fact, it was not matched complete avoidance parameter but the acoustic gaze control law has not yet been embedded into this model. The avoidance performance of the extended MOA model is expected to be improved with the acoustic gaze control law obtained from bats' navigation of unfamiliar space because the mathematical simulation was conducted without any pre-memorized spatial map. Moreover, it is possible to evaluate the improvement of navigation robustness by comparing new and original success probability maps. Mathematical simulations conducted for various conditions including both actual and imaginary conditions allows a quantitative evaluation of the capability of the acoustic navigation of bats, which is greatly beneficial for mathematical investigation. These considerations suggest that the MOA model is useful for the evaluation of the actual navigation behavior of bats.

The acoustic gaze control synchronized with the flight turn was simulated using the extending the MOA model (figure 5-6A). In the actual navigation of bats, the proportionality coefficient k of the linear correlation between the acoustic gaze and flight turn tends to be higher as bats become familiar with the space are around them. The effect of the proportionality coefficient k on the flight path was therefore investigated using a similar parameter γ. Differences in the bulge width of the flight turn were indirectly simulated by controlling γ using the same control law used for the proportionality coefficient k for bats (figure 5-7). A previous study reported that prey-capturing bats change the proportionality coefficient k among each of the search, approach and attacking phases. Adjusting the proportionality coefficient k seems to be an important strategy for bats to optimize their flight path regardless of the task of avoidance or chasing. These mathematical investigations reveal the essentials of the adaptation behavior of bats.

From an engineering point of view, multiple-echo processing of the MOA model inspired by the biosonar system of bats is a unique strategy. In a recent technology for the artificial sensing system of an autonomous vehicle, the whole of the surrounding space is covered by multiple sensors and directional sensing data for the closest obstacle distance are integrated employing a high-performance CPU. In contrast, the beam width of the pulse emitted by various species bats is ±20 to ±60°, which means that the scanning range of the echolocating bats is narrower than that of the artificial navigation system. For echolocating bats equipped with only one transmitter, multiple-echo processing could be considered a robust navigation strategy to compensate for less spatial information due to the limited scanning range. Instead of the limited scanning range, bats realize real-time decision making for acoustic navigation by the lower calculation cost requirement for spatial perception. Embedding a more critical bat-inspired navigation algorithm into the MOA model for further investigation could provide a useful algorithm for cheap and robust sensing.

5.5 *Summary*

This chapter presented an MOA model as an avoidance model based on ultrasound sensing using one transmitter and two receivers. The proposed model is designed such that the avoidance direction is calculated with information from multiple obstacles obtained from one sensing to compensate for the less spatial information provided by the limited scanning range in reality. Mathematical simulation showed that the MOA model could navigate the obstacle course using the actual navigation parameters of bats; i.e., the flight speed, IPI and beam width. Moreover, by extending the MOA model, acoustic gaze control synchronized with the flight turn, which is observed for the actual navigation of bats, was simulated. It is suggested that the MOA model is a useful platform for a bat-inspired navigation algorithm and the evaluation of the actual navigation behavior of bats.

Chapter 6. *Demonstration of an autonomous vehicle inspired by the bio-sonar strategy of bats*

6.1 Introduction

To determine how the observed behavioral strategies of bats improve the robustness of obstacle avoidance navigation based on cheap design sensing, we conducted an experiment involving a vehicle embedded with an obstacle avoidance algorithm employing ultrasonic sensors, which was inspired from the behavioral principles of bats during obstacle avoidance flight through an unfamiliar space. This study proposes a double-pulse scanning system as a bat-inspired navigation algorithm in which 1) the direction of a pulse emission is alternatively shifted between the preceding direction of movement and the obstacle direction and 2) the direction of movement is then calculated using the information of all echoes detected by double-pulse sensing. To quantify the double-pulse scanning system, a conventional scanning system was also developed whereby 1) the pulse emission is repeated in a neutral direction, which is the current moving on-axis, and 2) the direction of movement is calculated for each pulse emission.

6.2 Materials and methods

6.2.1 Vehicle design

We constructed a mobile vehicle (30 cm (H) × 15 cm (W) × cm 25 (L) cm), which included three ultrasonic sensor units, one transmitter (MA40S4R; Murata, Kyoto, Japan), two receivers (SPM0404UD5; Knowles, Itasca, IL, USA), two servomotor units and a microcomputer (Arduino Due; Arduino LLC, Somerville, MA, USA; fs = 140 kHz) (figure 6-1A). The CPU of the microcomputer had only a single core processor (with a clock speed of 84 MHz) that coordinated all of the navigation processes from the ultrasound sensing to the control of the vehicle movement in real time without serial communication with any additional personal computer (figure 6-1B). The autonomous vehicle could therefore be

regarded as having a cheap design relying on simple ultrasound sensing with a low-spec microcomputer.

One of the servomotors controlled the pulse direction from the transmitter and the other servomotor was connected to the left and right front wheel shafts so that the pulse direction could be adjusted independently of the control of the vehicle driving direction. The vehicle movement comprised two simple movements: 1) movement straight forward and 2) a pivot turn (without moving forward) that changes the driving direction toward the target direction.

A
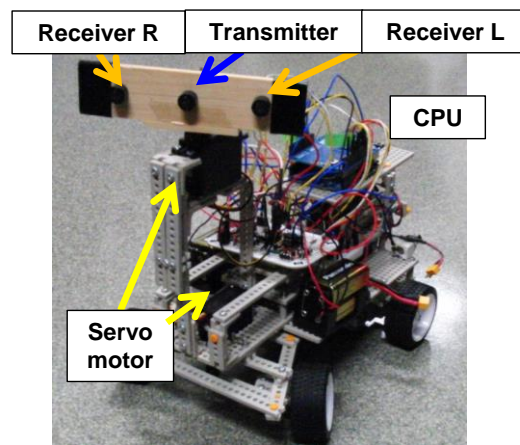
B
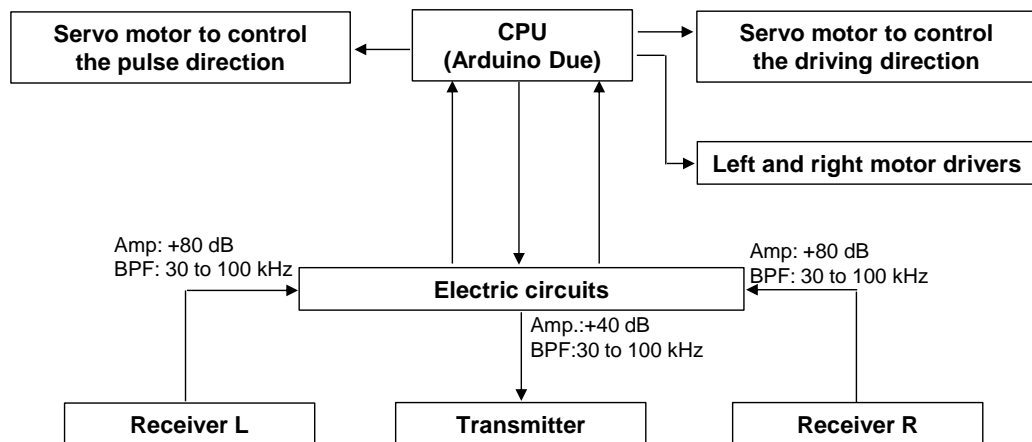
Figure 6-1 Design of an autonomous vehicle equipped with an ultrasound transmitter and receivers. (A) Custom-made autonomous vehicle called Mobius. (B) Schematic diagram of the vehicle operation system.

6.2.2 Signal processing for obstacle localization

Bats emit intense pulses of broad-beam ultrasound and receive multiple echoes from their surrounds during flight. The transmitter of our vehicle was thus chosen to have a broad beam width of the emission pulse. The transmitter emitted ultrasound at a central frequency of 40 kHz (for 2 ms in duration) and the beam width of the pulse (half amplitude angle from the beam axis at the energy maximum) was 50° at the central frequency (figure 6-2). The emission pulse was amplified by +14 dB by our original electric circuit, and the sound pressure level of the pulse was thus 128 dB at a distance 1 cm in front of the transmitter.
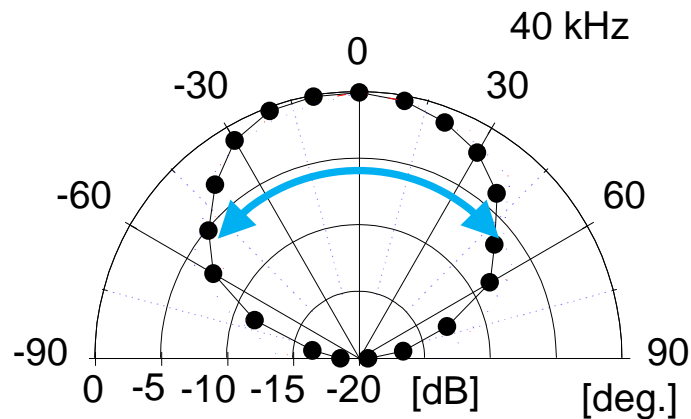
Figure 6-2 Ultrasound beam pattern of the transmitter. The beam width of the pulse was approximately ±50°.

In the receiver part, omni-directional sensors were used for left and right receivers and the obtained echo signals were amplified by +80 dB and bandpass filtered from 20 to 60 kHz by our original circuit to read the multiple echoes from the surrounds. The sampling rate of signal reading was 140 kHz, which was set according to the maximum speed of the analog-to-digital converter in the microcomputer. Figure 6-3A shows an example of time amplitude signals obtained from left and right receivers stored by the microcomputer on the vehicle. Zero time is the instant of the pulse emission. The figure confirms that the direct wave of the emission pulse (0–2 ms) was saturated but multiple echoes were completely stored with a good signal-to-noise ratio. The signal processing was designed to extract echo arrival times for all echoes. The arrival time of each echo was defined as the instant of the

initial rise above a voltage threshold. To avoid missing a reading because of the overlapping of the direct wave of the pulse and reflected echoes, the time window for the detection of the echo arrival was set at 1.7–30 ms from the instant of pulse emission (i.e., the detection distance range from the vehicle to the obstacle was restricted from 0.29 to 5.1 m) for each pulse emission. In a traditional method, echo detection is conducted only for the nearest object according to the initial rise of the signal sequence of the received echoes. Our original method can store information of many more echoes for one pulse emission in contrast with the traditional method. While driving, the times of echo arrival at the left and right receivers (t_{left}, t_{right}) were automatically determined by the microcomputer so that the position of each obstacle could be localized in real time (Figure 6-3B and C) using

$$r_{obs}(t,n) = \frac{c(t_{right}(t,n) + t_{left}(t,n))}{4} \tag{6-1}$$

$$\theta_{obs}(t,n) = \arcsin \frac{c(t_{right}(t,n) - t_{left}(t,n))}{d} + \varphi_p \tag{6-2}$$

where d indicates the distance between the right and left receivers, t indicates the pulse emission timing, n indicates the order in which echoes are detected by each receiver, r_{obs} is the distance from the vehicle to the obstacle, φ_p is the direction of the emission pulse relative to the vehicle driving direction, and θ_{obs} is the direction of the obstacle relative to the vehicle driving direction. Because the echoes arriving at the right and left receivers were paired in time-sequence order to calculate r_{obs} and θ_{obs} using equations (6-1) and (6-2), they were sequentially numbered; thus, the n of r_{obs} and θ_{obs} were defined as $r(t,n)$ and $\theta(t,n)$, respectively. Here, the number of all obstacles detected by the pulse emission at time t is defined as $N(t)$ for calculation of the vehicle navigation algorithm (see 6.2.4).
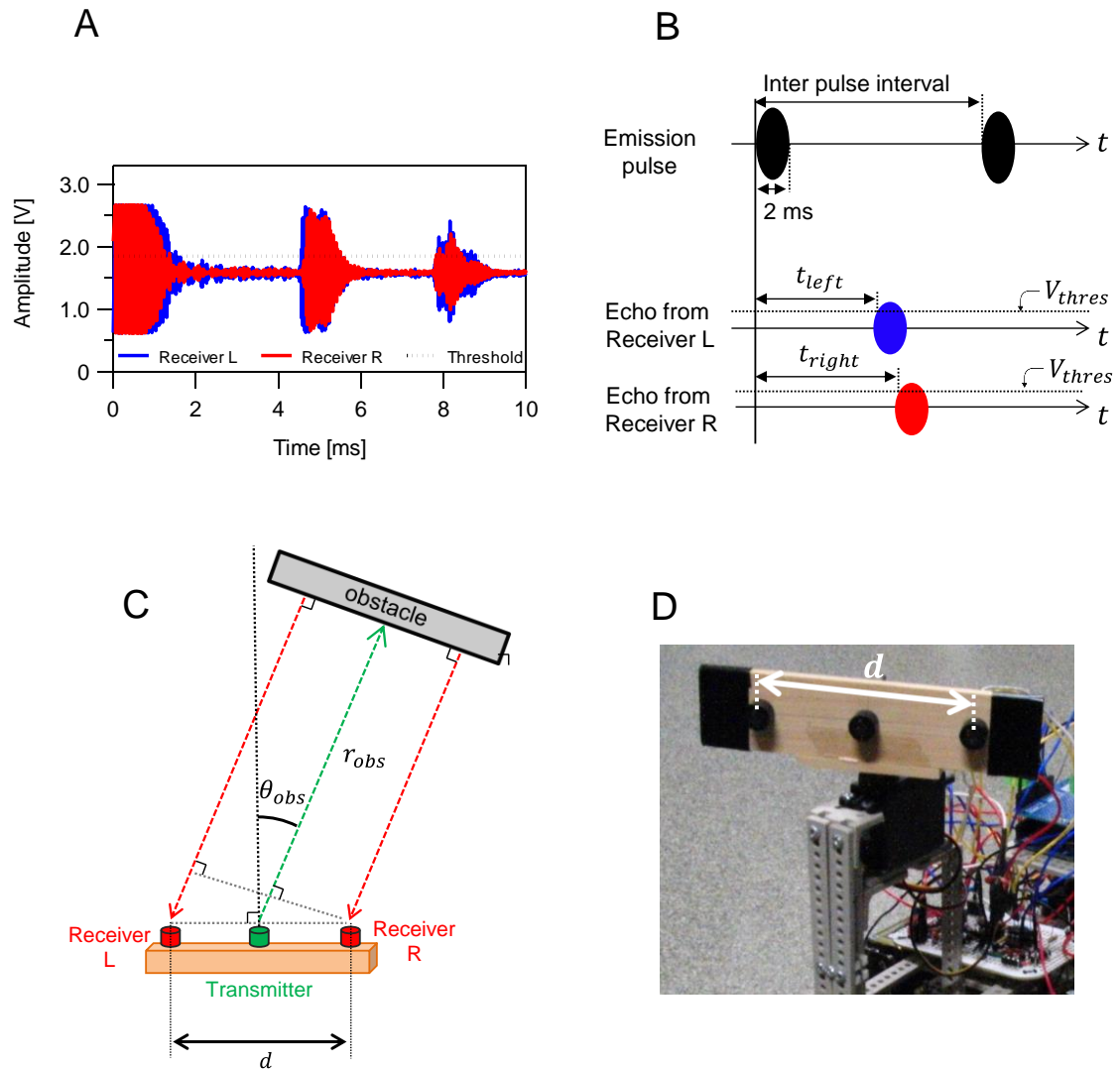
Figure 6-3 Signal processing procedure for obstacle localization. (A) Typical time amplitude echo signals recorded by left (blue) and right (red) receivers. The black dashed line indicates the threshold voltage. (B) Schematic diagram of the procedure for storing the echo information. The vehicle reads the time that the echo signal rises above a voltage threshold. Our original method was able to store information for many more echoes for one pulse emission. (C) Schematic diagram of the localization procedure. (D) Expanded view of vehicle sensors. The distance between the left and right receivers d was 8 cm.

The localization accuracy of the obstacle distance r_{obs} and the obstacle direction θ_{obs} was evaluated for a quiescent condition. The procedure for measuring the localization accuracy of obstacle direction θ_{obs} is shown in figure 6-4A. A stationary vehicle was placed on a turntable and it localized a target pole that was set at a distance 0.6 m from the vehicle

sensor unit. (Note that the pulse direction of the vehicle was fixed to the mid-line of the vehicle body.) The directional localization accuracy of the vehicle was evaluated by comparing the actual azimuth angle $\theta_{azimuth}$ (actual angle to the target pole from the pulse direction defined as 0°) and the localization angle θ_{obs} calculated by the vehicle. The measurement was made for 11 values of $\theta_{azimuth}$ ranging from −50° to 50° in steps of 10° by rotating the turntable set under the vehicle. For each condition, the vehicle repeated the sensing and localization calculation 100 times. Figures 6-4B shows the average localization angle θ_{obs} obtained for 100 repeated sensings at each actual azimuth angle $\theta_{azimuth}$. An error bar indicates the standard deviation for the 100 localizations and a dashed line indicates the ideal localization angle. The figure shows that the localization error and dispersion of the localization angle increased with the absolute azimuth angle. Maximum error was 14° ± 15° at $\theta_{azimuth} = 50°$. The localization error tended to increase to the outside of the target pole from the pulse direction. We therefore confirm that the directional error of localization increased as the obstacle detection angle departed from the beam axis.

The localization accuracy of the obstacle distance r_{obs} was also measured by setting the target pole in front of the vehicle sensor unit ($\theta_{azimuth} = 0°$; Figure 6-4C). The distance from the vehicle to the target pole r ranged from 0.3 to 1.4 m in steps of 0.1 m and the sensing was repeated 100 times for each distance condition. The localization error was evaluated as distance error Δr_{dist} and positioning error Δr_{posit}:

$$\Delta r_{dist} = \left| r - r_{obs} \right| \tag{6-3}$$

$$\Delta r_{posit} = \left\| r - r_{obs} e^{i\theta_{obs}} \right\| \tag{6-4}$$

Figure 6-4D shows the distance error Δr_{dist} and positioning error Δr_{posit} relative to the distance from the vehicle to the target pole r. The average distance error Δr_{dist} was within 2 cm for all distance conditions whereas the average positioning error Δr_{posit} was as high as 0.3 m and the dispersion of localization error increased when increasing the target

pole distance r. This result indicates that the localization error was dominated by angular error of the obstacle direction θ_{obs} rather than distance error of the obstacle distance r_{obs}.
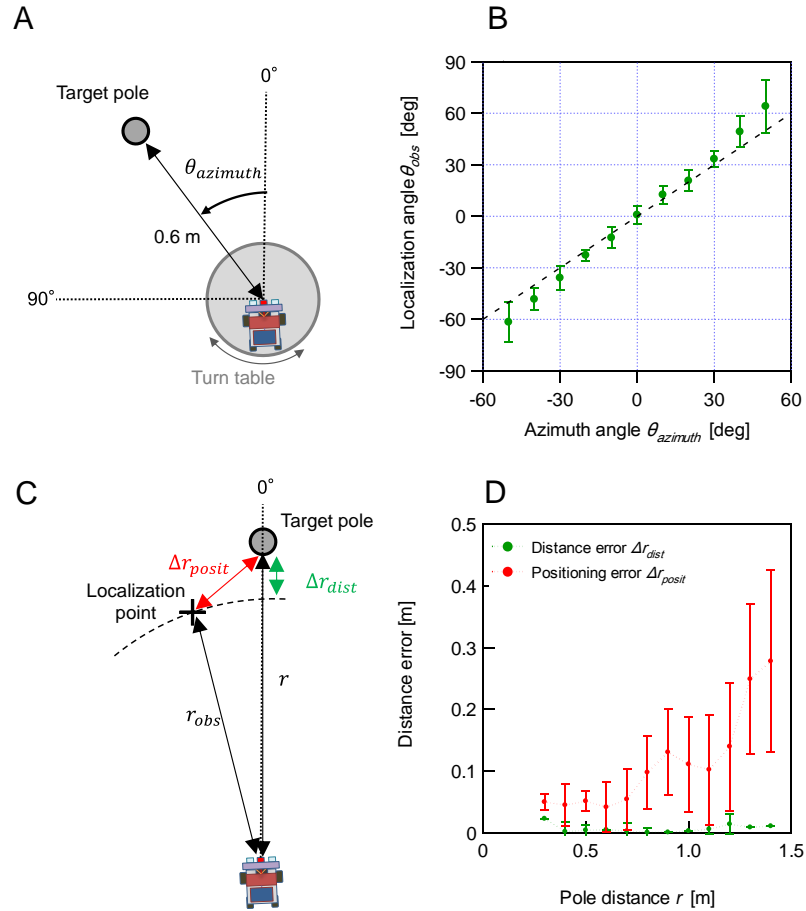
Figure 6-4 Evaluation of the vehicle localization accuracy in the stationary condition. (A, C) Procedures for measuring the localization accuracy of obstacle direction θ_{obs} and obstacle distance r_{obs}. Localization distance r_{obs} was evaluated as distance error Δr_{dist} and positioning error Δr_{posit}. (B) Average localization angle θ_{obs} relative to the actual azimuth angle $\theta_{azimuth}$ for 100 repeated sensings in each condition. An error bar indicates the standard deviation for 100 localizations and the dashed line indicates the ideal localization angle. (D) Average distance error Δr_{dist} (green) and positioning error Δr_{posit} (red) relative to the actual pole distance obtained by 100 repeated sensings in each condition. An error bar indicates the standard deviation of 100 localizations.

6.2.3 Vehicle movement setting

The vehicle was controlled based on two simple movements: 1) moving straight forward and 2) pivoting in place (without moving forward) to change the driving direction. Figure 6A and 6B provide schematic diagrams of the control dynamics for moving direction φ_d with the conventional scanning system and double-pulse scanning system, respectively. The timing of the ith pulse emission is defined as t_i. The moving direction φ_d of the conventional scanning system was changed by pivoting after pulse emission, with a response time Δt including both mechanical and echo processing time (Figure 6A). On the other hand, the moving direction φ_d in the double-pulse scanning system was calculated for every double-pulse emission (Figure 6B). Then, the vehicle moved straight forward for a duration τ, which was set at 0.6 s in the conventional scanning system and 1.2 s in the double-pulse scanning system. Because the response time Δt (<0.1 s) was sufficiently shorter than τ, we could consider the inter-pulse interval to be 0.6 s for both the conventional and double-pulse scanning systems, with the result that the inter-pivot interval (inter-pivot distance) of the double-pulse scanning system was twice as long as that of the conventional scanning system. The vehicle driving speed was set at ~15 times slower (21 cm/s) than the average flight speed of *R. ferrumequinum nippon* (2.7–3.0 m/s) during obstacle-avoidance flight. Therefore, the inter-pulse interval of the vehicle was set at 0.6 s, which was ~15 times that of the bats' average inter-pulse interval (~40 ms).
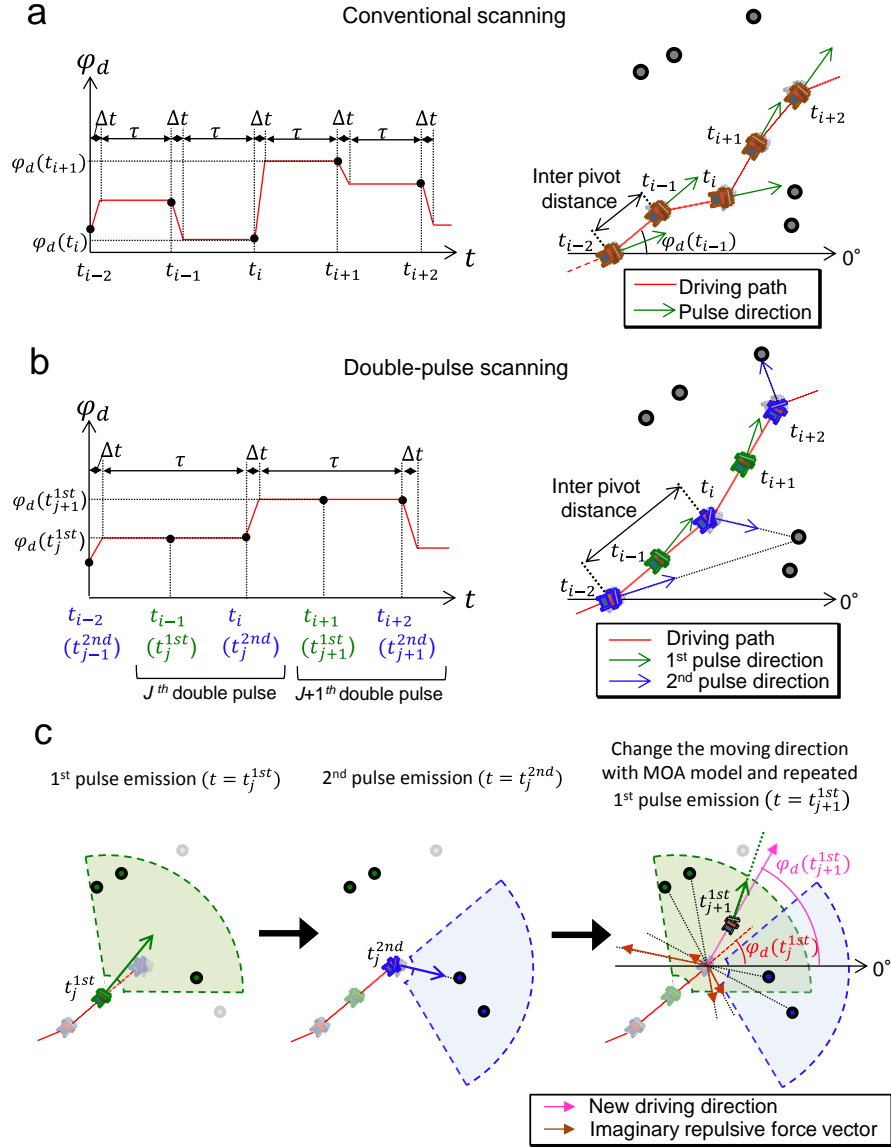
Figure 6-5 Comparison of vehicle movement between the conventional scanning system and the double-pulse scanning system. Schematic of temporal change in moving direction φ_d of the vehicle with the conventional scanning (a) and double-pulse scanning (b). The conventional scanning system repeated the pivot turn in the duration of response time Δt toward the calculated moving direction at every sensing. In contrast, the double-pulse scanning system was set for pivot turns every double-pulse emission. (c) Schematic of control law for pulse direction φ_p in the double-pulse scanning system. The 2nd pulse emission was directed towards the nearest obstacle among all obstacles detected by the previous two successive emissions, i.e. the 1st pulse emission of the jth double pulse and the 2nd pulse emission of the $(j-1)$th double pulse. Then, the direction of the 1st pulse emission of the $(j+1)$th double pulse was determined based on the amount of change in the moving direction φ_d between jth and $(j+1)$th double pulses.

6.2.4 Vehicle navigation algorithm

First, we constructed an obstacle-avoidance model for both the conventional and double-pulse scanning systems to control the vehicle's moving direction using multiple obstacle information (multi-obstacle-avoidance [MOA] model; see 5.2.1). To explain the MOA model briefly, we determined the moving direction φ_d in the case of the conventional scanning system using the following equation (Figure 6A):

$$\varphi_d(t_{i+1}) = \arg(e^{i\varphi_d(t_i)} - 2\sum_{n=1}^{N(t_i)} \sqrt{\frac{\alpha}{r(t_i,n)}} \sin\left(\arctan\frac{k}{r(t_i,n)}\right) e^{i\theta(t_i,n)}) \quad (6\text{-}5)$$

where $\alpha = 0.015625$ m, and $k = 1.3$ m. The moving direction φ_d was changed after the ith pulse emission. On the other hand, in the case of double-pulse scanning system, after the 2nd pulse emission of the jth double pulse, φ_d could be determined using the following equation (Figure 6B):

$$\varphi_d\left(t_{j+1}^{1st}\right) = \arg(e^{i\varphi_d\left(t_j^{1st}\right)} - 2\sum_{n=1}^{N\left(t_j^{1st}\right)} \sqrt{\frac{\alpha}{r\left(t_j^{1st},n\right)}} \sin\left(\arctan\frac{k}{r\left(t_j^{1st},n\right)}\right) e^{i\theta\left(t_j^{1st},n\right)}$$

$$-2\sum_{n=1}^{N\left(t_j^{2nd}\right)} \sqrt{\frac{\alpha}{r\left(t_j^{2nd},n\right)}} \sin\left(\arctan\frac{k}{r\left(t_j^{2nd},n\right)}\right) e^{i\theta\left(t_j^{2nd},n\right)} \quad (6\text{-}6)$$

where $\alpha = 0.0078125$ m, and $k = 1.3$ m. Thus, the moving direction φ_d in the double-pulse scanning system was calculated using all obstacle information obtained from the 1st and the 2nd pulse emissions. It should be noted that the positions of obstacles detected by the 1st pulse emission were corrected according to the movement of the vehicle to calculate the φ_d.

In the MOA model of both the conventional and double-pulse scanning systems, the moving direction φ_d can be calculated by adding the imaginary attraction force vector of the vehicle's current driving direction and imaginary repulsive force vectors. The imaginary repulsive force produced from each obstacle was determined by the distance $r(t,n)$ and the direction $\theta(t,n)$ ($n = 1,\ldots, N(t)$) of the obstacles. Furthermore, by assuming the imaginary width of individual obstacles according to the distance $r(t,n)$, the MOA model calculates the imaginary repulsive force, which corresponds to the concept of monoscopic depth cues

by visual sensing (i.e. the perceived object size decreases with distance). As a result, the driving direction can be defined by adding reconstructed imaginary two-dimensional images of surrounding objects that were derived from one-dimensional sound information.

In the conventional scanning system, pulse direction was fixed to the current moving on-axis at all times for every pulse emission (Figure 6a). In the double-pulse scanning system, the direction of the 1st pulse emission of the $(j+1)^{th}$ double pulse, $\varphi_p(t_{j+1}^{1st})$, was determined by the amount of change in the moving direction between the jth and $(j+1)^{th}$ double pulses (Figure 6C).

$$\varphi_p(t_{j+1}^{1st}) = \varphi_d(t_{j+1}^{1st}) + \beta\left(\varphi_d(t_{j+1}^{1st}) - \varphi_d(t_j^{1st})\right) \qquad (6\text{-}7)$$

where β was set at 0.6. After the vehicle detected the obstacles by the 1st pulse emission, the 2nd pulse emission was directed to the nearest obstacle among all obstacles detected by the previous two successive emissions, i.e. the 1st pulse emission of the $(j+1)^{th}$ double pulse and the 2nd pulse emission of the jth double pulse. As a result, in the double-pulse scanning system, the direction of pulse emission alternates between the direction of movement and the direction of the nearest obstacle, simulating the movement of bats flying in unfamiliar spaces. Figure 7*a* and 7*b* show flowcharts of the avoidance algorithm based on the MOA model for the conventional scanning and double-pulse scanning systems, respectively. The frequency of decision making for movement direction in the double-pulse scanning system was half that in the conventional scanning system. On the other hand, avoidance direction could be calculated using twice as much obstacle information by spatial integration obtained from double-sensing.

A
Conventional scanning

```
┌─────────────────────────┐
│      Move forward       │◄──┐
└─────────────────────────┘   │
             │                │
             ▼                │
┌─────────────────────────┐   │
│ Pulse direction was fixed to │
│ the current driving on-axis  │
└─────────────────────────┘   │
             │         No     │
             ▼                │
    ◇ Number of detected ◇────┘
      objects >0 ?
             │
             ▼ Yes
┌─────────────────────────┐
│ vector calculation by MOA model │
└─────────────────────────┘
             │
             ▼
┌─────────────────────────┐
│       Turn the body     │
└─────────────────────────┘
```

B
Double-pulse scanning

```
┌─────────────────────────┐
│      Move forward       │◄──┐
└─────────────────────────┘   │
             │                │
             ▼                │
┌─────────────────────────────┐
│     1st pulse emission      │
│  Pulse is emitted towards   │
│ the preceded moving direction│
└─────────────────────────────┘
             │         No     │
             ▼                │
    ◇ Number of detected ◇────┘
      objects >0 ?
             │
             ▼ Yes
┌──────────────────────────────────┐
│ Turn only the head to the nearest object │
└──────────────────────────────────┘
             │
             ▼
┌─────────────────────────┐
│      Move forward       │
└─────────────────────────┘
             │
             ▼
┌─────────────────────────┐
│     2nd pulse emission  │
└─────────────────────────┘
             │
             ▼
┌──────────────────────────────────┐
│ Integrate the positions of objects detected by │
│     1st and 2nd pulse emission   │
└──────────────────────────────────┘
             │
             ▼
┌─────────────────────────┐
│ Vector calculation by MOA model │
└─────────────────────────┘
             │
             ▼
┌─────────────────────────┐
│       Turn the body     │
└─────────────────────────┘
```

Figure 6-6 Comparison of navigation algorithms of the conventional scanning system and the new system inspired by bats. Schematic diagrams of vehicle navigation algorithms for the conventional scanning system (A) and double-pulse scanning system (B).

6.2.5 Experimental method

An obstacle course was constructed by arranging plastic poles (12 cm diameter) in a 4×2 m driving field. While driving on the obstacle course, obstacle distance and direction localized by the vehicle, and the pulse direction of the transmitted signal, were stored instantly in memory on the vehicle, and then transmitted using wireless serial communication (X-bee; Digi International Inc., Minnetonka, MN, USA) to a personal

computer in real-time. In addition, the vehicle driving path and moving direction were measured externally using two digital high-speed video cameras, with the same recording procedure used in the behavioural experiments with bats. The vehicle has a LED light that flashed in synchronization with pulse emission, so that the actual pulse emission timing could also be recorded by these video cameras. The localization errors of $r(t,n)$ and $\theta(t,n)$ ($n = 1,\ldots,\ N(t)$) were evaluated using the differences between the localized values from the vehicle and the values measured by the external cameras at every pulse emission. Furthermore, the obstacle-avoidance performance of a vehicle was measured to permit comparison between the conventional scanning and double-pulse scanning systems.

6.3   *Results of the vehicle experiment*

Examples of the path of motion and pulse direction of the vehicle during driving through the obstacle course are shown in figure 6-7A and B, respectively. With the conventional scanning system, the vehicle collided with the pole located at the center of the obstacle course even though the vehicle detected the pole (figure 6-7A) whereas the double-pulse scanning system could control the direction of movement to avoid the pole (figure 6-7B). Figure 6-8A and B also demonstrates the vehicle driving paths that were taken from the first 10 trials for each system. The vehicle frequently collided with the center pole in the case of the conventional scanning system whereas the double-pulse scanning system avoided a collision in all 10 trials, with the vehicle travelling along the left side, which was wider than the rout on the right side. Success rates for the 100 trials of obstacle avoidance driving (where success is defined as the vehicle passing through the course without collision) were 13% (13/100 trials) for the conventional system and 73% (73/100 trials) for the double-pulse scanning system. Collisions were categorized into two cases: collisions with the central obstacle pole (52% for conventional and 10% for double pulses) and collisions with the left and right poles (35% for conventional and 17% for double pulses).
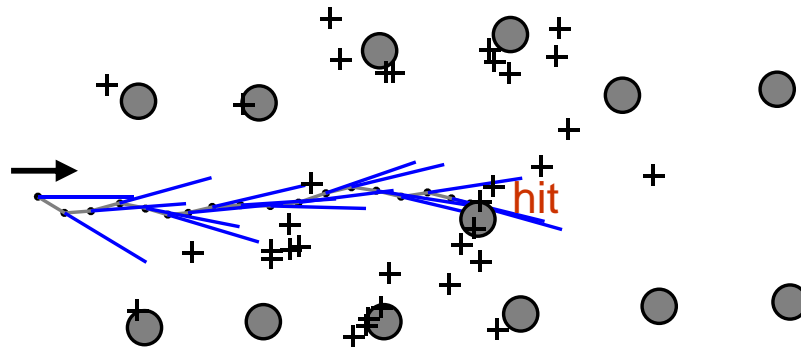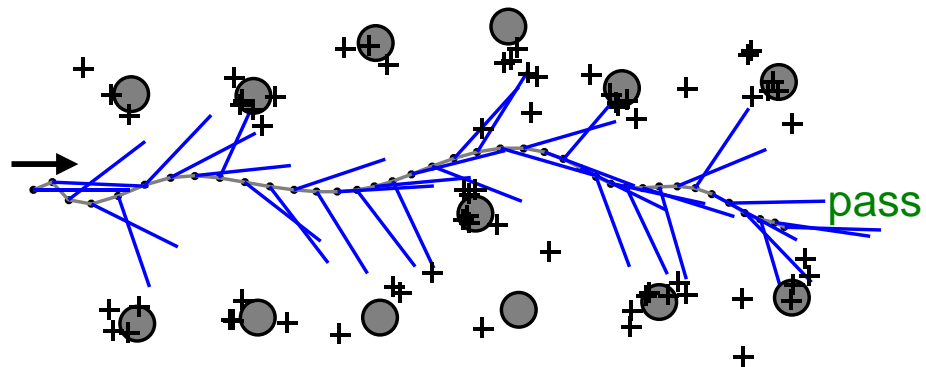
Figure 6-7 Demonstration of vehicle navigation during obstacle avoidance driving. Top views of representative driving paths (red line) and pulse directions (blue line) for the conventional scanning system (A) and the double-pulse scanning system (B). Cross plots indicate obstacle localization positions during driving.
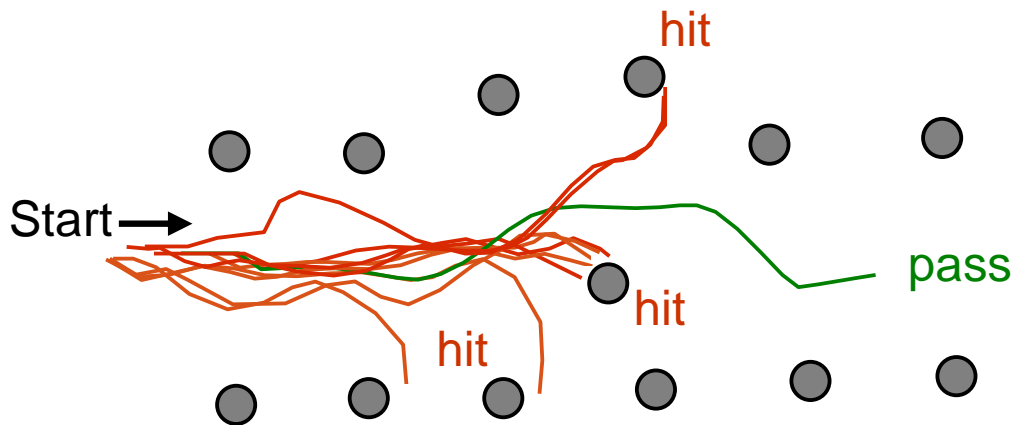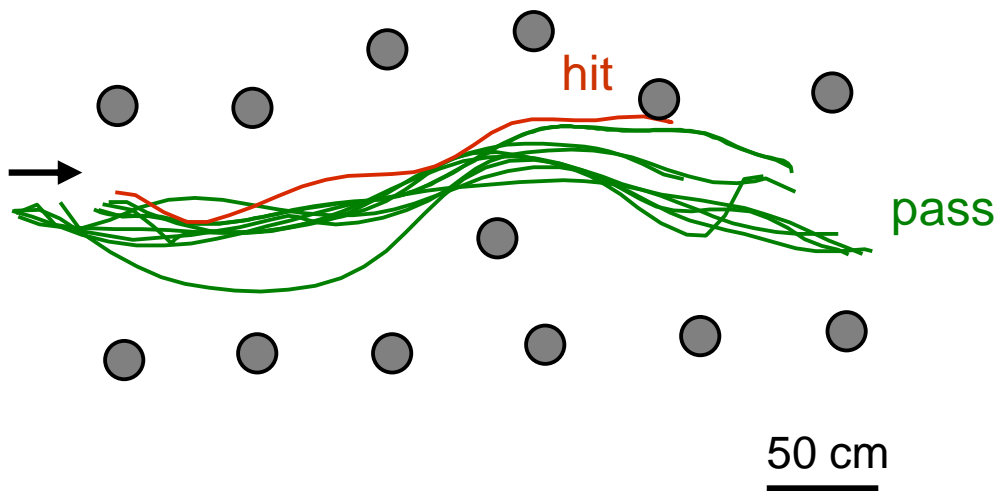
Figure 6-8 Comparison of driving paths for the conventional scanning system and double-pulse scanning system. Top views of driving paths for the conventional scanning system (A) and double-pulse scanning system (B) (10 trials per system).

All obstacle localization points detected by the vehicle are shown with cross marks in figures 6-7A and B. However, the localization points deviated from the actual obstacle positions; the error for the first 10 trials was 19 ± 12 cm in the case of the conventional scanning system, which was not significantly different from the error of 20 ± 12 cm in the case of the double-pulse scanning system (Mann–Whitney U test, $P = 0.07$) (figure 6-9A and B). Furthermore, figure 6-9C and D shows distributions of the angular error for all detected obstacles in the 10 trials. The angular error for the conventional system was not significantly different from that for the double-pulse scanning system (Mann–Whitney U test, $P = 0.54$). These results suggest that the localization accuracy for detected obstacles is not a critical reason for the difference in the obstacle avoidance performances of the conventional and double-pulse scanning systems.
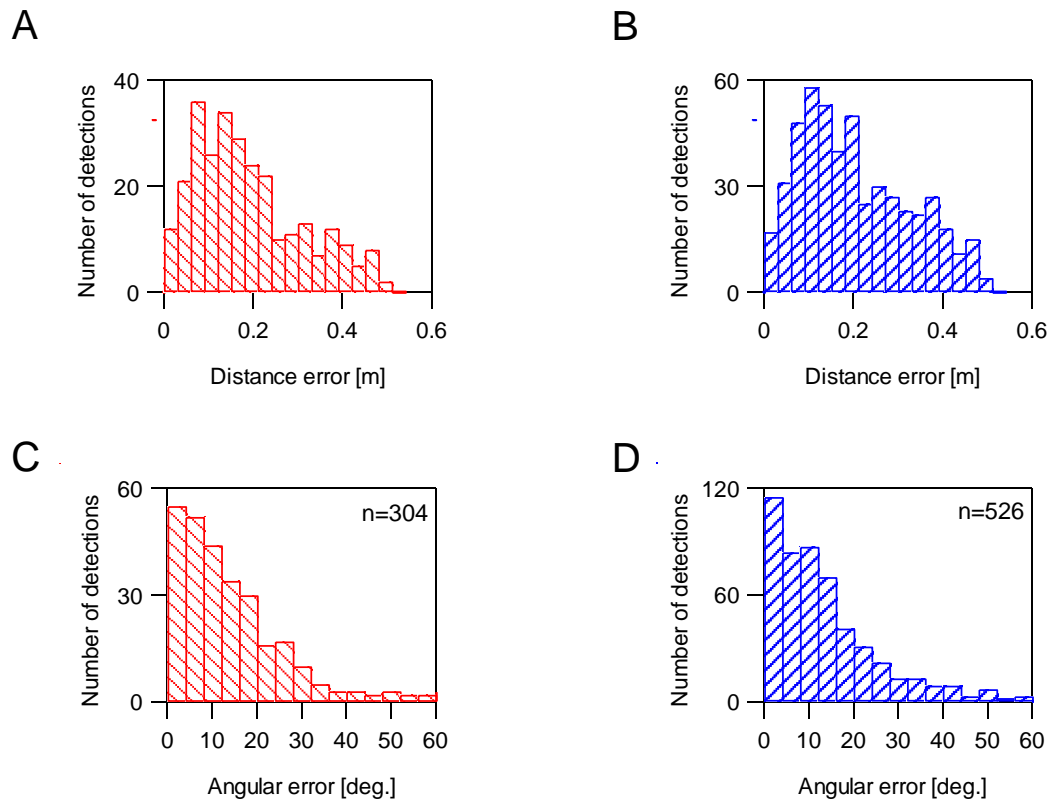
Figure 6-9 Comparison of localization error during obstacle avoidance driving with the conventional scanning system and double-pulse scanning system. Distributions of distance error in obstacle detection using the conventional (A) and double-pulse scanning systems (B). Distributions of the angle error in obstacle detection using the conventional (C) and double-pulse scanning systems (D).

Distributions of the number of obstacles N used to determine the direction of movement is shown in figure 6-10A. N in double-pulse scanning was 4.5 ± 1.3, which was twice that in conventional scanning ($N = 2.0 ± 1.0$) (Mann–Whitney U test, P < 0.01). The angles of detected obstacles relative to pulse direction were dominantly distributed around the center of the acoustic field in the double-pulse scanning system, whereas the conventional scanning system tended to detect obstacles to the left or right. Moreover, the rate of detection of the obstacle nearest the vehicle reached ~80% (334/526) for the double-pulse scanning system and was significantly higher than that for the conventional scanning system (50%, 186/304).

These findings suggested that a double-pulse scanning system has several practical advantages in obstacles detection; e.g., the vehicle can drive without losing the nearest obstacle within the acoustic field of view even though the frequency of decision making for the direction of movement is reduced by half.
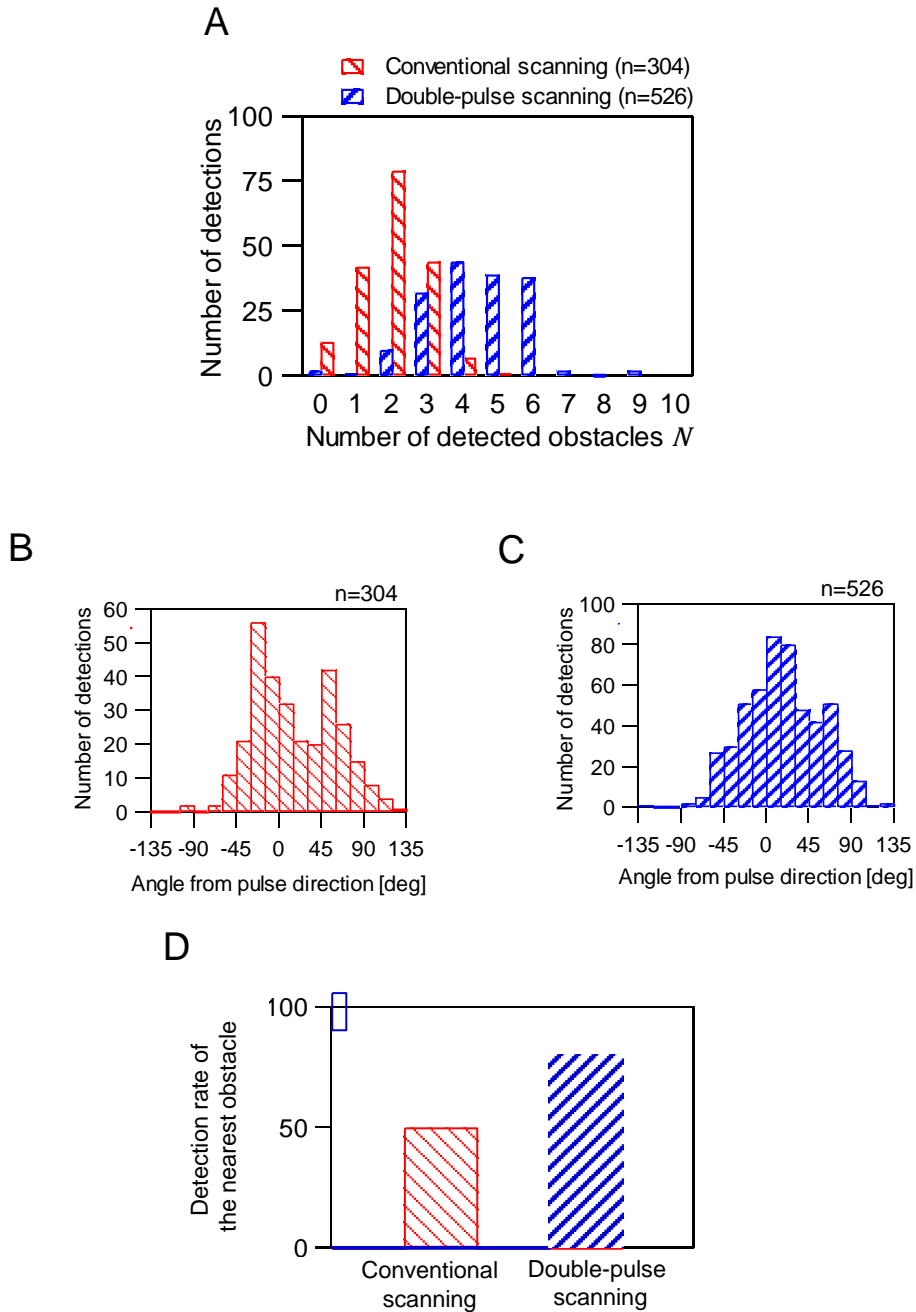
Figure 6-10 Comparison of the obstacle detection performance between the conventional and double-pulse scanning systems for the first 10 trial data. (A) Distributions of the number of obstacles N that were used to determine the direction of movement for the conventional and double-pulse scanning systems. Distributions of obstacle detection angle from the pulse direction for the conventional (B) and double-pulse scanning systems (C). (D) Comparison of detection rates for the nearest obstacles, according to vehicle coordination, between the conventional and double-pulse scanning systems.

6.4   Discussion

In chapter 4, we experimentally demonstrated that *R. ferrumequinum nippon* showed an adaptive behavioral change when it became familiar with the space around it; i.e., the pulse direction was observed to shift smoothly relative to the flight direction, whereas the pulse direction (acoustic gaze) alternately shifted between surrounding immediate obstacles and the intended flight direction in a time-sharing manner during flight through an unfamiliar space. We constructed an algorithm based on observed behavioral principles of bats during unfamiliar space navigation to experimentally investigate the possibility of applying a bat's cheap design of sensing to a vehicle. This is the first comprehensive study on bats involving behavioral and practical engineering experiments.

The findings suggest that bats may integrate information by sensing twice through the emission of double pulses. A double-pulse scanning system employing the hybrid scanning behavior observed during the flight of a bat in an unfamiliar space improved the avoidance performance of the autonomous vehicle. In the case of the conventional scanning system in which the pulse direction was always fixed to the current driving axis, the immediate obstacle was often outside the angle of the acoustic field of view of the vehicle when the vehicle changed direction to avoid the previous obstacle (figure 8a). In contrast, the double-pulse scanning system mimicking the bats' behavior to eliminate such a blind spot by keeping the critical obstacle point within the acoustic field of view that was spatially extended by integrating information obtained from double-pulse sensing. Furthermore, the vehicle calculated its own direction of movement using not only immediate obstacle information but also more distant obstacle information; this allowed the vehicle to select a more robust avoidance path (see figure 7d).

The recent technology trend of spatial sensing is to increase the number of sensor units so that the whole surrounding space is covered by integrating the spatial information of multiple sensors. Meanwhile, the vehicle in the present study had only one sensor unit. The double-pulse scanning system allows the vehicle to double-count a certain obstacle for two emissions. Because an imaginary repulsion force is calculated using all the detected obstacles, the double-pulse scanning system lays weight on the obstacles that are detected twice for control of the driving direction. This is considered to be temporal integration of obstacle information, which is one of the advantages of the double-pulse scanning system

because double-counted obstacles are usually located around the driving direction. A double-pulse scanning system thus extends not only spatially but also temporally its own acoustical field of view of the vehicle. Although the double-pulse scanning system reduces the frequency of decision making for the direction of movement to half that of the conventional scanning system (figure 6c), our findings suggest that the integration of information for two emissions(i.e., acoustic sight restricted to only one transmitter and two receivers) is effective, demonstrating that a small example of ingenuity can dramatically affect simple design sensing.

In this study, we investigated how echolocating bats determine spatial information selection and integration relative to the external world. Because the proposed double-pulse sensing used simple algorithms, such as temporal and spatial integration of obstacle information, it can be applied readily to various navigation systems with modest calculation costs. For example, simulation research for humanoid robot navigation with stereo vision has demonstrated that alternate gaze shift control, between the direction of movement and obstacle direction, is effective for avoidance without losing an obstacle positioned at a critical point (Seara *et al.*, 2003). We can compare gaze control by visually guided animals with simple acoustic sensing inspired by the bat biosonar system. The basis of our idea may not only provide new insight into the principles of representative ultrasonic sensing relying on cheap and simple systems but also link to future biomimetic research inspired by the processes of the decision making and conception of higher animals.

6.5   Summary

To confirm the practical effectiveness of the bat's behavior, a double-pulse scanning system was proposed as a bat-inspired navigation algorithm for navigation through an unfamiliar space in which 1) the direction of pulse emission was alternatively shifted between the preceding direction of movement and the obstacle direction and 2) the direction of movement was calculated using information of all echoes detected by double-pulse sensing. As a result, the success rate of an obstacle avoidance drive on a test course improved from 13% for conventional scanning to 73% with the proposed method. In the case of the conventional scanning system in which the pulse direction was always fixed to

the current driving axis, the immediate obstacle was often outside the angle of the acoustic field of view of the vehicle when the vehicle changed driving direction to avoid the previous obstacle. In contrast, the double-pulse scanning system mimicking the bats' behavior can eliminate such a blind spot by keeping the critical obstacle point within the acoustic field of view that was spatially extended by integrating information obtained from double-pulse sensing. Furthermore, the double-pulse scanning system allows the vehicle to double-count a certain obstacle for two emissions. Because the imaginary repulsion force is calculated using all the detected obstacles, the double-pulse scanning system lays weight on the obstacles that were detected twice for control of the driving direction. This is considered to be the temporal integration of obstacle information, and is one advantage of the double-pulse scanning system because double-counted obstacles are usually located around the driving direction. Thus, the double-pulse scanning system extends not only spatially but also temporally its acoustical field of view of the vehicle. These findings suggest that simple procedures inspired by animals, such spatial and temporal integration of sensing information from double-pulse scanning, can greatly affect the performance of acoustical navigation.

Chapter 7. *Conclusions*

In this study, changes in the pulse direction; pulse emission timing and flight path of *Rhinolophus ferrumequinum nippon* during an obstacle avoidance flight were experimentally investigated as the bats became familiar with the space. Furthermore, we constructed algorithm based on observed behavioral principles of the bats during unfamiliar space navigation so that the possibilities of bats' cheap design sensing could be experimentally investigated using the vehicle. This is the first comprehensive study by bat researches through behavioral and practical engineering experiments. In this chapter, main results of the dissertation and discuss directions for future work were summarized.

7.1   *Summary of the Main Results*

A. Echolocation behavior of CF-FM bats during long-term flight in an obstacle-filled environment (Chapter 3)

Ultrasonic sonar emissions and 3D flight paths of *R. ferrumequinum nippon* during long-term obstacle avoidance flight were measured to confirm the presence of adaptation behavior. Flight path analysis revealed that bats repeated the same circular or figure-of-eight flight path after several seconds to several tens of seconds of flight. Simultaneously, bats reduced the number of pulse emissions to half over 30 s by 1) prolonging the longer IPI and 2) replacing the triple+ pulse with a double or single pulse. In addition, the shorter IPI slightly increased and the distribution in the histogram of the shorter IPI was significantly narrower than the distribution in the histogram of the longer IPI so that bats did not change the duration of the IPI within a multiple pulse, suggesting that keeping the emission interval within the sonar sound group as short as possible was necessary in using the multiple pulse effectively. The use of the double pulse increased from the pre- to post-accustomed phase, suggesting that it was a special pulse used not only for exploring an unfamiliar space in the process of becoming accustomed to the space but also for negotiating a cluttered environment irrespective of whether the space was familiar. These findings suggest the bats are capable of spatial learning and that they adapt their flight path and pulse emissions to economically fly through an environment using spatial memory.

B. Echolocation behavior of CF-FM bats during repeated flights through a highly cluttered obstacle course (Chapter 4)

This chapter presented an adaptation strategy of bats mainly focusing on the directional control of sonar sound during repeated flights through a highly cluttered S-shaped obstacle course. The bats adapted their flight path to reduce the curvature of flight while increasing their flight speed in repeated trials. The number of pulse emissions decreased but the longer IPI did not increase, indicating that the timing control of a long-interval pulse was strongly affected by the cluttered environment. In addition, the emission of triple+ pulses decreased significantly with increasing trial number, suggesting that bats preferentially used the strategy of reducing the number of multiple pulses over the strategy of prolonging the pulse interval to reduce the pulse emissions in a cluttered environment. Further investigation of acoustic gaze control revealed that bats present an adaptive behavioral change as they became familiar with the space around them; i.e., the pulse direction was observed to shift smoothly relative to the flight direction whereas in flight through a unfamiliar space, the pulse direction (acoustic gaze) alternately shifted between surrounding immediate obstacles and the intended flight direction in a time-sharing manner. These findings suggests that bats adapt their acoustic gaze control synchronized with path planning and pulse emission timing in becoming familiar with an obstacle-filled environment.

C. Mathematical modelling of obstacle avoidance navigation (Chapter 5)

This chapter constructed the MOA model as an avoidance model based on ultrasound sensing using one transmitter and two receivers. The proposed model was designed such that the avoidance direction is calculated with information of multiple obstacles obtained from one sensing to compensate for less spatial information due to the limited scanning range in reality. Mathematical simulation revealed that the MOA model can navigate an obstacle course using the actual navigation parameters of bats; i.e., the flight speed, IPI and beam width. Moreover, by extending the MOA model, the acoustic gaze control synchronized with the flight turn, which was observed for the actual navigation of bats, was also simulated. These findings suggest that the MOA model is a useful platform for a bat-inspired navigation algorithm and the evaluation of the actual navigation behavior of bats.

D. Demonstration of an autonomous vehicle inspired by the bio-sonar strategy of bats (Chapter 6)

To confirm the practical effectiveness of the bat's behavior, a double-pulse scanning system was proposed as a bat-inspired navigation algorithm for navigation through unfamiliar space in which 1) the direction of pulse emission was alternatively shifted between the preceding direction of movement and the obstacle direction and 2) the direction of movement was then calculated using information of all echoes detected by double-pulse sensing. The success rate of obstacle avoidance driving on a test course vastly improved when using the proposed method rather than the conventional scanning system. The double-pulse scanning system mimicking the bats' behavior can eliminate a blind spot by keeping the critical obstacle point within an acoustic field of view that was spatially extended by integrating information obtained from double-pulse sensing. Furthermore, the double-pulse scanning system allows the vehicle to double-count a certain obstacle for two emissions. Because the imaginary repulsion force is calculated using all detected obstacles, the double-pulse scanning system lays weight on the obstacles that are detected twice for control of the driving direction. This is considered to be the temporal integration of obstacle information, and is one of the advantages of the double-pulse scanning system because double-counted obstacles are usually located around the driving direction. The double-pulse scanning system extends not only spatially but also temporally its acoustical field of view of the vehicle. These findings suggest that simple procedures inspired by animals, such as spatial and temporal integration of sensing information obtained from double-pulse scanning, can greatly affect the performance of acoustical navigation.

7.2   Future Works

1. Successive adaptation behavior

The present study demonstrated behavioral differences between navigation through unfamiliar and familiar spaces by investigating long-term or repeated flights in an obstacle-filled environment. Findings of the present study suggest that the acoustic gaze control contributes to spatial adaptation in flight path planning and pulse emissions. However, a successive adaptation strategy has not been revealed. In further investigation of the long-

term flight of bats through an obstacle circuit, behavioral changes by repeated round could be investigated to obtain the behavioral principles of the successive adaptation behavior of bats.

2. Spatial learning strategy of bats

The spatial scanning behavior of bats revealed that alternate shifting of the acoustic gaze is not synchronized with a reduction in the number of pulse emissions used to become familiar with a space, which means that bats change their spatial scanning strategy from an exploring phase to an economical navigation phase by relying on spatial memory. If the area of spatial scanning is estimated from the pulse direction and beam pattern, it is possible to investigate the space where put on the spatial memory. The compiling of spatial adaptation behaviors during flight through various obstacle layouts and search for a common appearance of a spatial scanning area can reveal the essentials of the spatial learning strategy of bats. Spatial learning is a unique and intelligent strategy relying on animal behavior. The spatial learning strategy adopted by bats contributes to a useful solution for cheap robust sensing as an artificial-intelligence system.

3. Mathematical evaluation of the acoustical navigation of bats

The present study revealed the MOA model to be a useful platform for a bat-inspired navigation algorithm and the evaluation of the actual navigation behavior of bats. A mathematical simulation was conducted for constant sensing parameters (i.e., IPI and detection range). Echolocating bats actively control acoustic characteristics relative to the surroundings so that there is a divergence in navigation between actual bats and simulation. Further studies are needed to evaluate the effectiveness of active control navigation employing the modified MOA model.

7.3 Towards engineering applications

Our behavioral investigations demonstrated that bats can adopt the animal intelligence navigation strategy referred to as spatial adaptation. Acoustic gaze control greatly contributes to flight path adaptation and pulse emission adaptation. Furthermore, actual vehicle investigations demonstrated that simple procedures for acoustic gaze control inspired by bats can greatly improve the performance of acoustical navigation with simple

ultrasound sensors. However, the present study is only a demonstration under simplified conditions (e.g., alternate shifting of the acoustic gaze with a double pulse during flight through an unfamiliar space). To develop useful solutions to technical problems of recent technology trends that rely on careful sensing using multiple sensors, not only double-pulse but also triple-pulse and single-pulse emissions should be assessed. The triple pulse was more often repeated during flight through an unfamiliar space and can thus be regarded as a "careful emission pulse" whereas a single-pulse emission was increasingly used as the bat became familiar with the space and can thus be regarding as an "economical emission pulse". Echolocating bats actively switch between careful and economical sensing in each situation, which differs from the case of artificial application. To be more precise, spatial adaptation behavior includes a spatial learning strategy and finding such a strategy may contribute to simultaneous localization and mapping technology (Newman *et al.*, 2005; Sunderhauf *et al.*, 2007) operated by a cheap signal processing unit. Bats thus have much to offer cheap robust navigation technology.

7.4 Final Remarks

The unique sensing strategy and auditory system of bats as an acoustically guided animal have been investigated through physiological analysis, behavioral measurement, mathematical simulation and engineering, separately. Our behavioral investigations demonstrated that bats are also capable of an animal intelligence navigation strategy referred to as spatial adaptation. Acoustic gaze control vastly contributes to flight path adaptation and pulse emission adaptation. Furthermore, actual vehicle investigations demonstrated that simple procedures for acoustic gaze control inspired by bats can greatly improve the performance of acoustical navigation with simple ultrasound sensors. This was the first comprehensive study of bats involving behavioral and practical engineering experiments. Further cross-correlational investigation will provide useful solutions to technical problems of recent technology trends that rely on careful sensing using multiple sensors.

REFERENCES

Aihara, I., Yamada, Y., Fujioka, E., and Hiryu, S. (**2015**). "Nonlinear dynamics in free flight of an echolocating bat," Nonlinear Theory and Its Applications, IEICE **6**, 313-328.

Arita, H. T., and Fenton, M. B. (**1997**). "Flight and echlocation in the ecology and evolution of bats," Trends in Ecology & Evolution **12**, 53-58.

Ashton, K. (**2009**). "That 'internet of things' thing," RFiD Journal **22**, 97-114.

Atzori, L., Iera, A., and Morabito, G. (**2010**). "The internet of things: A survey," Computer networks **54**, 2787-2805.

Barchi, J. R., Knowles, J. M., and Simmons, J. A. (**2013**). "Spatial memory and stereotypy of flight paths by big brown bats in cluttered surroundings," Journal of Experimental Biology **216**, 1053-1063.

Burgard, W., Fox, D., Hennig, D., and Schmidt, T. (**1996**). "Estimating the absolute position of a mobile robot using position probability grids," in *Proceedings of the national conference on artificial intelligence* (Citeseer), pp. 896-901.

Choi, B.-S., Lee, J.-W., Lee, J.-J., and Park, K.-T. (**2011**). "A hierarchical algorithm for indoor mobile robot localization using RFID sensor fusion," Industrial Electronics, IEEE Transactions on **58**, 2226-2235.

Cox, I. J. (**1991**). "Blanche-an experiment in guidance and navigation of an autonomous robot vehicle," Robotics and Automation, IEEE Transactions on **7**, 193-204.

Donges, E. (**1978**). "A two-level model of driver steering behavior," Human Factors: The Journal of the Human Factors and Ergonomics Society **20**, 691-707.

Eckmeier, D., Geurten, B. R., Kress, D., Mertes, M., Kern, R., Egelhaaf, M., and Bischof, H. J. (**2008**). "Gaze strategy in the free flying zebra finch (Taeniopygia guttata)," PLoS One **3**, e3956.

Fenton, M. B. (**2010**). "Convergences in the diversification of bats," Current Zoology **56**, 454-468.

Fenton, M. B. (**2013**). "Questions, ideas and tools: lessons from bat echolocation," Animal Behaviour **85**, 869-879.

Fenton, M. B., Faure, P. A., and Ratcliffe, J. M. (**2012**). "Evolution of high duty cycle echolocation in bats," Journal of Experimental Biology **215**, 2935-2944.

Fujioka, E., Aihara, I., Watanabe, S., Sumiya, M., Hiryu, S., Simmons, J. A., Riquimaroux, H., and Watanabe, Y. (**2014**). "Rapid shifts of sonar attention by *Pipistrellus abramus* during natural hunting for multiple prey," The Journal of the Acoustical Society of America **136**, 3389-3400.

Fujioka, E., Mantani, S., Hiryu, S., Riquimaroux, H., and Watanabe, Y. (**2011**). "Echolocation and flight strategy of Japanese house bats during natural foraging, revealed by a microphone array system," J Acoust Soc Am **129**, 1081-1088.

Ghose, K., Horiuchi, T. K., Krishnaprasad, P. S., and Moss, C. F. (**2006**). "Echolocating bats use a nearly time-optimal strategy to intercept prey," PLoS Biol **4**, e108.

Ghose, K., and Moss, C. F. (**2003**). "The sonar beam pattern of a flying bat as it tracks tethered insects," The Journal of the Acoustical Society of America **114**, 1120-1131.

Ghose, K., and Moss, C. F. (**2006**). "Steering by hearing: a bat's acoustic gaze is linked to its flight motor output by a delayed, adaptive linear law," J Neurosci **26**, 1704-1710.

Griffin, D. R. (**1958**). "Listening in the dark: the acoustic orientation of bats and men."

Griffin, D. R., Webster, F. A., and Michael, C. R. (**1960**). "The echolocation of flying insects by bats," Animal behaviour **8**, 141-154.

Grinnell, A., and Schnitzler, H.-U. (**1977**). "Directional sensitivity of echolocation in the Horseshoe bat, Rhinolophus ferrumequinum," Journal of Comparative Physiology A: Neuroethology, Sensory, Neural, and Behavioral Physiology **116**, 63-76.

Gustafson, Y., and Schnitzler, H.-U. (**1979**). "Echolocation and obstacle avoidance in the hipposiderid batAsellia tridens," Journal of comparative physiology **131**, 161-167.

Hartley, D. J., and Suthers, R. A. (**1987**). "The sound emission pattern and the acoustical role of the noseleaf in the echolocating bat, Carolliaperspicillata," The Journal of the Acoustical Society of America **82**, 1892-1900.

Hartley, D. J., and Suthers, R. A. (**1989**). "The sound emission pattern of the echolocating bat, Eptesicusfuscus," The Journal of the Acoustical Society of America **85**, 1348-1351.

Hartley, D. J., and Suthers, R. A. (**1990**). "Sonar pulse radiation and filtering in the mustached bat, Pteronotusparnelliirubiginosus," The Journal of the Acoustical Society of America **87**, 2756-2772.

Hase, K., Miyamoto, T., Kobayasi, K. I., and Hiryu, S. (**2016**). "Rapid frequency control of sonar sounds by the FM bat, Miniopterus fuliginosus, in response to spectral overlap," Behavioural processes **128**, 126-133.

Hiryu, S., Katsura, K., Lin, L.-K., Riquimaroux, H., and Watanabe, Y. (**2006**). "Radiation pattern of echolocation pulse in Taiwanese leaf-nosed bat, Hipposideros terasensis," Acoustical science and technology **27**, 108-110.

Hiryu, S., Shiori, Y., Hosokawa, T., Riquimaroux, H., and Watanabe, Y. (**2008**). "On-board telemetry of emitted sounds from free-flying bats: compensation for velocity and distance stabilizes echo frequency and amplitude," Journal of Comparative Physiology A **194**, 841-851.

Iida, F. (**2005**). "Cheap design approach to adaptive behavior: Walking and sensing through body dynamics," in *International symposium on adaptive motion of animals and machines* (Citeseer), p. 15.

Jakobsen, L., Olsen, M. N., and Surlykke, A. (**2015**). "Dynamics of the echolocation beam during prey pursuit in aerial hawking bats," Proceedings of the National Academy of Sciences **112**, 8118-8123.

Jakobsen, L., Ratcliffe, J. M., and Surlykke, A. (**2013**). "Convergent acoustic field of view in echolocating bats," Nature **493**, 93-96.

Jakobsen, L., and Surlykke, A. (**2010**). "Vespertilionid bats control the width of their biosonar sound beam dynamically during prey pursuit," Proc Natl Acad Sci U S A **107**, 13930-13935.

Jen, P. H.-S., and Kamada, T. (**1982**). "Analysis of orientation signals emitted by the CF-FM bat, Pteronotus p. parnellii and the FM bat, Eptesicus fuscus during avoidance of moving and stationary obstacles," Journal of comparative physiology **148**, 389-398.

Kinoshita, Y., Ogata, D., Watanabe, Y., Riquimaroux, H., Ohta, T., and Hiryu, S. (**2014**). "Prey pursuit strategy of Japanese horseshoe bats during an in-flight target-selection task," Journal of Comparative Physiology A **200**, 799-809.

Kortenkamp, D., and Weymouth, T. (**1994**). "Topological mapping for mobile robots using a combination of sonar and vision sensing," in *AAAI*, pp. 979-984.

Kothari, N. B., Wohlgemuth, M. J., Hulgard, K., Surlykke, A., and Moss, C. F. (**2014**). "Timing matters: sonar call groups facilitate target localization in bats," Frontiers in physiology **5**.

Kounitsky, P., Rydell, J., Amichai, E., Boonman, A., Eitan, O., Weiss, A. J., and Yovel, Y. (**2015**). "Bats adjust their mouth gape to zoom their biosonar field of view," Proceedings of the National Academy of Sciences **112**, 6724-6729.

Land, M., and Horwood, J. (**1995**). "Which parts of the road guide steering?," Nature **377**, 339-340.

Land, M. F., and Collett, T. (**1974**). "Chasing behaviour of houseflies (Fannia canicularis)," Journal of comparative physiology **89**, 331-357.

Land, M. F., and Lee, D. N. (**1994**). "Where we look when we steer," Nature **369**, 742-744.

Lu, T.-F. (**2013**). "Indoor odour source localisation using robot: Initial location and surge distance matter?," Robotics and Autonomous Systems **61**, 637-647.

Matsuta, N., Hiryu, S., Fujioka, E., Yamada, Y., Riquimaroux, H., and Watanabe, Y. (**2013**). "Adaptive beam-width control of echolocation sounds by CF-FM bats, Rhinolophus ferrumequinum nippon, during prey-capture flight," J Exp Biol **216**, 1210-1218.

Mogensen, F., and Møhl, B. (**1979**). "Sound radiation patterns in the frequency domain of cries from a Vespertilionid bat," Journal of comparative physiology **134**, 165-171.

Moss, C. F., Bohn, K., Gilkenson, H., and Surlykke, A. (**2006**). "Active listening for spatial orientation in a complex auditory scene," PLoS Biol **4**, e79.

Moss, C. F., and Surlykke, A. (**2010**). "Probing the natural scene by echolocation in bats," Front Behav Neurosci **4**.

Mourant, R. R., and Rockwell, T. H. (**1970**). "Mapping eye-movement patterns to the visual scene in driving: An exploratory study," Human Factors: The Journal of the Human Factors and Ergonomics Society **12**, 81-87.

Neuweiler, G. (**1984**). "Foraging, Echolocation and Audition in Bats," Naturwissenschaften **71**, 446-455.

Newman, P. M., Leonard, J. J., and Rikoski, R. J. (**2005**). "Towards constant-time SLAM on an autonomous underwater vehicle using synthetic aperture sonar," in *Robotics Research. The Eleventh International Symposium* (Springer), pp. 409-420.

Novick, A., and Vaisnys, J. R. (**1964**). "Echolocation of flying insects by the bat, Chilonycteris parnellii," Biological Bulletin **127**, 478-488.

Pfeifer, R., and Lambrinos, D. (**2000**). "Cheap Vision—Exploiting Ecological Niche and Morphology," in *International Conference on Current Trends in Theory and Practice of Computer Science* (Springer), pp. 202-226.

Riquimaroux, H., Gaioni, S. J., and Suga, N. (**1991**). "Cortical computational maps control auditory perception," Science **251**, 565-568.

Riquimaroux, H., Gaioni, S. J., and Suga, N. (**1992**). "Inactivation of the DSCF area of the auditory cortex with muscimol disrupts frequency discrimination in the mustached bat," Journal of neurophysiology **68**, 1613-1623.

Royer, E., Lhuillier, M., Dhome, M., and Lavest, J.-M. (**2007**). "Monocular vision for mobile robot localization and autonomous navigation," International Journal of Computer Vision **74**, 237-260.

Schnitzler, H.-U., and Denzinger, A. (**2011**). "Auditory fovea and Doppler shift compensation: adaptations for flutter detection in echolocating bats using CF-FM signals," Journal of Comparative Physiology A **197**, 541-559.

Schnitzler, H.-U., and Kalko, E. K. (**2001**). "Echolocation by Insect-Eating Bats We define four distinct functional groups of bats and find differences in signal structure that correlate with the typical echolocation tasks faced by each group," Bioscience **51**, 557-569.

Seara, J. F., Strobl, K. H., and Schmidt, G. (**2003**). "Path-dependent gaze control for obstacle avoidance in vision guided humanoid walking," in *Robotics and Automation, 2003. Proceedings. ICRA'03. IEEE International Conference on* (IEEE), pp. 887-892.

Seibert, A.-M., Koblitz, J. C., Denzinger, A., and Schnitzler, H.-U. (**2013**). "Scanning behavior in echolocating common pipistrelle bats (Pipistrellus pipistrellus)," PloS one **8**, e60752.

Seibert, A.-M., Koblitz, J. C., Denzinger, A., and Schnitzler, H.-U. (**2015**). "Bidirectional echolocation in the bat Barbastella barbastellus: Different signals of low source level are emitted upward through the nose and downward through the mouth," PloS one **10**, e0135590.

Shimozawa, T., Suga, N., Hendler, P., and Schuetze, S. (**1974**). "Directional sensitivity of echolocation system in bats producing frequency-modulated signals," Journal of Experimental Biology **60**, 53-69.

Simmons, J. A. (**1979**). "Perception of Echo Phase Information in Bat Sonar," Science **204**, 1336-1338.

Simmons, J. A., Ferragamo, M., Moss, C. F., Stevenson, S. B., and Altes, R. A. (**1990**). "Discrimination of jittered sonar echoes by the echolocating bat, Eptesicus fuscus: the shape of target images in echolocation," Journal of Comparative Physiology A **167**, 589-616.

Simmons, J. A., and Stein, R. A. (**1980**). "Acoustic imaging in bat sonar: echolocation signals and the evolution of echolocation," Journal of Comparative Physiology **135**, 61-84.

Speakman, J., and Racey, P. (**1991**). "No cost of echolocation for bats in flight," Nature **350**, 421-423.

Strother, G., and Mogus, M. (**1970**). "Acoustical beam patterns for bats: Some theoretical considerations," The Journal of the Acoustical Society of America **48**, 1430-1432.

Sunderhauf, N., Lange, S., and Protzel, P. (**2007**). "Using the unscented kalman filter in mono-SLAM with inverse depth parametrization for autonomous airship control,"

in *Safety, Security and Rescue Robotics, 2007. SSRR 2007. IEEE International Workshop on* (IEEE), pp. 1-6.

Surlykke, A., Ghose, K., and Moss, C. F. (**2009a**). "Acoustic scanning of natural scenes by echolocation in the big brown bat, Eptesicus fuscus," Journal of Experimental Biology **212**, 1011-1020.

Surlykke, A., Pedersen, S. B., and Jakobsen, L. (**2009b**). "Echolocating bats emit a highly directional sonar sound beam in the field," Proceedings of the Royal Society of London B: Biological Sciences **276**, 853-860.

SUTHERS, R. A., THOMAS, S. P., and SUTHERS, B. J. (**1972**). "Respiration, wing-beat and ultrasonic pulse emission in an echo-locating bat," Journal of Experimental Biology **56**, 37-48.

Thrun, S., Fox, D., Burgard, W., and Dellaert, F. (**2001**). "Robust Monte Carlo localization for mobile robots," Artificial intelligence **128**, 99-141.

Volos, C. K., Kyprianidis, I. M., and Stouboulos, I. N. (**2013**). "Experimental investigation on coverage performance of a chaotic autonomous mobile robot," Robotics and Autonomous Systems **61**, 1314-1322.

Warnecke, M., Lee, W.-J., Krishnan, A., and Moss, C. F. (**2016**). "Dynamic Echo Information Guides Flight in the Big Brown Bat," Frontiers in behavioral neuroscience **10**.

Wisniewska, D. M., Johnson, M., Beedholm, K., Wahlberg, M., and Madsen, P. T. (**2012**). "Acoustic gaze adjustments during active target selection in echolocating porpoises," Journal of Experimental Biology **215**, 4358-4373.

Yamada, Y., Hiryu, S., and Watanabe, Y. (**2016**). "Species-specific control of acoustic gaze by echolocating bats, Rhinolophus ferrumequinum nippon and Pipistrellus abramus, during flight," Journal of Comparative Physiology A **202**, 791-801.

Curriculum Vitae

Yasufumi Yamada

DATE of BIRTH: March 27th, 1989

PLACE of BIRTH: Osaka, Japan.

EDUCATION

2013	Doshisha University in Kyotanabe:
	M.S. Life and Medical Sciences
2011	Doshisha University in Kyotanabe:
	B.S. Electrical Engineering

AWARDS

2016	Student Presentation Award,
	Autumn Meeting of the Acoustical Society of Japan, Toyama, Japan.
2012	Student Poster Award,
	Autumn Meeting of the Animal Behavior of Japan, Nara, Japan.
2011	Poster Presentation Award,
	Meeting for young scientist of the Acoustical Society of Japan,
	Osaka, Japan.
2011	Student Presentation Award,
	Meeting of the Marine Acoustics Society of Japan, Tokyo, Japan.

PROFESSIONAL MEMBERSHIPS

Acoustical Society of Japan

November 2016